

Basic principles of MR imaging

PHILIPS
sense and simplicity

Basic Principles of MR Imaging

CONTENTS

- 7 Preface
- 9 How this book is organized

11 AN INTRODUCTION TO MAGNETIC RESONANCE IMAGING

- 14 Information content and clinical efficacy

17 PHYSICAL PRINCIPLES OF MAGNETIC RESONANCE

- 19 Magnetic properties of nuclei
- 20 The vector description of magnetic resonance and net magnetization
- 22 Larmor precession and resonance phenomena
- 23 Relaxation processes
- 24 Longitudinal (spin-lattice) relaxation
- 27 Transverse (spin-spin) relaxation
- 29 Magnetization transfer
- 29 The free induction decay, signal detection and fourier transformation
- 30 Spin echo development: rationale and methodology
- 32 NMR of nuclei other than protons

35 MAGNETIC RESONANCE INSTRUMENTATION

- 37 MR system components
- 38 The magnet system
- 39 Gradient coil system
- 40 RF coils
- 42 The acquisition and control system
- 42 The reconstruction system
- 42 Host computer, viewing, archiving, hardcopy
- 43 Magnetic shielding
- 44 RF shielding

45 THE THEORY OF IMAGE FORMATION

- 47 Introduction
- 48 Slice selection
- 51 Spatial encoding and image reconstruction
 - Using a read-out gradient*
 - Two-dimensional Fourier transform image reconstruction (frequency and phase encoding)*
 - Volume imaging or 3D imaging*
- 56 Spatial encoding and k-space

- 59 Imaging sequences
Pulse sequence fundamentals
Imaging based on the FID
- 60 Spin imaging
- 61 Gradient Echo Imaging Or Fast Field Echo (Ffe) Imaging
- 63 Variations on a theme - spin preparation in imaging sequences
Prepulses - Inversion Recovery
STIR
Suppression of CSF
SPIR
Contrast enhancement
- 67 Speeding up image acquisition - fast imaging enhancements
Imaging throughput enhancements: multi-echo and multi-slice
Multi-echo acquisition
Multi-slice acquisition
Imaging throughput enhancements: reducing the number of phase encoding steps
Reduced acquisition
Halfscan
Rectangular Field Of View
Keyhole - dynamic imaging with more images in shorter time
- 73 Fast image acquisition sequences
Turbo Field Echo (TFE)
Turbo Spin Echo (TSE)
Echo Planar Imaging
GRASE – Gradient And Spin Echo
Other ways to traverse k-space

81 PRACTICAL CONSIDERATIONS IN MR IMAGING

- 83 Introduction
- 84 Image quality
- 84 Voxel size and spatial resolution
- 86 Signal-To-Noise Ratio
- 88 Signal averaging
- 89 Pulse sequence parameters
Magnetic field strength
Effect of the rf coils
- 91 Image contrast
Sources of object contrast

- Proton density*
T₁ and T₂ relaxation
TR, TE and contrast in Spin Echo imaging
TR, TE, pulse flip angle and contrast in Gradient Echo imaging (FFE)
- 97 Flow phenomena
Inflow effects
Flow enhancement
Flow void
Misregistration
Phase effects
Turbulent flow
- 102 Magnetic susceptibility and paramagnetism
- 103 Artifacts and artifact reduction techniques
Motion artifacts
Fold-over suppression
Chemical shift artifacts
Magnetic material artifacts
- 107 Paramagnetic contrast agents
- 109 Cautions and contra-indications in magnetic resonance imaging

111 SPECIAL TECHNIQUES

- 113 Magnetic Resonance Angiography
Inflow MRA
Phase Contrast Angiography (PCA) and phase velocity mapping
- 123 Triggered acquisition sequences – cardiac imaging
- 124 Magnetic resonance spectroscopy chemical shift
Localization
Volume selective ³¹P spectroscopy
Local ¹H spectroscopy – suppression of the water resonance
Spectroscopic imaging
- 129 Functional imaging
Functional brain imaging
Functional imaging using contrast agents
Perfusion imaging
Diffusion imaging

133 INDEX

PREFACE

Few scientific analysis techniques have had as broad an influence as nuclear magnetic resonance (NMR). Since the nearly simultaneous discovery of NMR phenomena by Bloch and colleagues at Stanford University and Purcell and coworkers at Harvard in 1946, uses of the technique have developed rapidly. Initially valued by chemists and physicists as a probe of molecular structure, chemical reaction rates, and diffusion processes, NMR was quickly adapted to medical applications. Within thirty years of its discovery, magnetic resonance principles were used to acquire the first images of a human subject. In the ensuing years, the use of magnetic resonance imaging (MRI) has become an essential modality in clinical diagnostic imaging.

This book offers an introduction to the basic principles of magnetic resonance imaging. It is written for individuals with a clinical or scientific background, but does not assume prior knowledge of classical physics, quantum mechanics, or complex mathematics. Literature references and suggested additional reading are offered for readers who require a more thorough treatment of the material covered.

HOW THIS BOOK IS ORGANIZED

The information in this text is organized in the following fashion:

To Learn About:

The history of MR imaging and an overview of the role of MRI in clinical diagnosis

The physical principles underlying the nuclear magnetic resonance phenomenon including the magnetic properties of nuclei, Larmor precession, resonance behaviour and relaxation process

Basic MRI hardware components

The theory of image formation, including slice selection and spatial encoding, basic imaging sequences, spin preparation variations and fast imaging enhancements

Practical considerations for acquiring or interpreting MR images, including image contrast, signal-to-noise ratio, spatial resolution, the impact of flow, image artifacts and cautions and contraindications

MR angiography, cardiac imaging, MR spectroscopy and functional imaging

Read:

Chapter 1

Chapter 2

Chapter 3

Chapter 4

Chapter 5

Chapter 6

Chapter 1

An Introduction to Magnetic Resonance Imaging

The understanding that many nuclei possess an angular momentum and a magnetic moment - that they behave like small, charged, spinning spheres - was first observed in 1924, when Pauli demonstrated the existence of hyperfine splitting in atomic spectra. He suggested the behavior was the result of coupling between nuclear magnetic moments and those of the electrons. However, it was not until Bloch and Purcell independently measured nuclear magnetic resonance (NMR) absorption in bulk materials, work for which they jointly received the Nobel Prize for Physics in 1952, that the existence of nuclear spin was more clearly defined.

The full potential of this measurement went largely unnoticed until several years later when it was demonstrated that the precise frequency at which magnetic resonance occurs is a function of the specific chemical environment in which the nuclei reside. This behavior, called chemical shift, makes it possible to use nuclear magnetic resonance measurements as a nondestructive probe of chemical structure.

Through the 1950's and 60's, NMR was primarily an analytical tool for chemists and physicists probing chemical structure, configuration, and reaction processes. The first human applications were proposed in 1967 by Jasper Johns who had measured NMR signals from live animals. However, it was Lauterbur, some six years later in 1973, who modified a spectrometer to provide spatially encoded signals, through linear variation in the magnetic field. Using this approach, he produced the first images of an inhomogeneous object – two tubes of water – providing the first demonstration of magnetic resonance imaging (MRI).

FIGURE 1.
A Philips Achieva 3.0T TX
MRI system anno 2010.



From that crude beginning, the development of clinical MRI has been rapid. The first live human images were reported by Sir Peter Mansfield in 1976, hand and thorax images were described in 1977, and the head and abdomen in 1978. After creation of the first superconducting, whole body imager it was quickly recognized that an MR system could produce images with soft tissue contrast superior to that obtained by other imaging techniques. By 1983, continuous improvement in MR hardware and software had resulted in whole body imaging systems that were capable of producing high contrast images with spatial resolution of under 1 mm, in total imaging times of only a few minutes.

INFORMATION CONTENT AND CLINICAL EFFICACY

Medical images can be produced by the interaction of biological tissue with a number of different types of electromagnetic radiation. Biological tissue is generally opaque to intermediate wavelength radiation, such as the ultravissaging Frameworkkolet, infrared, or microwave bands (frequencies above 150 MHz and energy below 20 keV). However, the body is relatively transparent to short wavelength radiation (e.g. X-rays) which interact with atomic electrons, and to long wavelength, low frequency radio waves which interact with atomic nuclei.

Radiographic techniques (conventional X-ray, or X-ray computerized tomography) produce a shadow image resulting from the attenuation of X-ray photons by the body. Contrast differences are based on variations in tissue density, which are often very small. Overlapping structures are indistinguishable unless an alternate imaging angle is available. Furthermore, the use of ionizing radiation may entail unacceptably large doses when the need for serial monitoring is indicated.

Images can also be produced using ultrasound, where the signal brightness is the result of the relative amount of backscattered radio frequency signal. Ultrasound techniques avoid the use of ionizing radiation, bur offer relatively poor spatial resolution. Further, ultrasound is limited by the availability of a clear acoustic window between the external surface and the region of interest. This is especially restrictive in thoracic imaging where bone and lung tissue overlap.

Magnetic resonance images, however, are noninvasive, do not employ ionizing radiation, and rely on a different principle for image production. An MR image represents the relative response of specific nuclei to absorbed radio frequency energy. Like radiography or ultrasound, this image is a function of density - in this case, the distribution of the nuclei being observed. However, image contrast is influenced by other physical factors, including differences in the ability to re-emit the absorbed radio frequency signal (relaxation), and flow phenomena.

This dependence on multiple parameters means the information content of an MR image is very different from an X-ray or ultrasound image. Most MR images are designed to observe the hydrogen nucleus (proton NMR) because of its relative abundance in the body. Thus, an MR image is usually a tomographic map of the distribution of protons in the imaged sample. Further, the relative appearance of normal versus pathologic tissue can be modified by altering specific elements of the acquisition protocol to emphasize different physiochemical characteristics of specific protons, assuring exceptional tissue contrast across a wide range of tissue types. The imaging sequences can even be modified to visualize blood flow and to compensate for the blurring effects of cardiac or respiratory motion.

MR also offers the unique ability to acquire images in virtually any orientation, without repositioning the patient. This translates into greater convenience for medical staff and minimized patient discomfort. Plus, magnetic resonance provides chemical information not measurable with conventional radiography or ultrasonography. It is the combination of versatility, sensitivity and specificity as a diagnostic modality that has accelerated the acceptance of MRI.

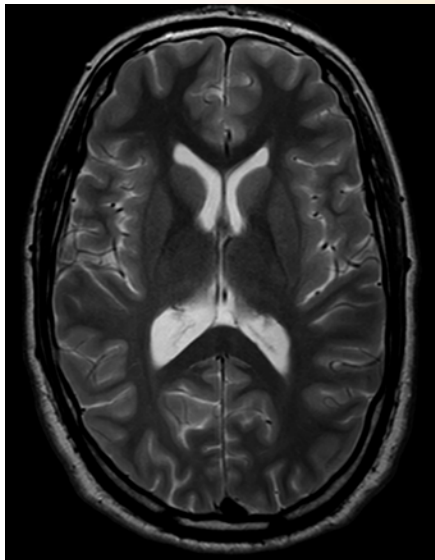


FIGURE 2
Typical MR images.

Chapter 2

Physical Principles of Magnetic Resonance

MAGNETIC PROPERTIES OF NUCLEI

The core of all atoms is the nucleus – a collection of positively charged and neutral particles that account for the bulk of the atomic mass. As theorized by Pauli, certain nuclei possess an inherent angular momentum, or spin. In fact, all nuclei that possess either an uneven atomic mass or uneven atomic number possess angular momentum, and have a characteristic spin quantum number, I , greater than zero. The spin characteristic of the nucleus, a charged particle, induces a magnetic field with an axis coincident with the axis of spin, and with a magnitude and direction represented by the magnetic moment (μ). (See Figure 3).

Normally, the magnetic moments in a collection of nuclei will be randomly oriented, as specified by the principles of Brownian motion. When a static magnetic field is applied, these magnetic dipoles tend to assume discrete orientations, either with (parallel) or against (antiparallel) the direction of the applied field. These orientations correspond to quantum mechanical energy states, the actual number of energy levels being determined by the spin quantum number, I . Figure 4 describes the quantization of nuclear spins in an applied field for nuclei with $I = 1/2$ (e.g. ^1H , ^{13}C , ^{31}P) and for $I=3/2$ (e.g. ^{23}Na , ^{39}K). Note that the spin quantum number assumes values $\pm n/2$, where $n=0, 1, 2, \dots$. The case of $n=0$ corresponds to nuclei with no magnetic moment. These nuclei are not NMR active - e.g. the major isotope of carbon (^{12}C).

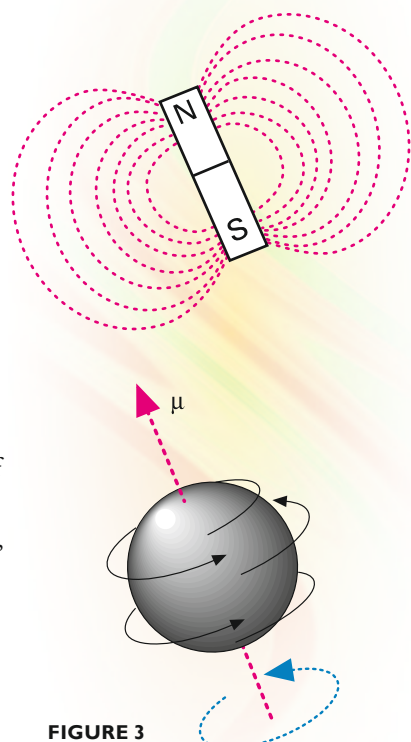


FIGURE 3

Rapidly spinning nuclei possessing a magnetic moment can be thought of as behaving like tiny bar magnets.

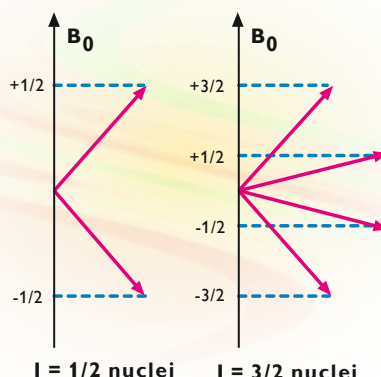


FIGURE 4

Quantized spin diagram for nuclei with spin $= 1/2$ and nuclei with spin $= 3/2$.

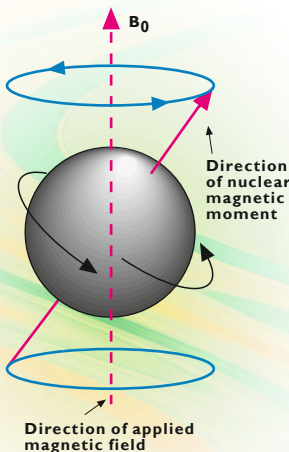


FIGURE 5

Precession of a spinning nucleus about the axis of an applied magnetic field.

In Figure 5, notice that the alignment of the magnetic moment with the applied field (B_0) is not perfect. In the presence of an applied magnetic field, the spin vectors of the nuclei experience a torque, called coupling, which causes them to rotate around the axis of the applied field with a precise frequency. This cone-shaped rotation, analogous to the rotation of a top in the presence of the earth's gravitational field, is called Larmor precession. The rate of precession is dependent upon the specific physical characteristics of the isotope involved and the strength of the applied magnetic field. This relationship is expressed as:

$$\omega = \gamma B_0$$

where ω is the Larmor (angular) frequency in MHz (1 megahertz = 10^6 cycles per second), γ is a constant of proportionality (gyromagnetic ratio) which is specific to the nucleus involved, and B_0 is the magnetic field strength measured in tesla (T, is the SI unit. 1 T = 10^4 gauss in cgs units). Larmor precession is a resonance phenomenon. If a system has a natural resonance, or frequency of oscillation, energy can be most efficiently transferred to the system at this frequency.

THE VECTOR DESCRIPTION OF MAGNETIC RESONANCE AND NET MAGNETIZATION

Since the ^1H nucleus (proton) is the type that is mainly used in MR imaging, we will limit ourselves to discussion of proton phenomena in the rest of this book. Up to now, we have discussed physical properties of individual nuclei. However, the body is composed of vast numbers of nuclei. Starting with an ensemble of spins, it is possible to define a net macroscopic magnetic moment which is a simple vector sum of the individual magnetic moments. As shown in Figure 6b, in the absence of an applied external magnetic field, the individual precessing magnetic moments are randomly oriented due to the motions produced by thermal energy, thus the macroscopic magnetic moment (M) is zero.

When an external magnetic field is applied to a collection of protons, the spins tend to align with the magnetic field, assuming one of the discrete orientations defined by their spin quantum number. Since the energy difference between these orientations is small relative to the thermal energy at room temperature, it can be shown that the probability of occupying either orientation is nearly identical. However, there is a slight excess favouring the low energy (i.e. parallel) orientation. This small imbalance creates a net magnetization oriented parallel to the applied field and with no measurable transverse component because the individual precessing nuclei are still randomly oriented with respect to the phase of their precessional motion.

The population of the available energy levels occurs as a dynamic balance, with continual transitions between the levels. The relative preference for the low energy state, and thus the strength of the net magnetization M , is a function of both temperature and the strength of the applied magnetic field, as shown in Figure 6. At a sample temperature of absolute zero, all spins would be aligned with the field and a large net magnetization produced. In the presence of a 0.1 tesla field at approximately room temperature (300 K), the alignment imbalance would be only about 1 part per million, or about a millionth of what it was at absolute zero. Since the energy difference between the two levels is directly proportional to field strength, increasing the applied field strength to 0.5 tesla results in a proportionally larger alignment imbalance and net magnetization. Note that in all of the room temperature cases, the actual difference was still quite small which explains why NMR signals are very weak.

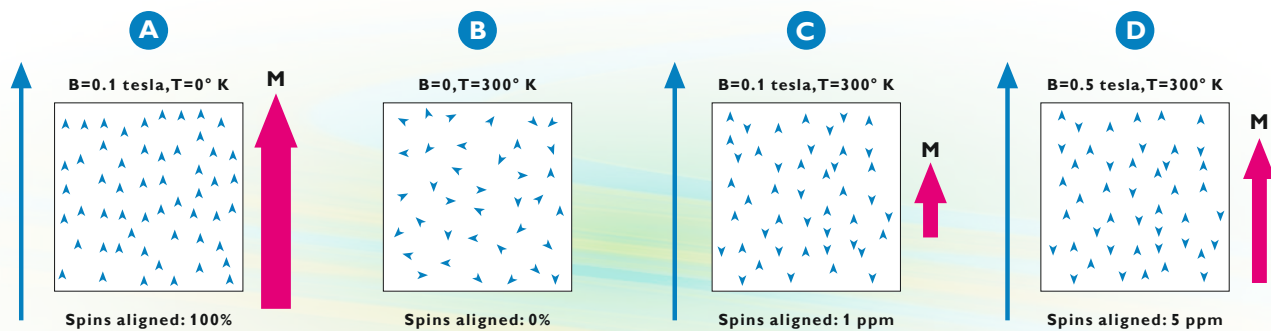


FIGURE 6 Representation of the influence of temperature and strength of the applied magnetic field on the net magnetization.

LARMOR PRECESSION AND RESONANCE PHENOMENA

The net magnetization vector in its equilibrium state is static and does not induce a current in a receiver coil, as defined by Faraday's law of induction. In order to obtain information from the spins, they must be perturbed or excited. This can be achieved by irradiating the spin system with an RF pulse – a short burst of radio frequency – matching the Larmor frequency of the nuclei of interest. This creates a time-dependent deflection of the net magnetization away from its equilibrium orientation. After this RF pulse, the net magnetization is precessing about the main magnetic field with the Larmor frequency or resonance frequency.

The use of a rotating frame of reference will simplify visualization of these complex motions. This coordinate system rotates around B_0 with the Larmor frequency. This has the effect of “freezing” the precession of the magnetization, analogous to observing the precession while being on the same “merry-go-round” that the precession is rotating on. In this rotating frame, the RF excitation pulse can be represented by an additional magnetic field, B_1 , which is perpendicular to B_0 and is switched on for a short period of time. The effect of applying the B_1 field is that the magnetization precesses about this second field, and hence rotates away from the vertical direction, toward the M_{xy} plane. This is represented in Figure 7. The angle of rotation about B_1 is a function of the amplitude and duration of the applied RF pulse, as described by the following equation:

$$\Theta = \gamma B_1 t$$

where Θ is the angle of rotation, B_1 is the amplitude of the RF pulse, γ is the gyromagnetic ratio and t is the duration of the RF pulse. The angle of rotation, Θ , is commonly referred to as the RF flip angle or RF pulse angle.

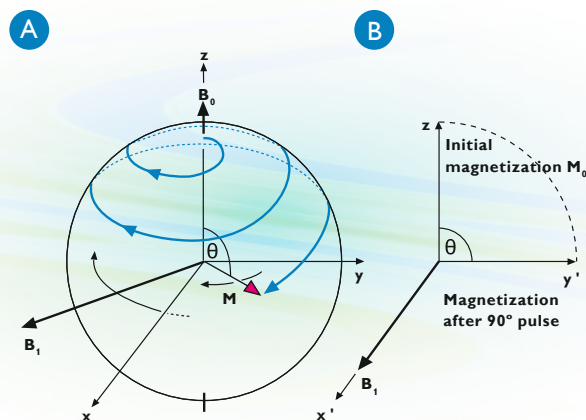


FIGURE 7

Precession of magnetization under influence of a stationary magnetic field B_0 and an oscillating field B_1 during a 90° pulse in the laboratory system (A) and in the rotating system (B).

As shown in Figure 8, the net magnetization \mathbf{M} can be thought of as having two vector components: M_{xy} in the transverse plane and M_z in the longitudinal plane. Since only the component in the xy plane can be detected, the maximum MR signal is achieved when the amplitude and duration of the RF pulse are adjusted to cause the magnetization to flip by 90° from its equilibrium state.

RELAXATION PROCESSES

After excitation, the nuclei return to equilibrium, losing energy by emitting electromagnetic radiation and by transferring energy to the lattice or between themselves. This process is called relaxation and commences at the termination of the RF pulse. During the relaxation process, both the longitudinal (M_z) and transverse (M_{xy}) components of the net magnetization return to their equilibrium values. That means the coherent precession of the spins reverts to random precession (i.e. M_{xy} disappears) and the net magnetization is restored to its original magnitude. In equilibrium, M_z is equal to M_0 which is proportional to spin density. The relaxation processes influencing the transverse and longitudinal magnetization components are independent. In fact, the transverse magnetization can disappear long before the longitudinal magnetization is restored. While both relaxation processes occur exponentially, the relative rates of relaxation are a function of the specific molecular structure, its physical state (i.e. liquid or solid), and temperature.

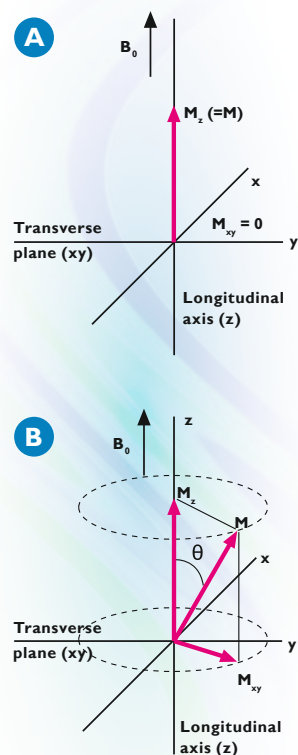


FIGURE 8

The precessing net magnetization \mathbf{M} can be viewed as having two vector components: M_z in the longitudinal direction and M_{xy} rotating in the transverse plane. (A) In equilibrium the magnetization \mathbf{M} aligns with \mathbf{B}_0 and there is no transverse component. (B) Application of the \mathbf{B}_1 field increases the magnitude of M_{xy} , the detectable component of the magnetization.

LONGITUDINAL (SPIN-LATTICE) RELAXATION

The molecular lattice in which the nuclei reside provides ample opportunity for energy exchanges between excited nuclei and the lattice. When nuclei interact, energy is transferred from the excited nuclei in discrete quanta and not in a gradual manner. Consequently, the net magnetization vector returns to its original magnitude in exponential fashion, reflecting the statistical probability of molecular collisions within the lattice. Termed spin-lattice relaxation, this process is characterized by a value T_1 , the spin-lattice relaxation time. T_1 is a time-constant which describes the time required for magnetization to return to 63% of its original value, as shown in Figure 9. Typical T_1 values in biological tissue range from about 50 milliseconds to a few seconds. Table 1 gives some examples.

FIGURE 9

The longitudinal and transverse magnetization during relaxation. T_1 is the time required for the longitudinal magnetization to return to 63% of its original value. T_2 is the time required for the transverse magnetization to fall by 63% of its original value. T_1 and T_2 are independent. T_2 is always shorter than T_1 .

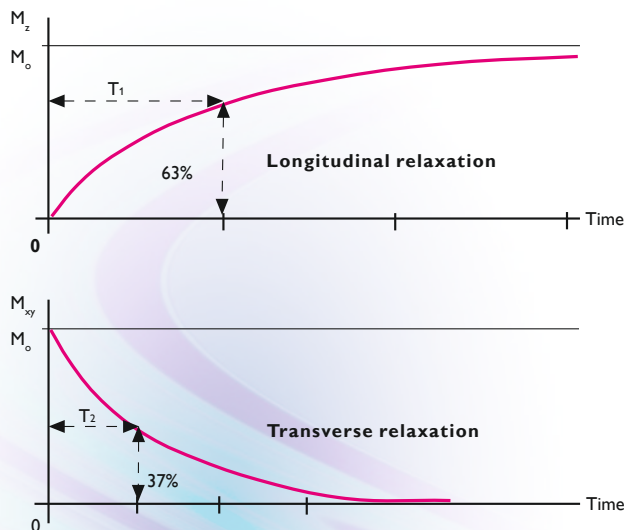
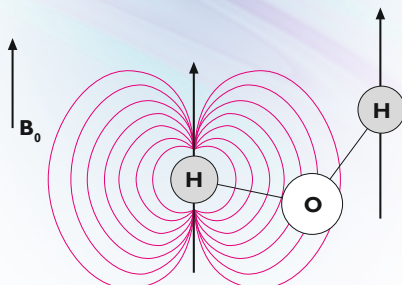


FIGURE 10

In a simple water molecule, the magnetic dipole field in one proton creates a lattice field, which influences relaxation behavior in adjacent proton nuclei. The interaction of an excited nucleus with adjacent lattice fields provides the mechanism for longitudinal relaxation.



The transfer of energy during longitudinal relaxation results from the interaction of an excited nucleus with the oscillating lattice fields created by surrounding magnetic nuclei. (Figure 10). For interaction to occur, the nearby lattice field must fluctuate at the Larmor frequency of the excited nucleus. Molecules which have an efficient means of energy transfer will exhibit a short T_1 relaxation time, while those without efficient transfer mechanisms have a long T_1 time. This is dependent on the size of the molecules, physical state of the lattice and the presence of macromolecules.

Efficient transfer of energy to the surrounding lattice is highly dependent on molecular motion – rotational, vibrational and translational (see Figure 11) – and hence the size of the molecules (although it is important to consider molecular structure as well, since similar atoms have similar vibrational energy levels and therefore are more likely to transfer energy). The relation between the frequency distribution of molecular motions and molecule size is depicted in Figure 12.

Motion of very large molecules generally occurs at a frequency too low for efficient energy transfer. Efficient longitudinal relaxation occurs most readily in medium-sized molecules, or via the terminal end-groups on larger macromolecules, which can rotate at higher frequencies than possible through translational motion. Figure 12 shows that medium sized molecules have higher relative abundance of motion at the Larmor frequency ω_L than large or small molecules.

Since the lattice field fluctuations result from random thermal activity the physical structure and state of the lattice play a major role in determining the efficiency of energy transfer, and accordingly, the T_1 relaxation time.

T_1 values are generally shorter in solutions than in solids. This reflects the fact that the vibrational frequencies present in a solid lattice (e.g. 10^{12} - 10^{13} Hz) are typically far higher than normal Larmor precession frequencies. For example, protons in ice can display T_1 values of hours at low temperatures. However, in pure liquids, small molecules move too fast, i.e. their translational motion is too rapid to permit efficient energy transfer. Thus, pure liquids also display relatively long T_1 values.

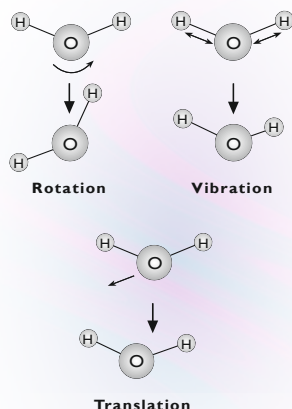


FIGURE II

Diagram showing three types of molecular motion - rotation, vibration,

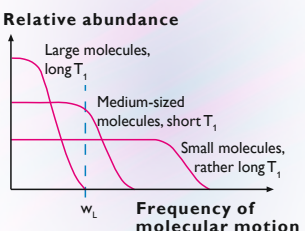


FIGURE 12 For molecules of different sizes the different distribution of molecular motion frequencies with respect to the Larmor frequency ω_L results in different relaxation times T_1 .

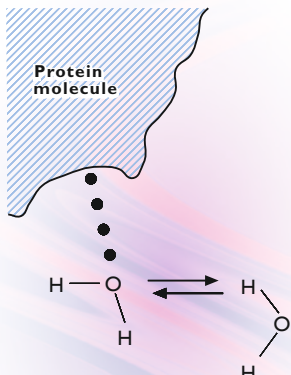


FIGURE 13

Bound and unbound water in the presence of macromolecules.

Finally, T_1 relaxation is affected by the presence of macromolecules, such as proteins, which possess available hydrophilic bonding sites. Water protons in tissue samples appear to relax much faster than water protons in pure water - on the order of milliseconds compared to 2-3 seconds. This results from the normal formation of hydration layers surrounding proteins and large macromolecules in solution. (See Figure 13). Hydration layers include both water which is hydrogen bonded to fixed sites on the macromolecule and water which is structured (its motion restricted but which is not actually bound). The formation of hydration layers slows the molecular motion of water, making it more effective at energy transfer, hence the shortened relaxation time. Because water molecules in a tissue sample are continually being exchanged at an equilibrium rate, the T_1 value measured is an average value for all the bound water at different sites on the molecule. Nevertheless, it has been demonstrated that this equilibrium may be perturbed by pathologies such as myocardial infarction, resulting in a change in the T_1 value. This altered T_1 value may be a sensitive indicator of tissue damage and/or edema in these pathologies.

TABLE 1

Some T_1 and T_2 values for human tissues. The differences in T_1 and T_2 are exploited in MR imaging to obtain contrast between different tissues.

TISSUE	T_1 at 1.5T (ms)	T_1 at 0.5T (ms)	T_2 (ms)
Skeletal muscle	870	600	47
Liver	490	323	43
Kidney	650	449	58
Spleen	780	554	62
Fat	260	215	84
Gray matter	920	656	101
White matter	790	539	92
Cerebrospinal fluid	>4000	>4000	>2000
Lung	830	600	79

TRANSVERSE (SPIN-SPIN) RELAXATION

In spin-lattice relaxation, energy was transferred from excited nuclei to the surroundings – the lattice structure. In transverse relaxation, energy is transferred between nuclei in different energy states – as one nucleus absorbs energy a neighboring nucleus releases energy. This process is referred to as spin-spin interaction and is measured by the T_2 , spin-spin (transverse) relaxation time.

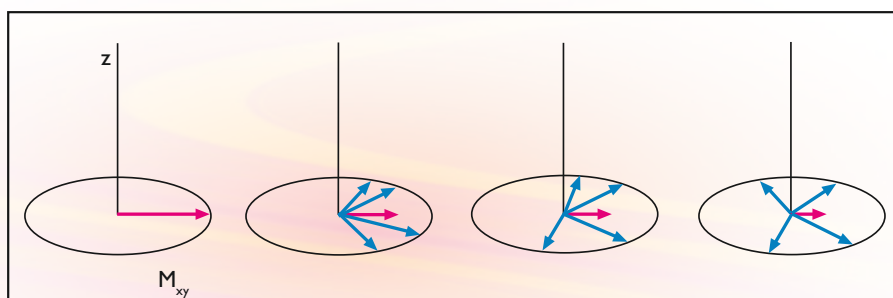
Immediately after excitation, the spins precess coherently (i.e. in phase), creating a transverse component of the magnetization. However, interactions between individual spins create random local magnetic field variations which, in turn, cause fluctuations in the precessional frequency of the individual nuclei. As a result, a gradual and random dephasing of the spins occurs causing a decay in the magnitude of the transverse component of the net magnetization. See Figure 9.

As illustrated in Figure 14, as the spins begin to dephase, some of the spins gain a few degrees on the net magnetization, while others fall a few degrees behind. This non-reversible dephasing process continues until the nuclei are precessing at random and complete decay of the transverse magnetization has occurred.

Physical state and molecular size also affect the transverse (T_2) relaxation rate. Solids and large molecules experience relatively rapid T_2 relaxation, since the fixed molecular structure is effective in maintaining the magnetic fields which are the basis for spin-spin interaction. Small molecules, such as free water, have relatively long T_2 relaxation times, since rapid translational motion tends to average the local magnetic field variations caused by interaction of precessing nuclei and thus reduce the efficiency of T_2 relaxation phenomena.

FIGURE 14

T_2 relaxation process: As the individual spins (dashed) begin to precess “out-of phase”, the magnitude of their sum M_{xy} – the transverse component of magnetization (red) – is reduced.



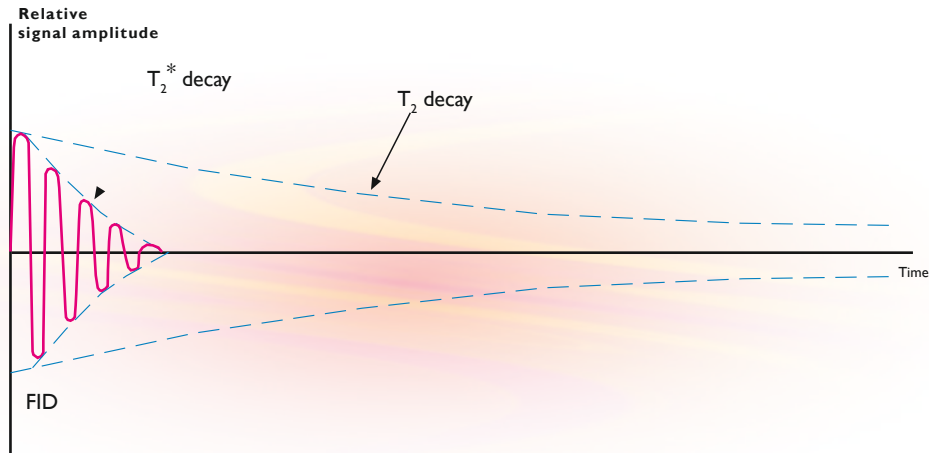
The presence of macromolecules in solution also shortens the T_2 relaxation times, although the relaxation mechanism is different from the T_1 process. In this case, the presence of the large molecules increases the efficiency of spin-spin interactions by reducing overall molecular motion, hence spin dephasing is faster and T_2 relaxation times shorter.

The same factors which affect T_1 relaxation rates also influence T_2 relaxation. However, T_2 values are independent of magnetic field strength and transverse relaxation is extremely efficient in solids where the fixed molecular structure maintains local field variations permitting rapid loss of phase coherence. Typical T_2 relaxation times in biological tissues range from a few microseconds in solids to a few seconds in liquids.

If the only contribution to the dephasing process were spin-spin interactions, the T_2 relaxation time could be readily determined. However, spin coherence is also affected by inhomogeneities in the applied magnetic field. The exponential decay in signal resulting from the combination of T_2 relaxation and field inhomogeneities is referred to as T_2^* —the effective transverse relaxation time. (See Figure 15).

FIGURE 15

Due to magnetic field inhomogeneities the decrease of M_{xy} , which is proportional to the relative signal amplitude, is considerably accelerated, i.e. T_2^* is smaller than T_2 .



MAGNETIZATION TRANSFER

In biological tissues, only spins in the free water pool contribute to the measurable MR signal, whereas spins in bound water do not. Recently, another mechanism for contrast involving free and bound water has been identified. Different tissues have different amounts of free water and bound water. Using a procedure called Magnetization Transfer Contrast (MTC), an RF prepulse is used to saturate the bound water pool, while keeping the free water pool intact. This may be a narrow bandwidth, high intensity off-resonance prepulse, see Figure 16, or a binomial on-resonance prepulse. Due to cross-relaxation between the free water pool and the bound water pool, a new equilibrium is created, where the tissue of interest has less available longitudinal magnetization, and also a shorter T_1 (spin-lattice relaxation time constant). The MTC mechanism is a potential source of contrast, because it makes tissues which are sensitive to the effect (e.g. muscle, cartilage, brain matter, tendons/menisci/ligaments) darker in MR images. Tissues such as fat, blood and CSF are hardly affected by MTC.

THE FREE INDUCTION DECAY, SIGNAL DETECTION AND FOURIER TRANSFORMATION

To this point, we have discussed alignment of a spin system using an external magnetic field and excitation of the system by application of a second (RF) field, causing a measurable signal in the transverse plane. This measurable signal, an induced current, is a quantity which varies with time and which conveys information about our spin system. Signals can be described by their temporal behavior or represented by their frequency components, including their amplitude and phase.

Figure 17 displays two simple time-domain signals and their related frequency spectra. The signal in (A) is a single frequency sine wave. Its spectrum is a single line at a point on the frequency spectrum. The height of the line defines the signal amplitude. The signal in (B) is a dual frequency sine wave where each of the individual components has identical amplitude.

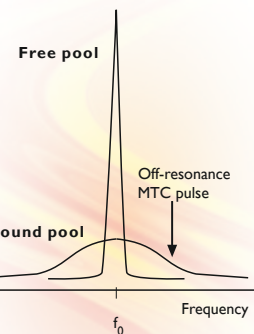
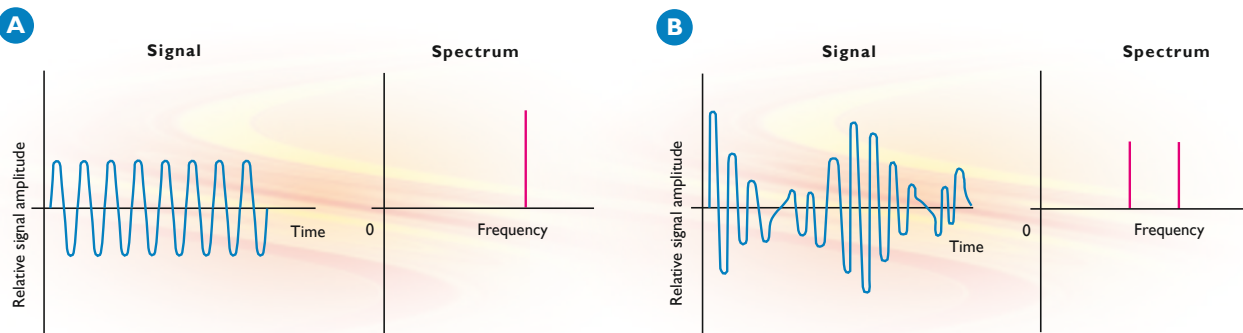


FIGURE 16

The spectral lines of the free pool and the bound pool are both centered at the same Larmor frequency f_0 . The free pool has a narrow line (relatively long T_2), the bound pool has a broad line ($T_2 < 0.1$ ms). Off-resonance MTC pulses employ the differences in line width to selectively destroy the bound pool.

FIGURE 17

Relationship between time-based signal and frequency.

(A) Single frequency.

(B) Two frequencies.

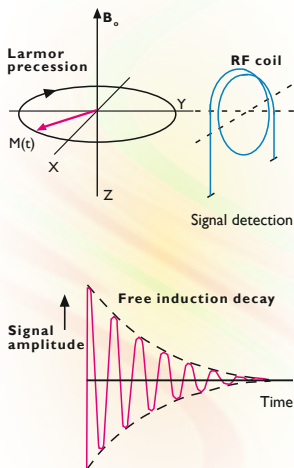


FIGURE 18

Measurement of a time-based signal and a typical free induction decay signal.

In general, for each time-dependent signal, the associated frequencies (spectrum) can be mathematically generated by Fourier transformation, and vice-versa.

In an MR measurement, the application of a 90° pulse causes the net magnetization vector to rotate to the xy plane, inducing a signal in an RF detection coil after the excitation pulse is terminated. This signal, which is a result of the free precession of the net magnetization in the transverse plane, is called the free induction decay (FID) signal, since it gradually decays due to the relaxation mechanisms. (See Figure 18).

The free induction decay signal in magnetic resonance has the following characteristics:

- it oscillates at the Larmor frequency of the excited nuclei
- it has an initial magnitude which is proportional to the density of observed nuclei in the sample being measured
- it decreases in amplitude exponentially with a time constant T_2^* , due to spin-spin relaxation and magnetic field inhomogeneities
- Subsequent Fourier transformation of the FID yields the frequency-based NMR spectrum on which MR images are based.

In our description of free induction decay signals, we assumed that the RF pulse and FID detection occur in one continuous, uninterrupted sequence. In fact, it is sometimes advantageous to not sample the FID directly, but rather to observe the signal as an “echo” – a reappearance of the signal a finite time after disappearance of the initial FID. Two approaches are routinely employed for creating an echo signal in magnetic resonance measurements: Spin echo and gradient echo. Spin echo is explained below, while gradient echo is first explained in Chapter 4.

SPIN ECHO DEVELOPMENT: RATIONALE AND METHODOLOGY

The two dephasing processes which excited nuclei experience (spin-spin interactions and field inhomogeneities) are fundamentally different. The spin-spin interaction which occurs between adjacent nuclei is a random, time-variant and irreversible process.

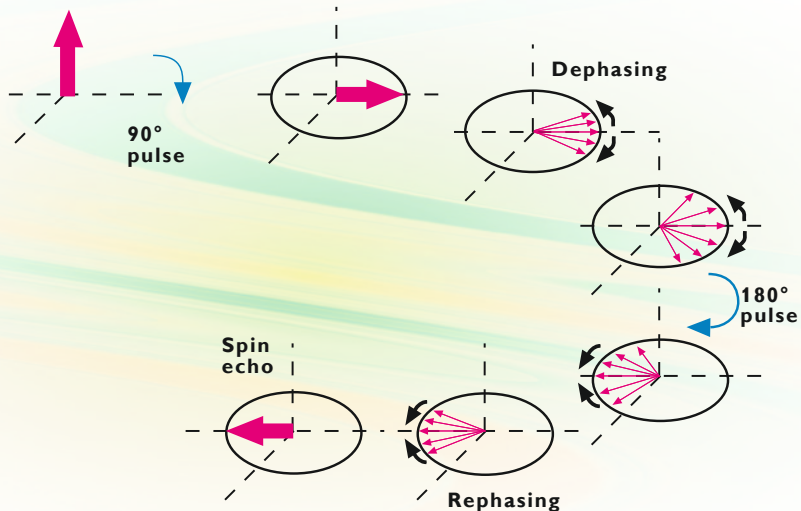
Magnetic field inhomogeneities, however, exert a constant static influence on the spin system and therefore, in theory, can be accounted for during the procedure. Measuring spin echo signal, instead of the FID, permits more complete evolution of spin-spin interactions while offering a vehicle for correcting the influence of static field inhomogeneities.

Consider runners on a circular track on a windy day. Before the start of the race, all the runners are together— they can be thought of as being “in phase”. After the start of the race, their different abilities and the gusting of the wind will cause the runners to spread out around the track, with the faster runners in the lead and the slower runners falling behind. If the runners are then instructed to turn around and reverse direction, the situation is reversed. Suddenly, the slow runners are in the lead. If the runners maintain their original steady speed, they will once again begin to come together as they approach the starting line, since the slower runners now have a shorter distance to run. When they cross the original starting line, they will be separated only by a distance caused by the random influence of the wind.

In a similar manner, the static effects of field inhomogeneity can be reversed by applying a 180° refocusing pulse at some time after the initial 90° pulse. The 90° excitation pulse flips the spins into the transverse (xy) plane where T_2 effects cause dephasing of the individual magnetic moments. At time $TE/2$ (TE = echo time), the time between the beginning of the 90° pulse and the maximum amplitude of the first echo signal), a 180° pulse is applied (the instruction to turn around), flipping the individual spins about the x-axis in mirror-like fashion. After an additional time $TE/2$, the spins once again begin to come back into phase (approach the starting line), rebuilding the FID and resulting in an echo. This sequence of events is summarized in Figure 19.

FIGURE 19

The effect of the 180° refocusing pulse on the spin system during spin echo generation.



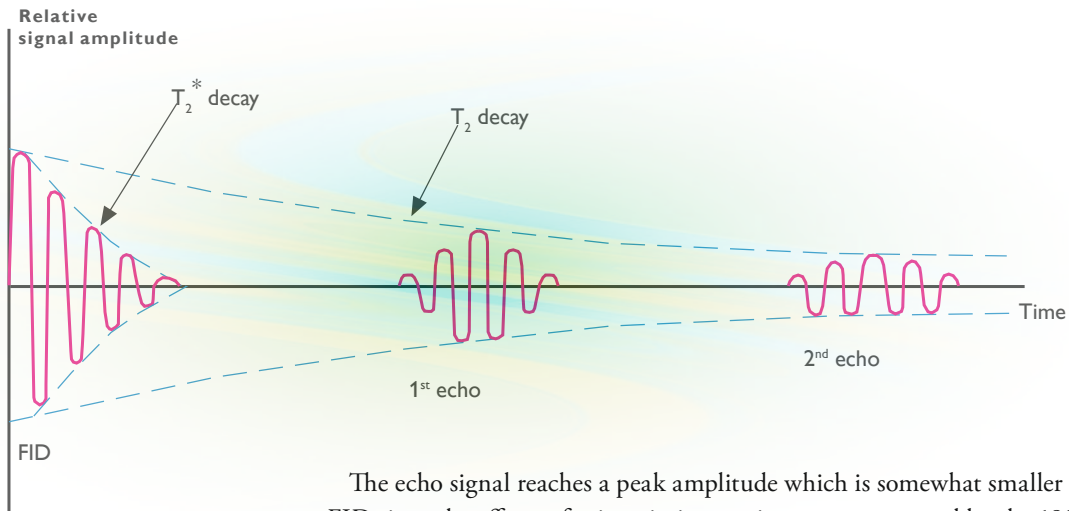


FIGURE 20

Successive echoes in a spin echo sequence, decay in maximum amplitude of the echo occurs at a rate characterized by T_2 .

The echo signal reaches a peak amplitude which is somewhat smaller than the original FID since the effects of spin-spin interaction are not reversed by the 180° pulse. If subsequent 180° pulses are applied, each separated by a time TE, each ensuing echo will continue to decline in amplitude due to this same effect. As shown in Figure 20, this successive decay of the echo signal occurs at a rate characterized by the true T_2 value.

NMR OF NUCLEI OTHER THAN PROTONS

While we have focused on “proton NMR,” any isotope that has nuclear spin and occurs in the body, or which could be introduced into the body, can be used for imaging. In practice, the usefulness of a particular isotope is dependent upon several factors, including:

- natural abundance in the body
- sensitivity.

Table 2 lists the common isotopes found in biological tissues in order of their natural abundance. While carbon and oxygen occur abundantly in the body, their isotopes with spin (^{13}C and ^{17}O) are scarce, while the abundant isotopes (^{12}C and ^{16}O) have no spin. Natural abundance is a critical factor in determining the suitability of isotopes for MR measurement. Likewise, the relative sensitivity of a given isotope affects its suitability for NMR measurements. Sensitivity is usually presented relative to ^1H sensitivity, since the bare proton is the most sensitive nucleus in NMR. While fluorine (^{19}F) is relatively sensitive, its natural abundance is very low. It could be useful in MRI when administered via labelled drugs to study certain effects. These factors, along with the gyromagnetic ratio of the nucleus, and experimental considerations such as the T_1 and T_2 values, have made ^1H the predominant nucleus used in MRI measurements. While other nuclei continue to be researched because of their potential clinical significance, only phosphorous-31 has seen significant application to date.

ISOTOPES WITH SPIN	MOLAR CONC. (MOI/L)	RELATIVE SENSITIVITY
^1H	99.0	1.0
^{14}N	1.6	
^{31}P	0.35	0.066
^{13}C	0.1	0.016
^{23}Na	0.078	0.093
^{39}K	0.045	0.0005
^{17}O	0.031	0.029
^2H	0.015	0.096
^{19}F	0.0066	0.830

TABLE 2

Concentration in biological tissue and relative sensitivity of isotopes with spin.

Chapter 3

Magnetic Resonance Instrumentation

MR SYSTEM COMPONENTS

A magnetic resonance imaging study uses a combination of a static magnetic field, local variations of this magnetic field (magnetic field gradients) to encode spatial information on the nuclei within a tissue sample and RF pulses, applied through a radio frequency pulse generation system, to generate a signal. An RF receiver system then detects re-emitted RF energy and transports this signal to a computer system for digital processing and image display. To accomplish these goals, an MR imaging system must include the following components:

1. Magnet for generating the static magnetic field.
2. Magnetic field gradient system, consisting of gradient amplifier and gradient coils.
The gradient system is required for spatial selection and spatial encoding.
3. RF amplifier and RF transmit coil for production of measurement pulses to excite the nuclei.
4. RF receive coil and amplifier to detect the re-emitted signal from the nuclei.
(Transmit coil and receiver coil may electronically and physically be integrated)
5. Acquisition and control system for digital signal processing, image processing, and data acquisition control.
6. Physiology hardware to measure a patient's ECG and respiratory cycle, necessary for some types of examinations.
7. Reconstruction system.
8. An operation/viewing console for display of the images and for operator input of control parameters.
9. Archiving system.
10. Magnetic shielding to minimize the effect of the fringe magnetic field on the areas surrounding the MR imager.
11. RF shielding to protect the system from external RF interferences and vice versa.
12. Patient table for positioning the patient in the magnet during an exam.
13. Patient monitoring equipment to monitor the patient during the exam.

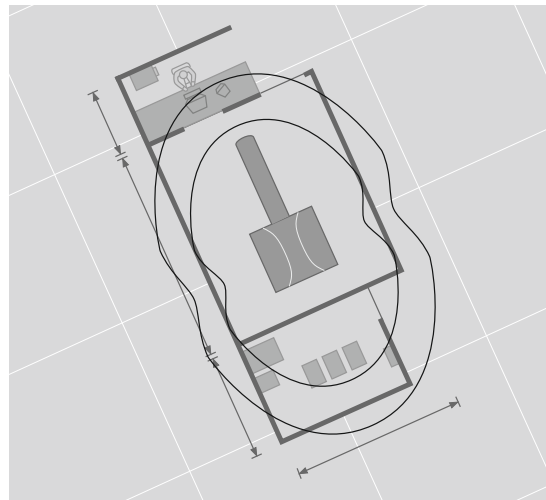


FIGURE 21

Typical site layout for an MR imaging system.

THE MAGNET SYSTEM

Commercial magnet systems are available in field strengths ranging from 0.01 to 4 tesla. For comparison: The earth's magnetic field varies between 0.2 and 0.7 gauss (1 gauss is 0.0001 tesla). Proton images have generally been acquired with fields ranging from 0.04 tesla to 4.0 tesla. As explained in chapter 2, a higher field strength results in higher net magnetization and therefore potentially higher signals, although image contrast may decrease with increasing field strength. The use of higher field strength magnets has been limited by several considerations. First, the resonance frequency and, generally, the RF absorption increases with increasing field strength. As a result, improvements in signal-to-noise ratio generated by higher field strength is offset by losses due to RF attenuation in the body. Further, the high levels of RF energy required for operation at high field strengths can, in some instances, exceed current guidelines for power deposition in the patient.

In addition to magnetic field strength, magnetic field homogeneity – the measure of field uniformity within the measurement area of the magnet – is an important parameter in the magnet system. Optimal field homogeneity is crucial to generating images free from distortion and with the maximum possible signal-to-noise ratio. Field homogeneity must be achieved over a substantial volume. In practice, it is common to specify field homogeneity of approximately 2 ppm over a 25 cm spherical volume located at the isocenter of the magnet system or approximately 5 ppm over body sizes.

Three types of magnets can be distinguished, being resistive magnets, permanent magnets and superconducting magnets. Resistive magnets consist of coil windings through which a strong electrical current is flowing, thereby creating a magnetic field. However, the combination of constant field strength and high homogeneity is difficult to obtain. Permanent magnets need no power supply to create the magnetic field, but are only used with a maximum field strength of 0.3 T. These systems are stable only if temperature is very well controlled. Besides, permanent magnets are very heavy, with the weight increasing with field strength. Initial and running cost (determined by air conditioning costs) can be relatively low.

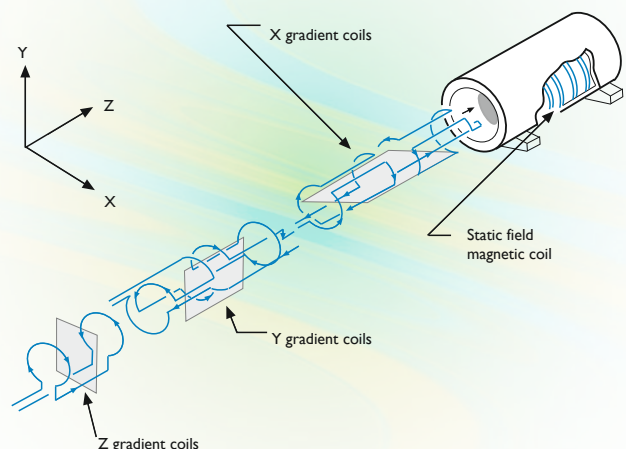
For higher magnetic field strengths, superconducting magnets are used, which have magnetic coil windings immersed in cryogenic fluids (liquid helium). Sometimes liquid nitrogen surrounds the liquid helium reservoir. Both helium and nitrogen will slowly boil off and have to be refilled regularly. At liquid helium temperature, the coil windings become superconducting, so that once an inductive current has been introduced into the magnet coils, the system can be disconnected from the external power supply, while the current is maintained and thus also the magnetic field. This design provides excellent stability and field homogeneity. After manufacture, the magnet should be “ shimmed” by placing pieces of iron into the magnet bore (passive shimming) to optimize homogeneity. New imagers also incorporate software, such as dynamic field-of-view shimming, which allows adjustment of the field homogeneity through tuning of the gradient coils with the patient in the magnet and the desired image region identified. This permits optimal setting of the homogeneity, which is useful since introducing a body in the field always causes some field distortion.

GRADIENT COIL SYSTEM

As will be explained in chapter 4, magnetic resonance imaging utilizes magnetic field gradients to create spatial differentiation of the signals emitted from the region of interest in a patient. A magnetic field gradient is a weak magnetic field, that changes linearly with position and is superimposed on the main magnetic field. The magnetic field gradients in the x, y, and z directions required for an imaging study are produced by three sets of orthogonally-positioned coils. A typical coil arrangement is depicted in Figure 22.

FIGURE 22

Typical coil arrangement in an MR imager.



Each coil set is connected to an independently controlled power supply. In addition to producing gradients oriented along the x, y, or z axes, by powering the gradient coils in combination, it is possible to generate magnetic field gradients in any orientation. The gradients generated by these coils should be linear over the imaging volume, and should be stable for the duration of the applied gradient.

A complicating factor is the occurrence of eddy currents. These eddy currents are generated by the changing gradients in conducting parts like the metal shields of the magnets. The eddy currents in turn also produce an unwanted gradient field at the place of interest, which causes problems, like artifacts in images, and additional helium consumption. The effects of eddy currents are minimized by the design of actively shielded gradient coils, where the effect of the eddy current field is counteracted by a field generated by an additional coil surrounding the original gradient coil.

The currents through the gradient coils are in the order of several hundred Amperes. Consequently, large forces act on the mechanical parts so that these start oscillating during gradient switching, thereby producing the acoustic noise characteristic of MR measurements.

RF COILS

The RF coils in a magnetic resonance imager are used for excitation of the nuclei and/or for signal detection. The coils must be able to produce a uniform field (or well-defined) throughout the region being imaged. A separate coil may be used for excitation and detection purposes, or the same coil may be used for both. In either case, coils with a high sensitivity are desired. The coils must be tuned to match the resonance frequency of the type of nucleus being observed. In older systems, the RF source and the transmitting coil must also be impedance matched to avoid energy reflection which could damage the source amplifier. When a patient is placed inside the RF coil, resistance is added to the coil circuitry. This is referred to as coil loading. At field strengths typical of MRI systems (0.5T to 1.5T), the noise introduced by the patient dominates the inherent noise produced by the RF circuitry.

For optimal signal detection, the object being imaged should fill the majority of the detection coil. Typically, a filling factor of 70% or higher is desired. Therefore a surface coil usually yields a better signal-to-noise ratio than a standard body coil. Typical signal-to-noise enhancements of a factor of 3-5 can be achieved using surface coils.

The Philips flexible surface coils (see Figure 23) allow maximum freedom for positioning and ensure best patient comfort. For instance in abdominal imaging, body coil images may be acceptable, but the signal-to-noise ratio can be improved by using a body-wrap around coil. For imaging the head or extremities, a smaller coil placed close to the region of interest is generally substituted.

The use of a quadrature RF coil (see Figure 23) gives a further improvement in the signal-to-noise ratio. A quadrature transmit coil reduces the required RF power and thus the energy dissipation within a patient. The quadrature coil is made up of an arrangement of two coils with their axes meeting at a right angle. While both coils pick up an identical signal, the induced noise voltages are almost uncorrelated. By a proper combination of the output signals, a gain up to a factor of $\sqrt{2}$ in signal-to-noise ratio may therefore be expected. This could be traded-in against shortened total imaging time and greater applications flexibility. Although the RF homogeneity of a quadrature volume coil is better than that of a wrap around coil, the filling factor of a flexible coil is often higher, especially in small field-of-view imaging, resulting sometimes in a favorable signal-to-noise ratio with a flexible surface coil.



FIGURE 23

Examples of alternate coil designs:
Left: quadrature head coil;
Below: flexible surface coil.

The synergy coil concept exploits the signal-to-noise advantages of small coils and quadrature detection, but makes it applicable to a large field of view. A synergy coil is made up of an array of quadrature coils receiving the MR signal simultaneously, therefore without increase in scan time. Each coil covers a different part of e.g. a spine and after a measurement, the images of all coil elements can be combined into one large field of view image, e.g. 45 cm. In this image, the signal-to-noise is better by about 50% in comparison to images of a flexible surface coil of the size of one coil element.

THE ACQUISITION AND CONTROL SYSTEM

The acquisition and control subsystem is located between the host computer, the reconstructor and the front-end (RF-, gradient- and physiology hardware). This subsystem performs execution of the MR method programs, acquisition and demodulation of the MR signals and transport to the array processor, acquisition and processing of physiology signals to synchronize the MR programs to the patient's physiology, automatic calibration of the front-end for the required scan (preparation phase), calibration and test facilities for the front-end. The MR spectrometer is part of the acquisition and control system.

THE RECONSTRUCTION SYSTEM

The measured data are reconstructed and displayed. In many acquisitions the data set size is a major consideration, e.g. in 3D image acquisitions or with the largest matrix sizes.

HOST COMPUTER, VIEWING, ARCHIVING, HARDCOPY

Patient administration, scan-control, sensor signal display, image viewing, image processing, archiving and hardcopying are accessible from the operator's console. All can be done in parallel. An LCD display on the front magnet cover can be used to display images and sensor signals. The reconstructed images of a scan are initially stored on the system disk of the host computer. Long-term archiving is typically done on (rewritable) optical discs.

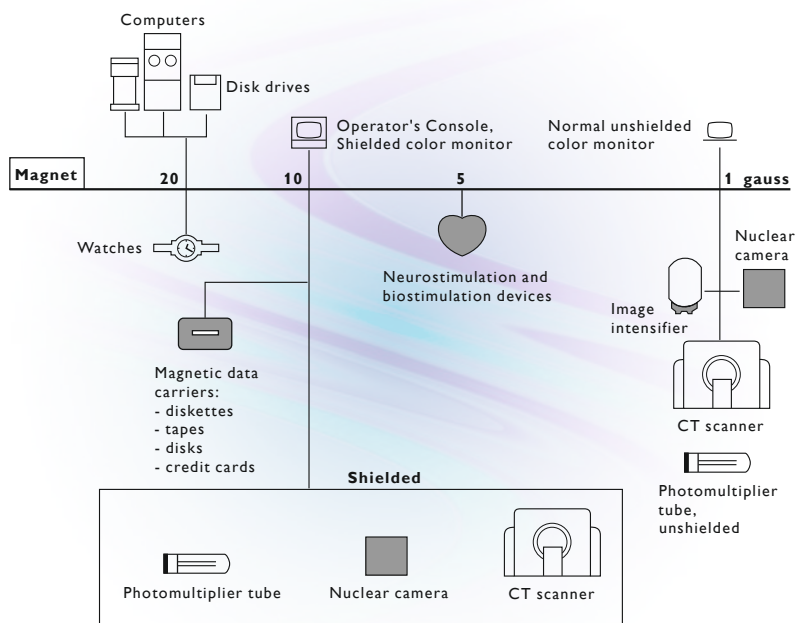
MAGNETIC SHIELDING

Magnetic shielding is required to protect the surrounding environment from the effects of fringe fields which surround a magnet. Watches, tapes, credit cards etc. may be damaged by a magnetic field. Of greater clinical concern is the effect of magnetic fields on devices such as pacemakers. To avoid unexpected safety hazards, it is necessary to isolate the magnet in an area where suspect individuals will not pass through potentially hazardous magnetic fields, and to construct magnetic shielding to limit the extent of the fringe field. The magnetic field strengths that can typically be tolerated by equipment found in a typical hospital are indicated in Figure 24. Besides, to maintain magnetic field homogeneity shielding is necessary from field distorting effects from the environment, like those caused by passing cars, trains, or elevators.

Magnets may be passively shielded by surrounding the magnet room with heavy, iron platings, but this adds additional weight. In an actively shielded magnet an inner superconducting coil set produces the main magnetic field, while an outer superconducting coil set, in which current flows in the opposite direction, contains and reduces the fringe field.

FIGURE 24

The strength of magnetic field that can typically be tolerated by equipment found in a typical hospital.



RF SHIELDING

The MRI signal is relatively weak, hence small external RF interferences can significantly degrade image quality. As a result, MR systems generally require that the imaging room be shielded from external sources of RF energy. For most systems, this involves building RF shielding into the walls, floor and ceiling of the MR site. RF shielding also prevents that RF signals generated during MR measurements disturb radio signals outside the MR room.

Chapter 4

The Theory of Image Formation

INTRODUCTION

When a patient is placed in an imaging magnet, nuclei with a magnetic moment align along and precess about the applied magnetic field. If a radio frequency pulse is then applied through a coil perpendicular to the applied magnetic field, at the proton Larmor frequency, proton nuclei are excited and brought into phase. When the applied pulse is terminated, an MR signal is detected. The problem is that all the nuclei within the area covered by the detection coil would resonate at about the same frequency and the signal would contain no information on spatial distribution.

In order to reconstruct an image, it is necessary to encode the emitted signal so that its components can be related to the spatial position of the nuclei which contribute to them. This imaging process can be divided into two fundamental operations:

- selection of an image slice (or volume);
- spatial encoding of the magnetic resonance signal emanating from that slice.

Both are achieved on the basis that the frequency at which a nucleus resonates, its Larmor frequency, is a function of the strength of the static magnetic field in which it is located. It follows that if we alter the strength of the applied magnetic field as a function of position - that is, by means of a magnetic field gradient – we alter the specific resonance frequency as a function of spatial position.

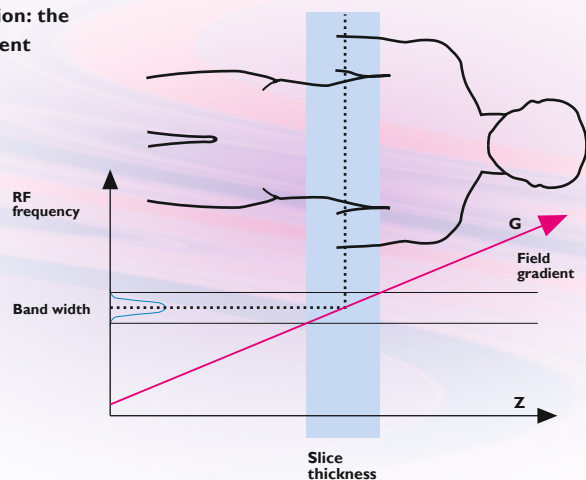
SLICE SELECTION

It is possible to superimpose a weak magnetic field, that changes linearly with position, on the main static field to create a magnetic field gradient. If this gradient is oriented from head-to-toe, then every transverse slice in the patient resonates at a different Larmor frequency. (See Figure 25).

If the patient is then exposed to a radio frequency pulse with a narrow range of frequencies (a narrow bandwidth), only those nuclei in the thin slice where the Larmor frequency matches the frequencies of the RF pulse, will actually absorb the RF energy. This process is called slice selective excitation. Since the absorption of RF energy by precessing nuclei occurs precisely at the Larmor frequency, the magnetic field gradient necessary for slice selection is relatively small. In addition, the direction of the magnetic field gradient is perpendicular to the slice orientation. By convention, the main field direction is always aligned along the z-axis, but the gradient may be created along the x-, y-, or z-axis, or along any oblique angle.

FIGURE 25

Slice selective excitation: the steepness of the gradient and the RF bandwidth determine the slice thickness.



Slice thickness is controlled by two factors: the amplitude of the magnetic field gradient, and the bandwidth of the radio frequency pulse (i.e. the range of frequencies included in the pulse). The RF pulse shape also relates to slice thickness and shape. Figure 26 shows that a sharp rectangular slice profile requires a slice selection pulse shaped like a decaying sine wave - a sinc function, since slice profile and pulse shape are each others Fourier transform. Accordingly, a sinc waveform with sufficiently narrow bandwidth can be used to describe a thin slice with steep, well-formed edges. Use of a precisely defined slice minimizes slice interference or “crosstalk.” (See Figure 27).

FIGURE 26
The sinc wave function becomes a sharp rectangular frequency function after Fourier transformation, and vice versa.

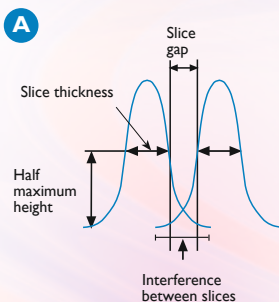


FIGURE 27
Definition of slice thickness, slice gap and slice interference for two cases. Contiguous slices are defined as consecutive image slices which touch at half maximum height.

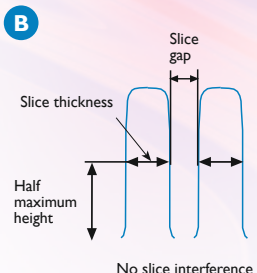
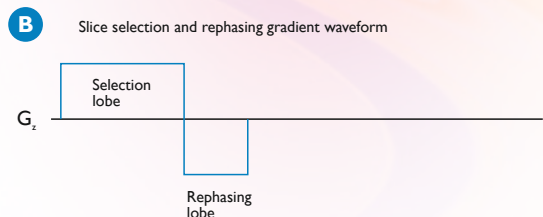
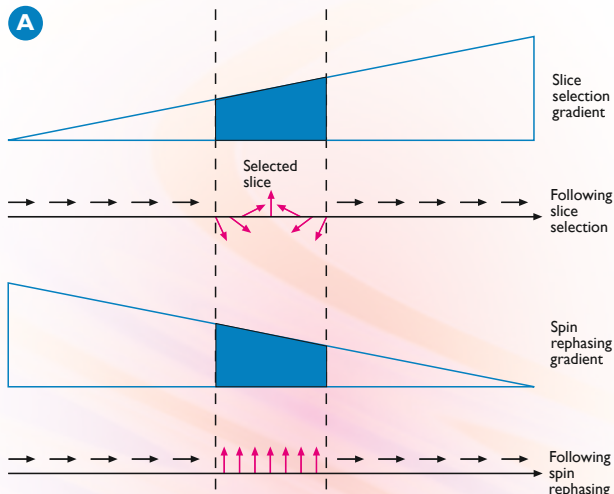


FIGURE 28

(A) Phase distribution of spins following slice selection and gradient rephasing.

(B) The slice selection and spin rephasing gradient waveform forms.

Under the influence of the magnetic field gradient, spins across the thickness of the selected slice will precess with slightly varying frequencies, since via $\omega = \gamma B$, these are a function of the local field strength. As a result, the selected spins will dephase – spread out like steps on a spiral staircase (See Figure 28). The position of a slice can be changed by off-centering the gradient or by changing the RF pulse frequency. However, to achieve the maximum signal intensity, it is necessary for all the spins in the selected slice to be brought back into phase. This is accomplished through the use of a spin rephasing gradient which is simply a field gradient of opposite polarity from the initial slice selection gradient. The spin rephasing gradient “unwinds” the spiral, creating phase coherence among the nuclei in the selected slice.



SPATIAL ENCODING AND IMAGE RECONSTRUCTION

The slice selection gradient and RF pulse define a slice. Now, we must define how the slice is spatially resolved to generate an image.

USING A READ-OUT GRADIENT

If a second magnetic field gradient, G_x , is applied orthogonally to the slice selection gradient while receiving the signal, the frequency of the emitted signal can be related to its position along the G_x gradient axis. Only nuclei in the centre line will continue to precess at the original frequency. The Fourier transform of the detected signal is a projection onto the x-axis. The amplitude of each frequency component – the intensity at each position along the x-axis – is proportional to the summed signal in the y-direction for that x-position. See Figure 29. The G_x gradient is termed the “read-out gradient” or measurement gradient or frequency encoding gradient. By repeated rotation and application of the read-out gradient, spatial information in more than one direction can be obtained, from which an image of the plane can be constructed using a technique known as projection reconstruction. It is the technique used by Lauterbur for his original imaging experiments and it is similar to the methodology used to construct computed tomography (CT) images. However, it is sensitive to magnetic field inhomogeneities and has rarely been employed in the last few years, although interest in the technique has been revived with recent hardware advances.

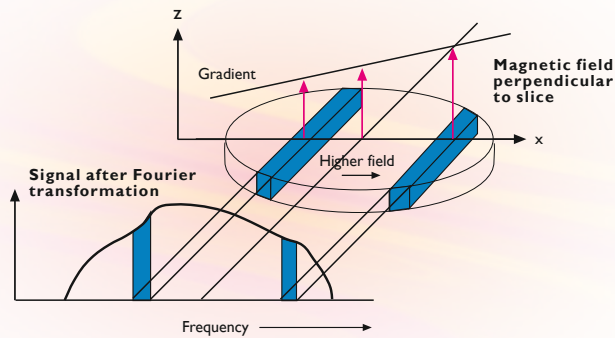


FIGURE 29

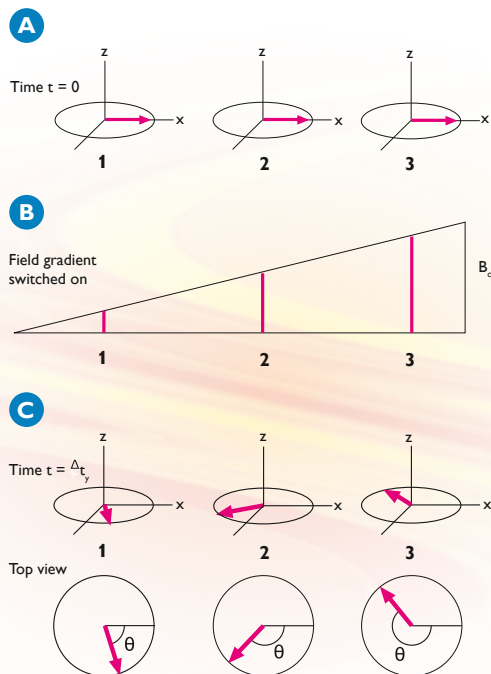
The gradient G_x causes the excited nuclei to precess at increasing frequency along the x-axis. The frequency distribution spectrum of the response signal shown provides a one-dimensional profile of signal intensity in the subject.

TWO-DIMENSIONAL FOURIER TRANSFORM IMAGE RECONSTRUCTION (FREQUENCY AND PHASE ENCODING)

A read-out gradient (G_x) provides spatial information along one axis of an image slice. If we fix the read-out gradient, and introduce a third gradient field - the phase-encoding gradient, G_y , which is applied prior to and at right angles (orthogonally) to G_x , we can complete the spatial encoding of the spins. This combination of gradients is the basis for two-dimensional Fourier transform techniques, since the resulting data is analyzed via the use of sequential Fourier transformations. After application of the slice selection gradient together with the requisite RF excitation pulse, all spins in the selected slice commence precession in phase with each other at the same nominal frequency. If a phase-encoding gradient G_y is subsequently turned on, the spins will have their resonant frequencies, and hence their rate of precession, altered according to their position along the y -axis. When the phase-encoding gradient is switched off, spins at points along the y -axis again begin to precess at the same frequency, however, their phases will no longer be the same - the individual nuclei have their phases altered according to their relative position along the y -axis, behavior referred to as "phase memory." (See Figure 30).

FIGURE 30

Principle of phase encoding.
After the 90° pulse, all spins precess at the same frequency and are in phase (A). When the y -axis gradient is switched on at time $t=0$, the nuclei precess at different frequencies, depending on their location (in this example 1, 2, or 3) along the gradient (B). When the gradient is switched off, all nuclei precess at the same frequency again, however, the spins retain the relative phase variation accumulated while the gradient was applied (C).



After switching on the read-out gradient G_x , the frequency of precession now varies as a function of position along the x-axis. This is illustrated in Figure 31, where nuclei in the selected slice vary by frequency along the x-axis and vary by phase along the y-axis. The individual spin vectors along the y-axis are oriented like steps on a spiral staircase.

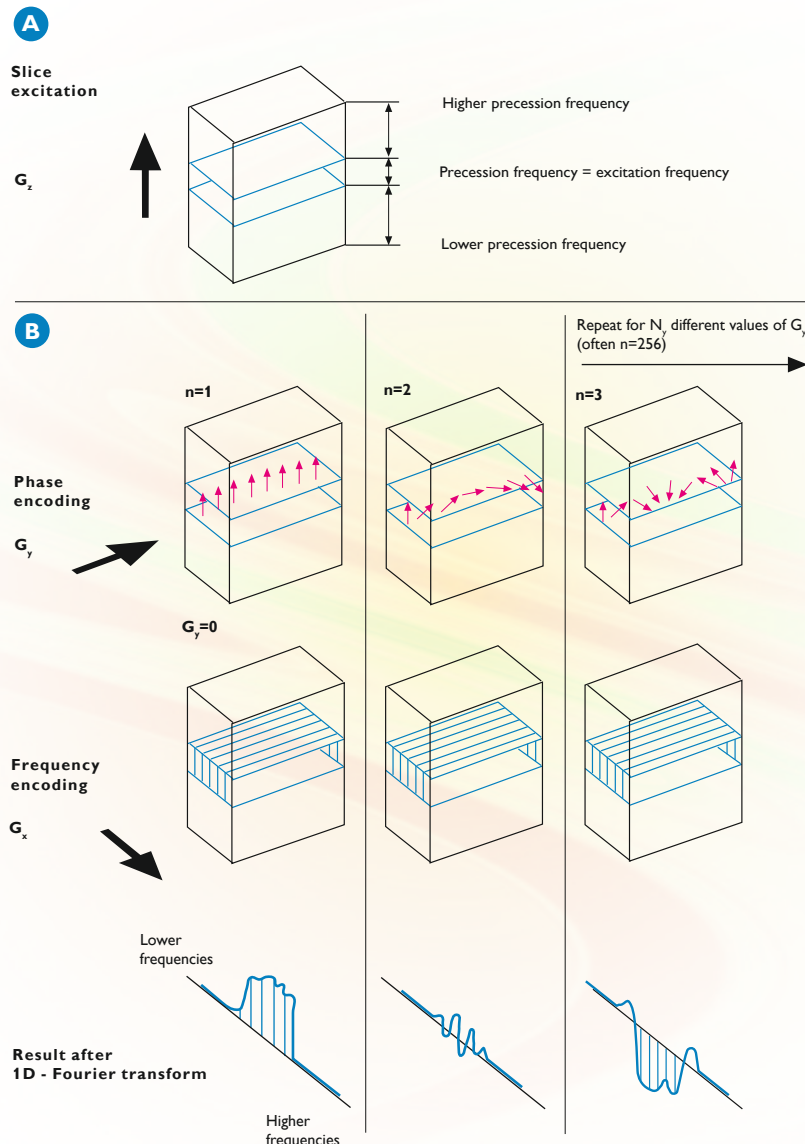


FIGURE 31

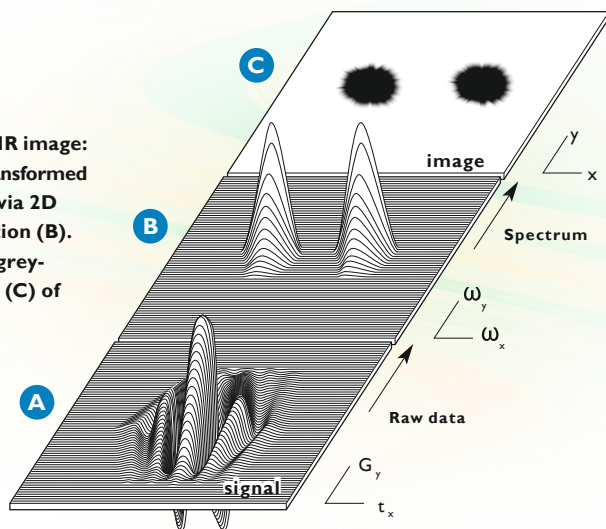
In a 2D Fourier transform imaging acquisition, slice selection takes place before each measurement by exciting the slice under gradient G_z (A). In N_y successive measurements, successive values of phase encoding gradient G_y are applied. The frequency gradient G_x is applied during slice data registration (B).

The signal component at a particular frequency (position) along the x-axis is the sum of all the vector contributions from a row of spins in the y-direction (Again, refer to Figure 31). The signal generated represents a composite of all the frequency components along the x-axis.

During the time that the read-out gradient is applied, we sample the signal, acquiring N_x data points. Repeating the measurement N_y times for different values of the y-gradient, yields a matrix of $N_x \times N_y$ amplitude points. For the general case of an image with $N \times N$ pixels, the phase-encoding step must be repeated N times with different values for G_y . To process our data array, we extend the Fourier transformation to a second dimension. Using an $N_x \times N_y$ raw data matrix, we sequentially perform two Fourier transformations, along the x- and y-axes, to produce a 2-dimensional spectrum of $N_x \times N_y$ pixels whose intensity is representative of signal distribution in the imaging slice. The final MR image is a gray-scale representation of this two-dimensional spectrum. (See Figure 32).

FIGURE 32

The creation of an MR image:
the raw data (A) is transformed
into a 2D spectrum via 2D
Fourier transformation (B).
The final image is a grey-
level representation (C) of
this 2D-spectrum.

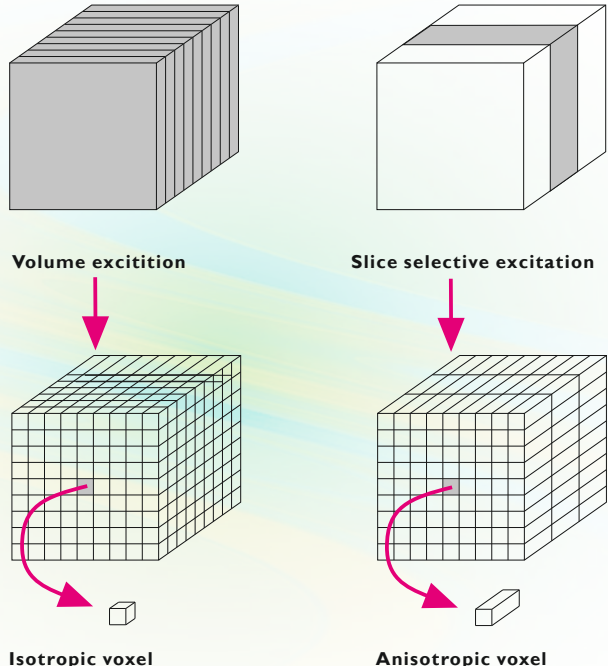


VOLUME IMAGING OR 3D IMAGING

Instead of measuring a number of slices in the described way, the method of volume imaging could be applied: an entire volume is excited by RF pulses, with all nuclei in the volume resonating at the same frequency – no slice selection gradient is applied. Instead, spatial localization in the third dimension is created through application of a second phase encoding gradient perpendicular to the desired slice orientation. The number of phase encoding steps in this slice selection direction – i.e. the number of discrete values of the additional field gradient – determines the number of slices in the volume. The advantages of volume imaging include a higher intrinsic signal-to-noise ratio, since the MR signal is derived from the entire volume rather than from a single slice. Remember that in normal 2D-FT imaging, noise is always detected from the full volume while the signal arises only from the selected slice. In addition, image slices can be very thin (as small as 1 mm) and very closely spaced without suffering from interference effects. In addition, it is possible to set up the imaging sequence so that the spatial resolution is nearly equivalent in all directions – in other words the voxels are nearly isotropic, see Figure 33 – permitting the 3D data set to be analyzed via successive reformatting in any plane, with equal image quality, and without the need for further image acquisition to obtain views in other orientations.

FIGURE 33

General concept of 3D volume imaging in comparison with slice selective excitation. Note that with volume imaging a voxel may be isotropic.



If data processing by multiplanar reformatting is the objective, it can be beneficial to perform the 3D acquisition with overcontiguous slices. If slices are overcontiguous, only half the selected number of slices is measured, but with doubled slice thickness.

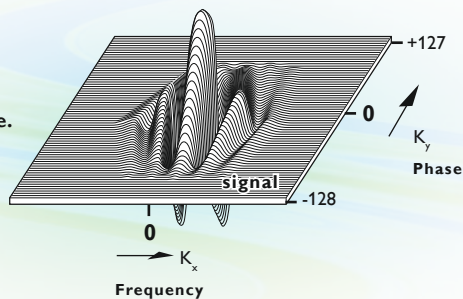
Afterwards all slices are interpolated from this acquired data. The number of displayed slices is equal to the selected number of slices! but the thickness of the displayed slices is twice the selected slice thickness, so that the displayed slices are overlapping by half a slice thickness. The result is that scan time is halved, while signal-to-noise ratio increases by $\sqrt{2}$ and conspicuity of small pathologies is improved. The major disadvantage of 3D volume acquisition is greater total imaging time due to the increase in the number of phase-encoding steps – the imaging cycle has to be repeated $N_z \times N_y$ times. For a volume acquisition with 16 image slices, the total imaging time increases by a factor of 16. In addition, image reconstruction time also increases as a result of the larger data set.

Spatial Encoding and K-Space

In addition to encoding spatial information into a data set, each MRI method must have an accompanying decoding strategy which “unravels” the coded information to produce a spatially resolved image. While there may be more than one way to analyze a data set, in no case can the final image be any better than the information which was coded into it. Unlike most imaging modalities, MRI permits a variety of ways for encoding spatial information into a sample, with image quality varying greatly depending on the method used. A k-space consists of the raw data that is collected during image acquisition, but not yet reconstructed to an anatomical image (Figure 34). Every single image has its own k-space data set. The horizontal axis describes the value of k that corresponds to the time (integral) of the measurement gradient. It is usually denoted k_x . Along the vertical axis the phase encoding steps are plotted – each phase encoding step is represented by a k_y -value which is proportional to the gradient strength used to phase encode. In this way, the k-space actually consists of all the acquired profiles or echoes above each other. The profile with $k_y=0$ is the echo measured after a zero phase encoding gradient was applied.

FIGURE 34

An example of k-space.



The k-space formulation can model an MR imaging method. In addition, the k-space formulation permits quantitative assessment of the influence of variations in gradient design, relaxation phenomena, and alternate sampling schemes. Regardless of the acquisition method, as long as you can determine how k-space was mapped, it is possible to properly structure the resulting data for two-dimensional Fourier transformation. The basic principle of the k-space formulation is that, during the encoding process for imaging, the time integral of the gradients traces a path in a two-dimensional space, “k-space.” The coordinate in k-space at which a sample is acquired (k_x , k_y) corresponds to the frequencies of the sinusoidal waves that form the basis for the Fourier transform in the x- and y-directions, respectively (Figure 35).

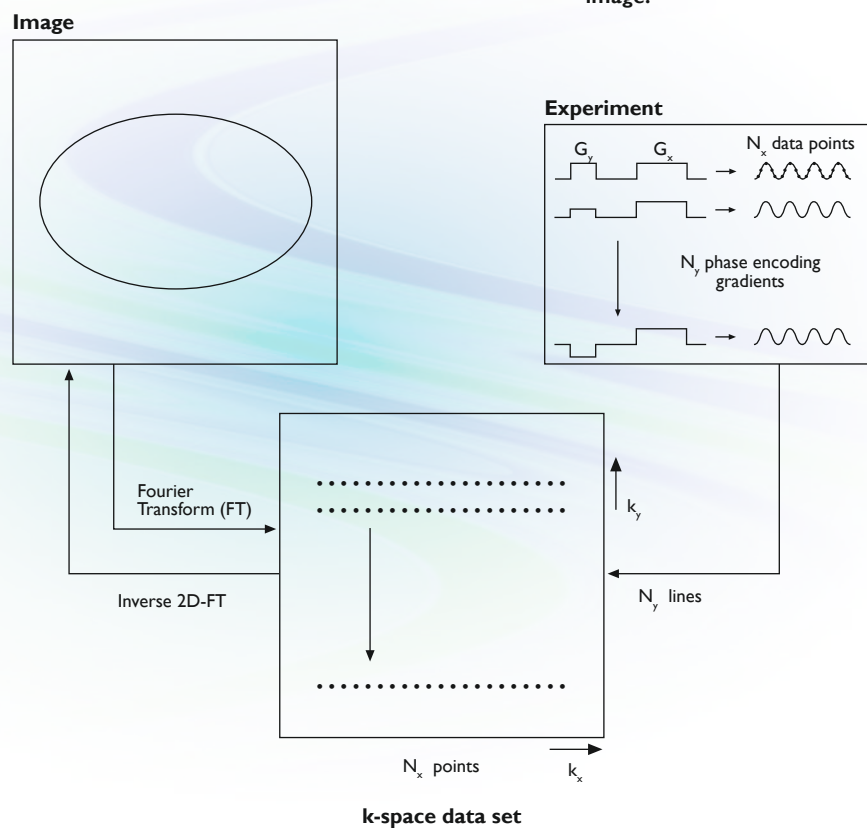


FIGURE 35

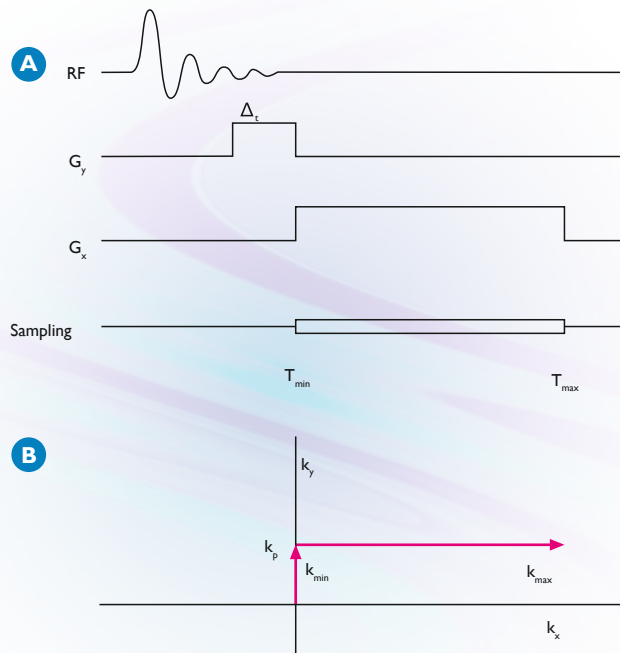
Understanding k-space. The k-space data is created through the sampling of the MR signal. The correctly ordered k-space undergoes an inverse Fourier transform to create the image.

Figure 36 provides a simple illustration of how k-space is mapped. After an RF pulse is applied, the y-gradient is applied briefly (Δt) to create a phase progression along the y-axis – this drives the spin system up the k_y -axis to k_p . The read-out gradient (G_x) is then applied to permit frequency distribution along the x-axis - i.e. progression along the k_x -axis. While the G_x gradient is on, the MR signal is sampled. The sampling process involves integrating the signal over the time interval between successive points. Each row of samples, collected at a given value of the y-gradient, represents a single k-space line (a profile). By varying the y-gradient and acquiring additional k-trajectories we can successfully acquire sufficient information for Fourier transformation and image creation.

FIGURE 36

Acquiring a k-space trajectory. The gradient sequence used (A) creates a horizontal line in k-space (B). Repeated acquisitions using variations in the G_y gradient are used to completely map the k-space.

Assuming that we wish to produce a final image with $n \times m$ pixels, we need to acquire m data points from each echo, and sample n lines in k-space to completely map the k-domain. In a typical 2D-FT sequence, k-space is sampled on a rectangular grid – the individual k-trajectories run parallel to a k_x -axis. Therefore, it is possible to create a “well-formed” spatial frequency array which can be presented directly to the Fourier transform. However, there are a virtually unlimited number of ways to map the k-domain, many of which involve k-trajectories which are neither linear nor parallel to a k-axis, making it necessary to perform mathematical interpolation before presenting the data for Fourier transformation.



IMAGING SEQUENCES

For an image to have diagnostic utility, there must be contrast between the MR signal of different tissue types. If MR signal intensity was purely a function of proton density, the sources of contrast would be limited. However, the intensity of magnetic resonance signals is a function of several parameters, including proton density, relaxation times T_1 and T_2 , chemical shift, and motion. The relative contribution of each parameter is controlled by adjusting the RF pulses and gradients applied and the timing of the data acquisition. These parameters are set in the imaging sequence, also called the pulse sequence or pulse program.

PULSE SEQUENCE FUNDAMENTALS

A typical magnetic resonance imaging pulse sequence can be separated into two functional parts:

1. spin preparation – manipulation of the MR signal characteristics through the use of RF pulses or magnetic field gradients.
2. signal production – the steps necessary to generate the magnetic resonance signal and encode this signal with spatial information.

Using this two part definition, it is possible to characterize virtually all MR pulse sequences (as partially illustrated in Figure 37), and to make it easier to understand the process of modifying an existing program or creating an entirely new sequence.

We can distinguish three ways of generating an MR signal:

- free induction decay (FID)
- spin echo
- gradient echo.

Integrating these signal types with the gradient sequences necessary for spatial encoding produces the fundamental magnetic resonance imaging pulse sequences.

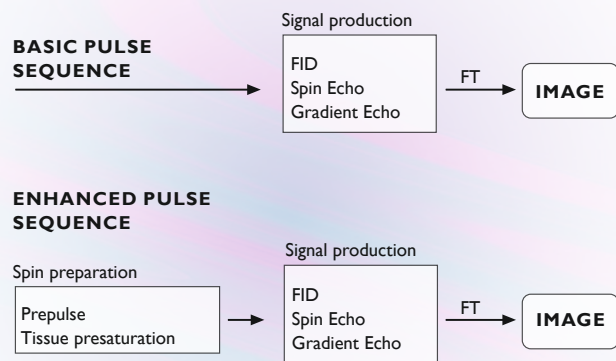


FIGURE 37

A pulse sequence can be separated into two functional elements: a signal production component and a spin preparation component.

IMAGING BASED ON THE FID

As discussed, the maximum MR signal intensity is created by the application of a 90° RF pulse. If an FID signal is sampled immediately after termination of the 90° pulse, MR signal intensity is proportional to the net equilibrium magnetization. The sampling must begin as soon as possible after termination of the pulse because any delay allows signal reduction due to transverse relaxation (T_2^*)

FIGURE 38

(A) The spin echo timing sequence. (B) The associated k-space map. The evolution in k-space before and after sampling is shown for one value of k_y . Usually only the evolution during sampling is shown.

Since the FID decays within a time defined by T_2^* , typically on the order of 20 ms, there is only a short time to spatially encode the FID. This has led to imaging strategies based on spin echo.

SPIN IMAGING

Spin echo signal generation accommodates the time requirements of phase encoding, while allowing more complete evolution of spin-spin interactions.

Figure 38A shows a standard spin echo imaging sequence. The combination of the 90° pulse and the selection gradient define the image slice. The 90° pulse flips the magnetization to the horizontal plane. The 180° pulse is the refocusing pulse given at exactly $TE/2$. The time between excitation and the maximum echo signal is TE , which is typically 10 to 200 ms. The sequence is repeated N_y times, with N_y different values for the phase encoding gradient G_y . The time between successive excitations is called the repetition time TR . TR must be long enough to allow sufficient build-up of longitudinal magnetization again via T_1 relaxation. In spin echo measurements, TR is typically 200 to 2000 ms. The total scan time needed to perform the complete experiment equals $N_y \times TR$.

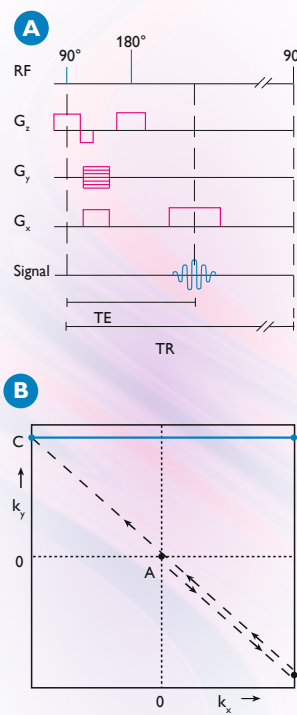


Figure 38B shows how k-space is mapped in spin echo acquisition. The programmable y axis phase encoding gradient G_y evolves the spin system along the k_y axis, while simultaneously the gradient G_x creates a phase variation along the x axis - in k-space terms, both evolve the spin system to one extreme corner (A to B), as shown. The 180° pulse then reverses the effects of magnetic field inhomogeneities, creating the echo signal, and also reverses the phase evolution along the k_x and k_y axes (B to C). The measurement gradient is re-applied following the 180° pulse and sampling is initiated, as indicated by the bold line C to D. Repeating this sequence for different amplitudes of the G_y gradient completes the k-space map. Note that this is a “well-formed” acquisition protocol which produces a rectangular data array in k-space that can be presented directly for 2DFourier transformation.

GRADIENT ECHO IMAGING OR FAST FIELD ECHO (FFE) IMAGING

Instead of applying a 180° pulse to rephase the spins into an echo, it is possible to use the FID-domain for signal detection. In a gradient echo imaging sequence, a gradient is applied for a limited time, in the read-out direction, following the excitation pulse. This causes spins to precess at different rates, according to their position along the x-axis, so that dephasing occurs and the signal drops. The gradient is then reversed, so that spins that were in a positive field are now in a negative field and vice versa. This reversal leads to a rephasing of the spins, and an echo signal. A gradient is in fact a controlled way of introducing magnetic field inhomogeneities and therefore the symbol T_2^* is also used to characterize the signal drop after switching on the gradient. It is evident that the value of this T_2^* is smaller than the one that characterizes the signal drop of an FID without gradient on.

Figure 39 illustrates the timing pattern in a gradient echo sequence. This example illustrates that in reversing the field, it is the product of gradient strength and duration of application which controls echo production – i.e. the two lobes on the waveform must have equal area beneath the curve. For example, the rephasing field can be applied for half the time, as long as the field strength is double that of the dephasing field.

One significant difference between gradient and spin echo formation is a sensitivity to magnetic field inhomogeneities. Unlike the spin echo sequence, gradient echo acquisition does not cancel field inhomogeneities which act like static, nonlinear gradients that dephase the spins.

As discussed, the completion of an image requires repeated measurement of echoes. These repetitions take place once every repetition time. In spin echo imaging, the excitation pulse is a 90° pulse and the repetition time varies between a few hundred milliseconds and a few seconds. This rather lengthy repetition time is required to avoid saturation: Immediately following a 90° pulse, there is no effective longitudinal magnetization. As the spin system begins to relax, however, a longitudinal component of magnetization is restored. Complete restoration requires a time equal to or greater than several T_1 . If longitudinal relaxation is incomplete before the next excitation pulse, the effective magnetization tipped into the transverse plane is smaller. Thus, if multiple excitation is employed, only a small magnetization component is tipped into the transverse plane - an effect referred to as saturation.

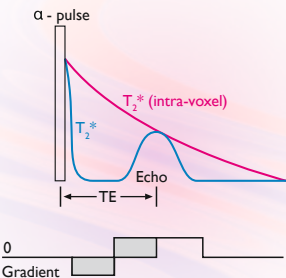


FIGURE 39

Creating a signal using the gradient echo technique.
The initial gradient application leads to loss of phase coherence; the reversal of the gradient permits reformation of an in-phase signal.

The gradient echo sequence is compatible with the use of smaller flip angles, shorter echo times and shorter repetition times than spin echo measurements, with a resulting decrease in total imaging time. If we reduce the repetition time, TR, from 1 second, typical for spin echo measurements, to 15-30 milliseconds, we would see an approximately 50-fold decrease in the total imaging time. However, this would lead to strong saturation of the spin system and unacceptably low signal.

It follows that when a shorter TR is employed, the excitation pulse angle must change to a value less than 90°. Following a limited flip angle excitation (e.g. 15°-45°), the time required to restore normal longitudinal magnetization is greatly reduced. Under these conditions, the spin system reaches a steady state (after a few pulses) in which a significant, measurable transverse magnetization component is generated by each pulse, while most of the net magnetization remains in the longitudinal direction. (See Figure 40).

While this approach allows a very short recovery time, it is not compatible with the use of 180° pulses for generating the signal echo. Since a large fraction of the net magnetization remains in the longitudinal plane, a 180° pulse would primarily invert longitudinal magnetization. Even at low excitation flip angles, this would drive the net magnetization to zero as TR shortens. Thus, the use of gradient echoes instead of spin echoes is necessary to create significant echo signal in the case of small flip angles and short TR's. Although gradient echo acquisition does not cancel static magnetic field inhomogeneities, this drawback is balanced by the ability to acquire an image very rapidly - a single image can be obtained in about 2 seconds.

FIGURE 40

Signal intensity as a function of flip angle in a gradient echo sequence for some values of TR/T_1 . Limited flip angles lead to a greater transverse component with short TR.

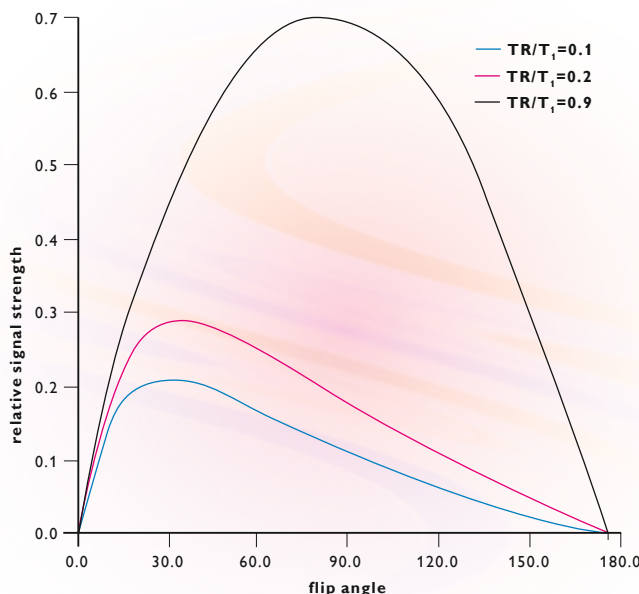


Figure 41 illustrates a typical gradient echo imaging sequence along with its associated k-space map. As in the spin echo sequence, an excitation pulse and slice selection gradient (G_z) define the image slice. The programmable y-axis preparation gradient (G_y) evolves the spin system along the k_y axis. In this case, however, the simultaneous measurement gradient is used first to evolve the spin system to one extreme on the k_x axis (A to B), then it is reversed to evolve the system back along the k_x line (B to C). Sampling is initiated after reversal of the measurement gradient. Repeating this sequence for varying amplitudes of the G_y gradient completes the k-space map. Again, this acquisition protocol produces a rectangular data array in k-space which can be presented directly for 2D Fourier transformation.

Virtually all major MRI vendors have developed some version of the gradient echo imaging sequence. Each version differs slightly in its specific implementation, however, each utilizes the same basic limited flip angle, gradient reversal strategy. The major sequences include: Philips' FFE (fast field echo), FLASH (fast low angle single shot), and GRASS (gradient recalled acquisition in the steady state).

VARIATIONS ON A THEME - SPIN PREPARATION IN IMAGING SEQUENCES

One of the strengths of MR imaging is the ability to adjust the imaging parameters to accommodate different clinical requirements. These variations in pulse sequence are used by the diagnostician to bring out, in an appropriate way, a clear contrast between tissues of interest. In some cases, however, choosing various combinations of TE, TR and flip angle α , offer inadequate combinations to reach a desired contrast in a clinically acceptable fashion. For example, spin echo measurements using long TR (2-3 s) are desirable for T_2 -weighting, but require a long acquisition time. The use of modified RF or gradient pulse sequences prior to signal generation – termed spin preparation – offer additional flexibility in adjusting the contrast. Some common spin preparation techniques include:

- Prepulses (Inversion pulses, saturation pulses).
- Contrast enhancement in FFE.
- Fast image acquisition modifications.

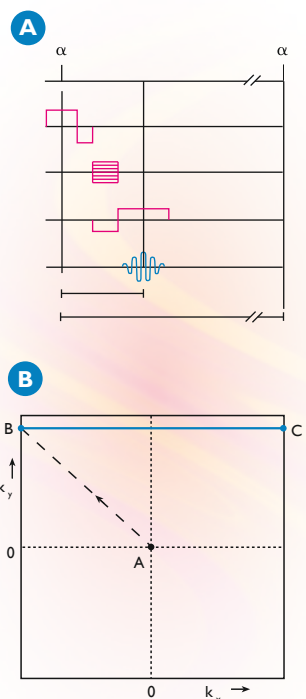


FIGURE 41
(A) The gradient echo timing sequence.
(B) The related k-space map.

PREPULSES - INVERSION RECOVERY

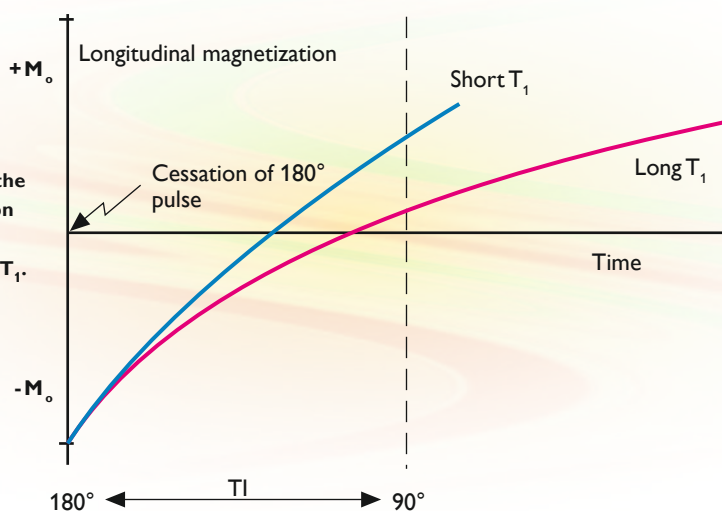
Prepulses can be executed in conjunction with either a gradient echo or a spin echo sequence. An inversion prepulse is applied to generate images which are primarily dependent upon T_1 relaxation effects (T_1 -weighted), and also as part of tissue presaturation protocols.

As its name implies, an inversion pulse inverts the net magnetization - i.e. flips the magnetization 180° from its initial orientation (a magnetization along the positive z-axis is brought to the negative z-axis). When the pulse is terminated, the spins begin to relax and the magnitude of the net magnetization gradually recovers, passing from a maximum negative value, through zero, then building up in the positive direction. See Figure 42. This relaxation occurs in exponential fashion, at a rate characterized by T_1 . Since the net magnetization has not been tipped into the transverse plane, there is negligible MR signal throughout this process.

To generate a detectable MR signal, a signal generation scheme is then applied. For example, a 90° pulse can be applied and the FID measured, with the initial amplitude of the FID proportional to the value of the net magnetization at the time of the measurement. Note that the magnitude of the signal is dependent on T_1 . Tissue with a short T_1 may be almost fully recovered by the time the 90° pulse is applied; therefore, a large signal will be detected. Tissue with a long T_1 , however, may have recovered to around zero and contribute little signal. Thus, tissue with a short T_1 will appear bright and tissue with a long T_1 displays dark.

FIGURE 42

Return to equilibrium of the longitudinal magnetization for tissue with a short T_1 , and for tissue with a long T_1 .



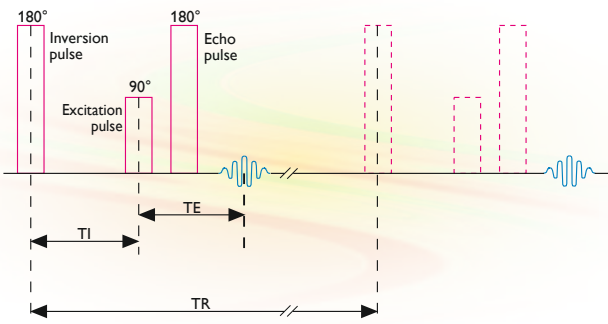


FIGURE 43

Timing diagram for inversion recovery sequence.

It is more typical, however, to couple inversion pulses with a spin echo sequence. This combination is referred to as an “inversion recovery” (IR) sequence. By varying the time between the 180° inversion pulse and the 90° read pulse (i.e. the inversion time, TI, as shown in Figure 43) it is possible to control the T_1 weighting of the image. Between successive measurements, the spin system must be allowed to relax, so that inversion recovery sequences are usually run with a long TR.

STIR

For imaging in the orbit, breast, lower abdomen or of stress fractures where the signal from lipid can often complicate image acquisition, it is helpful to selectively null the fat signal through inversion pulses by proper choice of the inversion time (TI). When TR is sufficiently long to permit nearly complete relaxation between successive pulses ($TR > 3 \times T_1$), this condition occurs at approximately $0.6 \times T_1$ of fat. This method, called STIR – Short TI Inversion Recovery, has been successfully employed in a wide range of applications.

Note that when STIR is used to null the lipid, most tissues still have negative magnetization, because their T_1 is longer than that of lipid. For such tissues, the signal strength increases with T_1 as well as T_2 , resulting in an attractive contrast for some applications. This is illustrated in Figure 44.

SUPPRESSION OF CSF

A relatively recent item of attention is the use of an inversion pulse to null the signal from CSF, a method sometimes called Fluid Attenuated Inversion Recovery (FLAIR). Contrary to nulling of lipid, this application requires a very long TI (around 2000 ms). The corresponding TR is 6-9 seconds. When used in combination with spin echo imaging, this technique produces T_2 -weighting in an image in which CSF is black. The image acquisition time is prohibitively long, unless some means of fast imaging (like IR-TSE) is used.

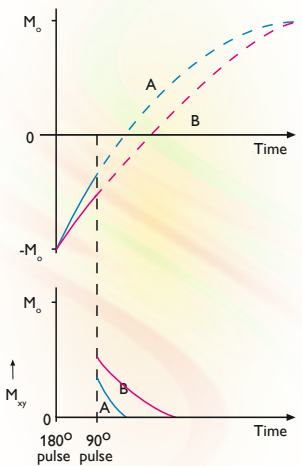


FIGURE 44

Time Contrast phenomena in inversion recovery measurement with short TI.
Tissue A has short T_1 and short T_2 , while tissue B has long T_1 and long T_2 . This example illustrates the additive effect of T_1 and T_2 differences with STIR imaging.

SPIR

The fat suppression method of Spectral Presaturation with Inversion Recovery (SPIR) utilizes the difference in resonance frequencies between water and fat (about 3.4 ppm). A frequency selective inversion pulse excites the lipid bound protons. After an appropriate delay time between the inversion pulse and the start of the normal spin echo sequence, a pure water image is generated.

CONTRAST ENHANCEMENT

Gradient echo signals result from the refocusing of local field inhomogeneities caused by the presence of a magnetic field gradient. As illustrated in Figure 40, an RF pulse of flip angle α produces a FID which is subjected to a magnetic field gradient. The FID signal decays rapidly as a function of T_2^* , but is refocused to form an echo at time TE by reversal of the applied gradient. Note that in successive applications of the RF pulse, since the repetition time is generally shorter than the average T_1 for all the tissue types in the image, the signal will contain a contribution that is the spin echo of a prior excitation, so that the total signal now equals the sum of the FID and spin echo signal. This concept is illustrated in Figure 45.

To control contrast behavior, or create “contrast enhancement”, it is possible to apply additional gradient pulses, called spoiler pulses, to dephase signal arising from either the FID component or the spin echo component. In T_1 -weighted contrast enhanced Fast Field Echo (T1-FFE) measurements, spoiler gradients are applied to eliminate the formation of spin echoes from previous RF excitations. To obtain T_2 -weighting (T2-FFE) spoiler gradients before the echo formation are used, preventing the formation of a contribution from the FID, and leaving only the spin echo signal from the previous two pulses. An alternative means of spoiling the spin echo contribution in T1-FFE is achieved by stepping the phase of the excitation pulses – phase cycling. The advantage of this method is improved efficiency in timing.

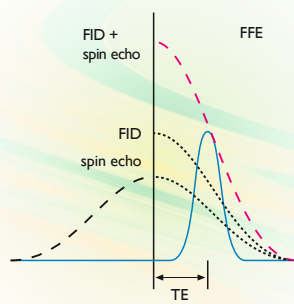


FIGURE 45

The contributions to the signal in an FFE (gradient echo) sequence.

SPEEDING UP IMAGE ACQUISITION - FAST IMAGING ENHANCEMENTS

Starting with our basic signal production schemes (spin echo, gradient echo), we can modify the pulse sequence to produce image data faster. Let's look at two ways of speeding up image acquisition times:

- Throughput enhancements which are more time efficient implementations of "standard" pulse sequences.
- Fast imaging protocols which are specifically designed for very fast acquisition of image data.

IMAGING THROUGHPUT ENHANCEMENTS: MULTI-ECHO AND MULTI-SLICE

During the course of a spin echo study; it is normal to acquire images for several anatomic "slices" to provide a clear image of morphology. In addition, multiple excitations (signal averages) are often required for each image slice to obtain satisfactory signal-to-noise ratio. Performing this acquisition sequentially – i.e. the multiple repetitions for each slice are completed before moving to next slice – would be extremely inefficient, since there would be long periods of inactivity (dead time) between the echo and successive excitation pulses. This inefficiency results from the requirement for a relatively long repetition time – typically 500 to 2000 ms – to allow the spins to relax sufficiently between pulses (See Figure 46). The inefficiency decreases patient throughput and increases the likelihood of image degradation due to patient motion. The protocol can be greatly improved by either acquiring data from multiple spin echoes within each repetition or by interleaving the acquisition for multiple image slices – acquiring data from other slices during the time between evolution of the echo and the end of the repetition time.

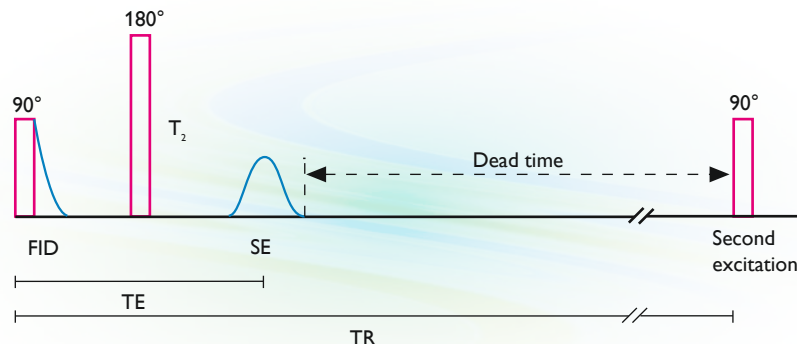
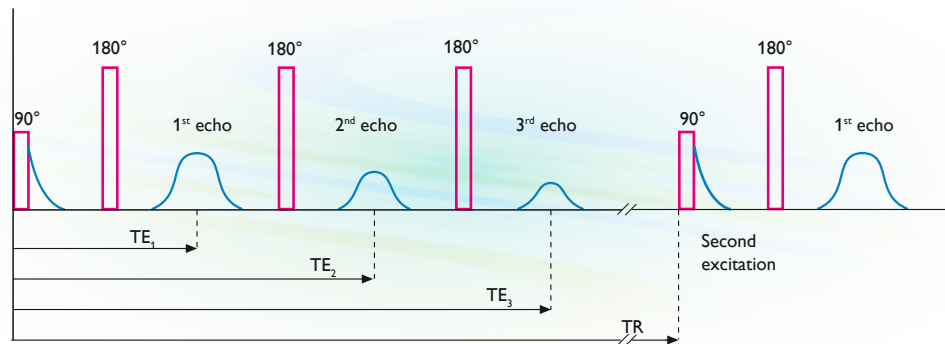


FIGURE 46

Dead time during a standard spin echo image acquisition results in inefficient use of patient imaging time during a normal multi-slice study (Typical values for a normal T_2 -weighted spin echo study are $TE = 90$ ms and $TR = 2000$ ms).

FIGURE 47

Multi-echo image acquisition using equidistant 180° pulses.



MULTI-ECHO ACQUISITION

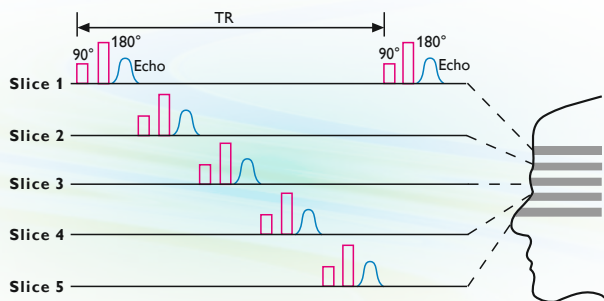
Multi-echo acquisition protocols operate by applying a series of 180° pulses, as shown in Figure 47. This generates a series of spin echo maxima which can be used to produce first, second, third, fourth, ... echo images. In a multi-echo imaging scheme, it is not necessary to have a fixed increment in TE, since TE can be varied by the timing of the 180° pulse. Different TE values (e.g. TR = 2000 ms, TE = 20/90 ms) are often used to obtain different types of contrast from one experiment (e.g. proton density and T₂-weighted).

MULTI-SLICE ACQUISITION

Multi-slice image acquisition operates by acquiring data from other image slices during the “dead time” – the time between echo formation and the end of the repetition time, as shown in Figure 48. This reduces total image acquisition time for acquisition of images from multiple slices – that is, it allows acquisition of multiple slices in the same time as acquisition of one slice. The gain in efficiency can vary but is typically a factor of 10 or greater. A shorter echo time or a longer repetition time both increase the maximum number of slices which can be packaged within a given TR period. See Figure 49.

FIGURE 48

Multi-slice image acquisition using a typical spin echo timing sequence.



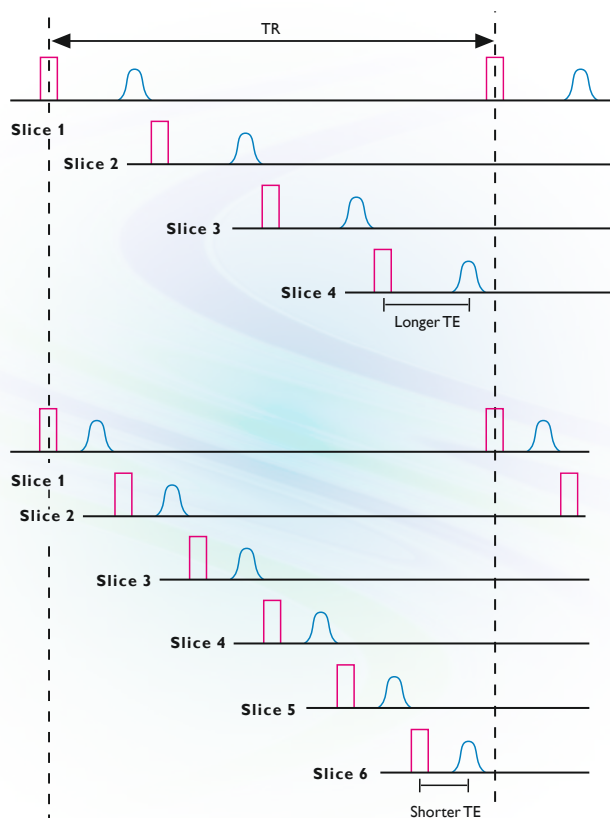
The individual layers in a multi-slice acquisition can be contiguous (i.e. adjacent slices touching at the full width at half maximum), overlapping or separated (e.g. a radial stack acquisition). For a strategy in which all slices are addressed within one TR, in practice usually (SE), a small gap is maintained between slices to avoid crosstalk. More freedom of selection in the slice gap – even involving overlapping slices (i.e. negative slice gaps) – can be obtained by distribution of the slices over two packages. For example, you can deal with odd numbered slices in the first half of the scan time and the even numbered slices thereafter.

When using multi-slice acquisition, inflow of blood or other fluids excited in adjacent slices can result in typical artifacts in an imaging slice. This topic is covered more thoroughly in Chapter 5, “Practical Considerations in MR Imaging.”

Multi-slice techniques can be applied to FFE imaging as well. The TR is then chosen sufficiently long to accommodate the excitation of all other slices. Complete contiguity is permitted and does not lead to crosstalk. Note, however, that it is often attractive to use gradient echo imaging with the shortest attainable TR. In such cases, there is no time to interleave acquisition from other image slices. The total imaging time for a multi-slice gradient echo acquisition is then a simple multiplicative factor (the number of images slices acquired) greater than a single slice acquisition. Finally, multi-echo and multi-slice protocols can be combined into a multi-echo, multi-slice acquisition.

FIGURE 49

In multi-slice image acquisition the result of selecting a longer TE might be that less slices fit into a TR period. In other words less slices fit into a package.



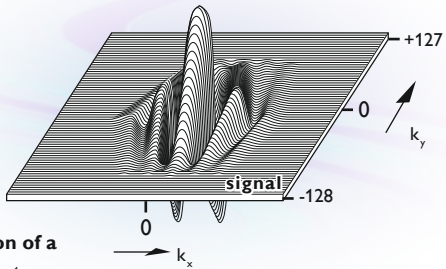


FIGURE 50

K-space representation of a typical 2D data set. Note that the signal is symmetrical in both the x and y direction.

IMAGING THROUGHPUT ENHANCEMENTS: REDUCING THE NUMBER OF PHASE ENCODING STEPS

A second common strategy for improving image throughput is reducing the number of phase-encoding steps N_y , which can reduce total imaging time, since imaging time is proportional to $N_y \times TR$. Two approaches are routinely used: Reduced acquisition (zero-filling) and Halfscan. Both methods rely on data symmetry and interpolation to reduce the total amount of data which must be acquired.

In a typical MR exam, the data along the x-axis, represents the acquired signal per echo. Note that the shape of the echo signal is symmetrical around the mid-point. Each successive line is displaced along the y-axis as a result of a phase-encoding step in the acquisition protocol. The complete data set is symmetrical around the central line, as shown in Figure 50.

REDUCED ACQUISITION

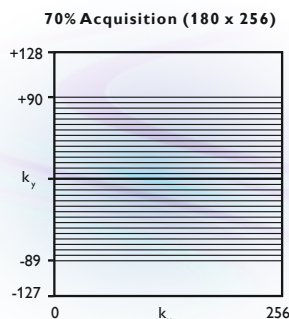


FIGURE 51

K-space data set in reduced acquisition mode: For a matrix size of 256, a scan percentage of 70% means that 180 lines of 256 points are acquired.

In reduced acquisition, zeroes are substituted for data lines at the “fringes” of the y-axis (the outer lines) where there is little contribution to image contrast (See Figure 51). In order to apply Fourier transform methods, data sets must be structured as powers of 2 (e.g. 128, 256, 512, etc.). If we sample less than a full power of two data lines, then we must zero-fill the remaining lines to produce a “complete” data set. This permits application of the Fourier transform while largely preserving the information content of the image, although some loss of spatial resolution does occur. In fact, this loss of spectral resolution leads to an increase in signal-to-noise ratio. Reduced acquisition to 80% of the “full” data set is routinely applied in many applications. Further reduction, however, visibly decreases the image sharpness, but remains useful for scanning uncooperative, restless, claustrophobic or high-risk patients, since at least some image information can be obtained.

Instead of not measuring the outer profiles, a method called k-space shutter can be applied, especially for 3D imaging. With a k-space shutter, the outer corners of k-space are not measured, but filled with zeroes. In this way spatial resolution is preserved better than with reduced acquisition, since parts of the outer lines, which contain resolution information, are still measured.

HALFSCAN

With Halfscan or half-Fourier imaging, instead of filling the outer edges of the data set with zeroes, we acquire only an asymmetric fraction of the data set, then synthesize the balance, based on symmetry of the data, using a technique called conjugate data synthesis (See Figure 52). Halfscan is possible because the data samples resulting from negative values of the phase encoding gradient are identical to the data samples acquired using the corresponding positive value with the exception of the phase of the MR signal. Just over half of the total phase-encoding steps are required to permit use of Half scan, since this provides sufficient data for execution of phase-correction algorithms to correct for the inherent phase error. Using Halfscan, spatial resolution is preserved, but reduction in signal-to-noise ratio does occur and the technique is sensitive to magnetic field inhomogeneities. Halfscan is valuable when scan times are long, the expected signal-to-noise ratio is ample, and full spatial resolution is required. It is particularly useful in scans with a large field of view and relatively thick slices, and with 3D scans with many slices.

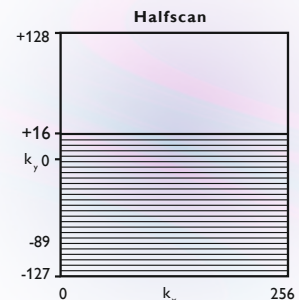


FIGURE 52

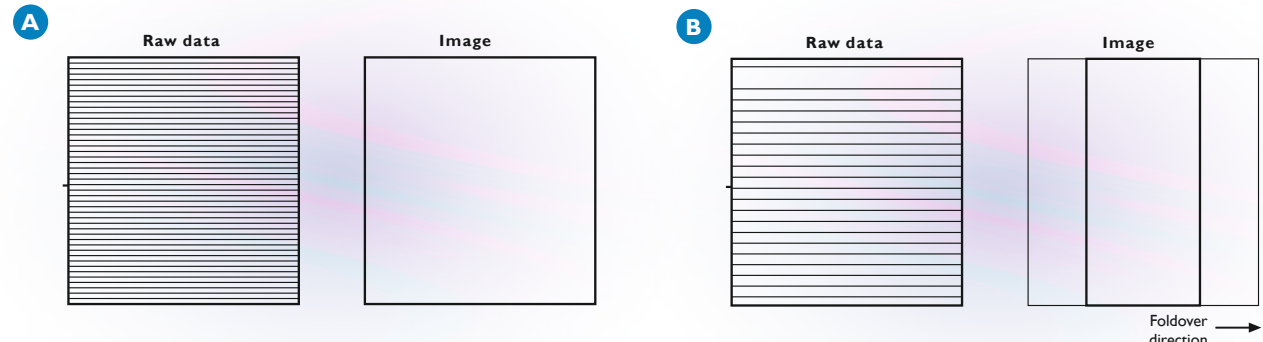
K-space data set using Halfscan.

RECTANGULAR FIELD OF VIEW

An image with a rectangular field of view is obtained when the spacing between the lines in k-space is enlarged, but still the same area is contained within the outer lines. If, for example, only 50% of the lines in k-space are measured by skipping every second line, scan time will be reduced by 50%, while the field of view in the image is reduced by 50% in the preparation direction, as shown in Figure 53. Spatial resolution remains unaffected by selecting a rectangular field of view and the pixels in the image are still square. However, the signal-to-noise ratio decreases by a factor proportional to the square root of the fraction of sampled lines. Rectangular field of view may be useful in imaging of spine or extremities, angiography, volume imaging and pediatric imaging.

FIGURE 53

Raw data and image size of (A) a normal square image (B) an image with 50% rectangular field of view.

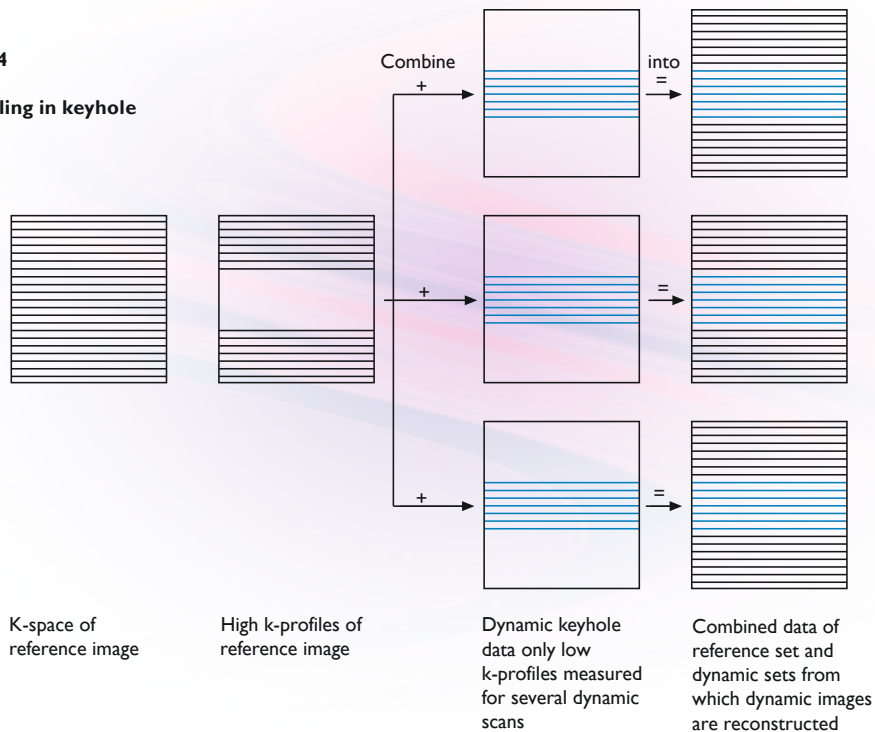


KEYHOLE - DYNAMIC IMAGING WITH MORE IMAGES IN SHORTER TIME

Dynamic imaging is applied when several images are needed for diagnosis. This may concern the examination of a joint in several positions or time resolved studies e.g. contrast agent wash-in and wash-out. Keyhole imaging is a method that makes efficient use of the available time for dynamic contrast studies. Instead of repetitively acquiring all profiles for each image, a complete reference image is acquired only once. For all subsequent images, only the central profiles which contain the contrast information are measured. Before Fourier transformation is performed, the central profiles of the dynamic images are combined with the outer profiles of the reference dataset, which contain information on edge definition and sharpness. See Figure 54. The result is a set of images of good sharpness and with contrast sampled at very short time spacings. This method offers good signal-to-noise ratio and spatial resolution for cases where the dynamic process is not too fast and where not too many slices are needed.

FIGURE 54

Data handling in keyhole imaging.



FAST IMAGE ACQUISITION SEQUENCES

Rapid image acquisition is essential for applications such as abdominal imaging where image quality can be degraded by respiratory motion or peristaltic flow artifacts. Fast acquisition also permits effective dynamic imaging, such as cardiac perfusion studies. Further, the shorter the examination, the higher the degree of patient acceptance and lower the chances of patient movement.

The throughput enhancement strategies discussed so far did not affect the imaging sequence per se. While effective at reducing the total imaging time, these strategies generally compromise either spatial resolution or signal-to-noise ratio. By comparison, an optimized imaging technique would provide reduced imaging times along with excellent contrast, signal-to-noise ratio and spatial resolution.

Improvements in MR imaging hardware and software have permitted the development of routine imaging sequences with scan times of 1-4 seconds per slice. Two important optimizations in imaging technique are TFE (Turbo Field Echo) and TSE (Turbo Spin Echo). These sequences are modifications of standard spin echo or gradient echo measurements.

TURBO FIELD ECHO (TFE)

The Turbo Field Echo sequence allows gradient echo imaging with very short echo and repetition times. It is optimized to obtain the highest image quality possible within a very short scan time. Typically, the echo times in a TFE measurement are 3-5 ms while the repetition times are 7-10 ms. These short repetition times allow complete data acquisition to occur successively per slice, rather than in multi-slice mode where data from several slices are acquired per phase encoding step.

The major application of TFE is the reduction of artifacts due to respiratory motion and abdominal peristaltic motion. Other applications of TFE include the imaging of restless patients and dynamic studies to monitor contrast agent wash-in/wash-out (e.g. for perfusion imaging, differential diagnosis, rejection of transplanted organs, etc.).

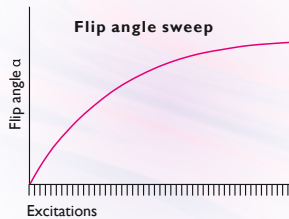


FIGURE 55

The use of flip angle sweep as typically employed in a turbo field echo measurement.

In normal gradient echo (FFE) scans, care is taken to “run-in”, after which all profiles are acquired with the spins in the steady state. The “steady state” is the point in time where the reduction of the magnetization along the z axis caused by RF pulse excitation equals the relaxation due to T_1 during each TR period. A major difference between Turbo Field Echo and a standard gradient echo scan is that data acquisition in TFE is actually proceeding while the spin system is approaching the “steady state.” Since TFE scans can even be complete before steady state conditions are established, each profile reflects a different set of initial conditions. Without the necessary precautions, ghost artifacts would be introduced since the approach to steady state can be highly oscillatory.

TFE uses a technique called Flip Angle Sweep to counter this problem. By incrementing the flip angle with each successive pulse profile, the approach to steady-state is smoother and artifact generation is minimized. As shown in Figure 55, the scan is commenced with a low flip angle. During the scan, the flip angle is increased for successive excitations, up to the prespecified angle. The flip angle sweep not only suppresses artifacts, but also allows use of larger flip angles without introducing too much saturation, and therefore gives increased signal-to-noise ratio and contrast.

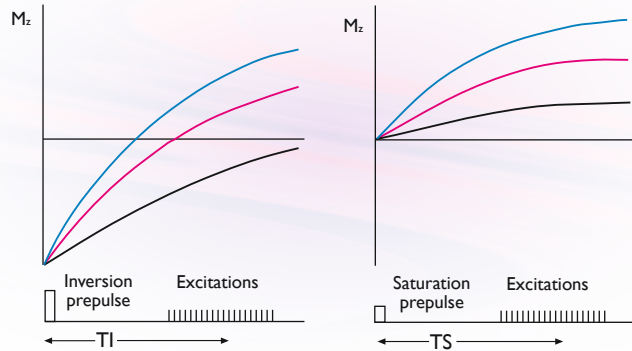


FIGURE 56

Use of prepulses in TFE measurements: Recovery of M_z after an inversion prepulse (left) or a saturation prepulse (right). TI and TS define the delay time between the prepulse and the $k=0$ profile.

When the imaging times are of the order of T_1 , the contrast will tend to be mildly T_1 -weighted, because spin saturation does not dominate. The degree of T_1 -weighting can be controlled further through the application of inversion or saturation prepulses. Inversion pulses in TFE work the same as inversion pulses in the Inversion Recovery (IR) technique. Signal is inverted and returns to equilibrium due to the static magnetic field. Tissues with different T_1 values have different recovery curves, thus contrast can be manipulated by selecting the proper delay time for the inversion prepulse. The application of a saturation pre-pulse instead of an inversion prepulse leads to a smaller increase in the T_1 -weighting. See Figures 56 and 57.

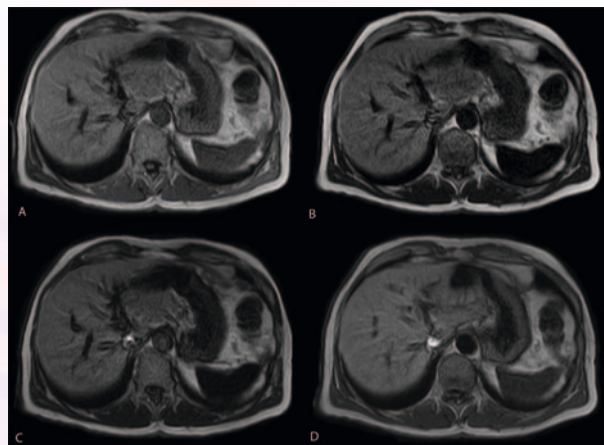


FIGURE 57

Contrast behavior in an image as a function of prepulse variations:

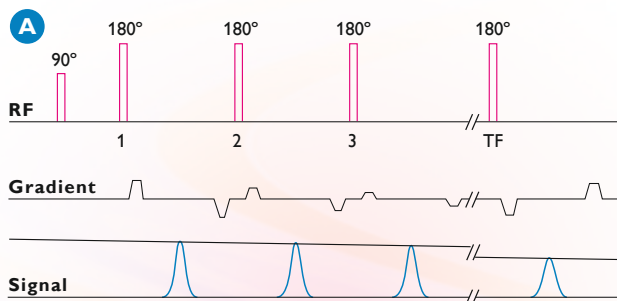
- (A) Saturation prepulse with delay time of 650 ms.
- (B) Inversion prepulse with delay time of 650 ms.
- (C) Inversion prepulse with delay time of 750 ms.
- (D) Inversion prepulse with delay time of 1050 ms.

TURBO SPIN ECHO (TSE)

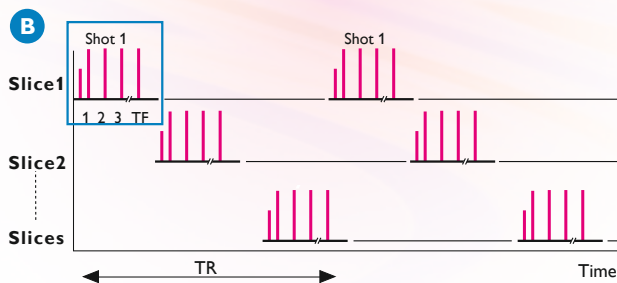
The Turbo Spin Echo (TSE) technique combines the acquisition of multiple profiles per excitation with the multi-slice mode to dramatically reduce imaging times. In the classic spin echo method, a single k-profile or phase encoding step is acquired per excitation (TR). Thus, for a 256×256 matrix, 256 excitations are required to collect all 256 profiles needed to produce the image. In TSE, multiple k-profiles are acquired per excitation. A train of closely-spaced (e.g. 20 ms), consecutive 180° refocusing pulses are applied per excitation and after each of these refocusing pulses, an echo is measured. This creates shots with a corresponding number of differently phase encoded echoes. The shots are acquired at regular intervals (TR) until the image is complete (See Figure 58).

FIGURE 58

(A) Turbo spin echo acquisition scheme. Each excitation is followed by a number of refocusing pulses. Each group of pulses/profiles is referred to as a shot.



(B) Shots are acquired at regular intervals (repetition time TR) until the image is complete. The corresponding shots for a number of additional slices can be acquired within the same TR.



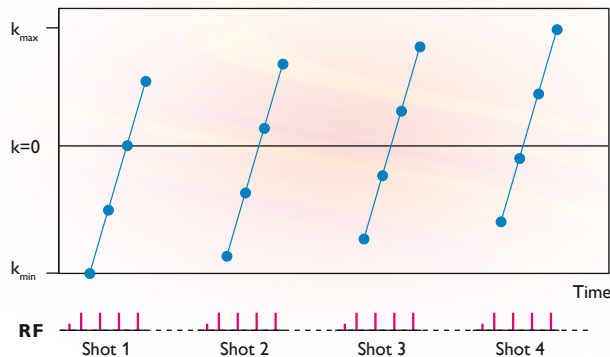


FIGURE 59

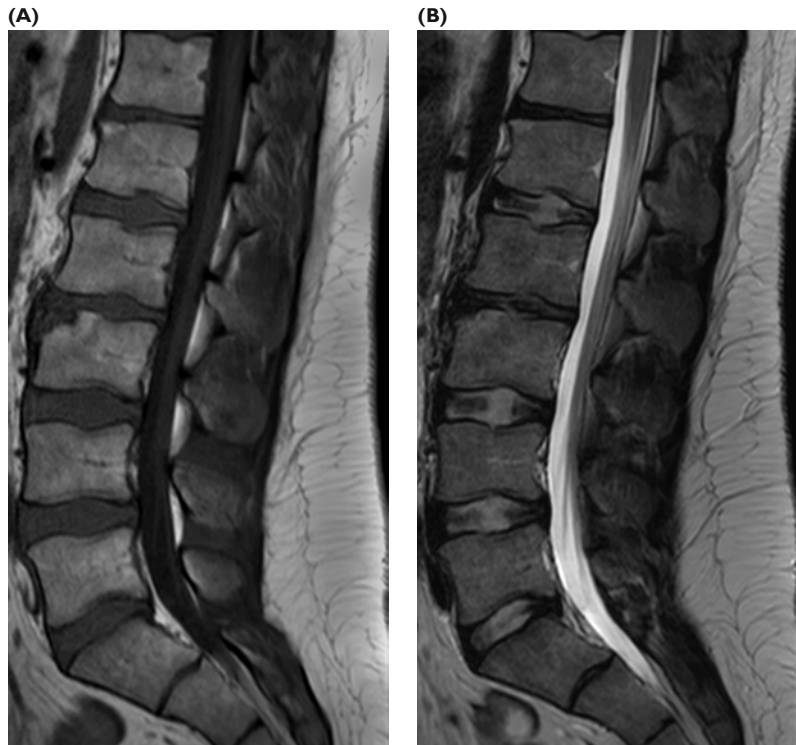
Segmented linear profile order for a multi-shot T_2 weighted turbo spin echo scan. Each line represents a multi-echo shot with a given TR. Successive shots are used to create the full image.

If 32 echoes are measured per excitation, the measurement will only require 8 TR's in order to acquire all the 256 profiles necessary to make an image with a 256×256 matrix (See Figure 59). By performing this in multi-slice mode, additional slices are obtained within the same scan time by acquiring corresponding segments for other slices within the same TR. TSE permits acquisition of a T_2 -weighted scan in a fraction of the time required for normal spin echo scan and with reduced susceptibility to motion artifacts. Unlike TFE, the turbo spin echo technique is insensitive to field inhomogeneities, since it retains the use of 180° refocusing pulses.

The contrast in a TSE image is similar to that of a spin echo image with the same TR and an equivalent TE. However, fat is usually brighter and some MTC effects are inherently present. See Figure 60. In TSE, contrast is dominated by the echo with the lowest k_y value. Usually, this is the central echo in the train, although it is possible to change the order of the phase encoding gradients profile order in order to locate the effective echo time early in the train or nearer to its end.

FIGURE 60

TSE images of a sagittal spine showing different types of contrast that can be obtained:
(A) Contrast is dominated by T_1 influence (TE 18 ms).
(B) Contrast is dominated by T_2 influence (TE 150 ms).



With TSE, a single shot acquisition – i.e. all phase encoding steps measured after a single excitation – is possible. However, the technique is generally implemented with only a subset of the necessary phase encoding steps or profiles acquired per repetition time. The echo train length or number of profiles measured per excitation is usually between 3 and 128, and is referred to as the Turbo Factor of the scan.

Dual echo imaging is equally possible in TSE as it is in spin echo. The allocation of the echoes within a shot, in such a case, is not to one image, but to two different images. Accordingly, the k_y value order can be adapted to obtain two effective echo times at the user's choice.

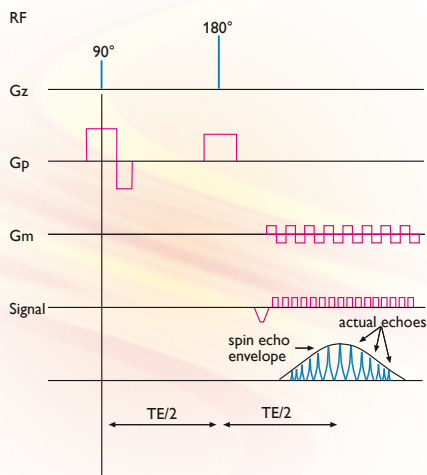
The turbo spin echo technique can be used in all parts of the body where T_2 -weighting, high resolution and short scan times are relevant. It also allows examinations which were previously impossible or impractical because of exceedingly long scan times. TSE is especially valuable in neurological imaging (brain, spine) where detailed resolution and a high number of slices is required and in abdominal imaging, where TSE permits the acquisition during breath-hold of practically motion-free images.

ECHO PLANAR IMAGING

The most condensed approach to MR imaging would encode all spatial information into the MR signal after a single excitation. While Turbo Spin Echo achieves a dramatic reduction in total imaging time by acquiring many echoes with different phase encoding per repetition time, the ultimate implementation of this idea is echo planar imaging (EPI), in which an even more favorable timing is reached by collecting gradient echoes with different phase encoding, providing complete spatial encoding after a single excitation.

FIGURE 61

An echo planar imaging (EPI) pulse sequence with a train of gradient echoes centered around one spin echo.



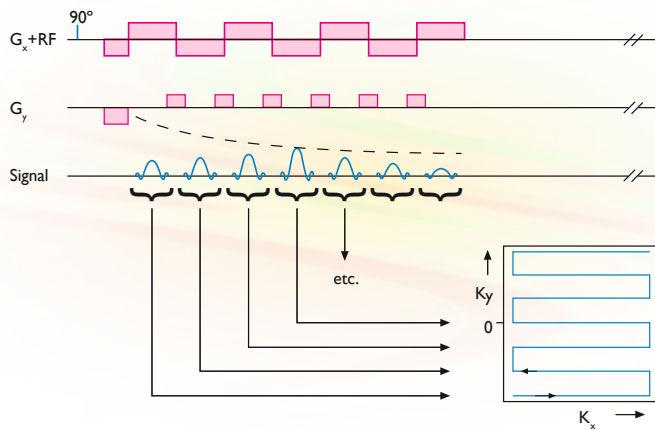


FIGURE 62

An echo planar imaging (EPI) sequence with a train of gradient echoes and the k-space trajectory.

Figure 62 illustrates the k-trajectory (in k-space) for an echo-planar image acquisition. Notice that the k-space is fully mapped by a single, sawtooth-pattern path. As illustrated in Figure 61 a spin echo version of EPI also exists. In practice, the signal-to-noise ratio of single shot EPI is often disappointing. Image quality improves by employing EPI in two or more shots instead of one to map the whole k-space. This will, however, lengthen the imaging time.

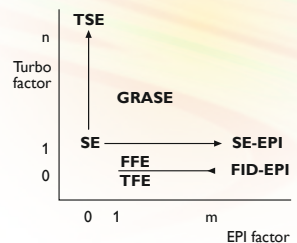
The EPI technique requires a high speed data acquisition system and rapidly switched magnetic field gradients. EPI has only recently become available for clinical use and its potential will have to be proven.

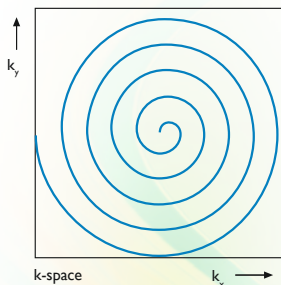
GRASE – GRADIENT AND SPIN ECHO

GRASE is in fact a combination of the turbo spin echo technique and echo planar imaging. One shot in GRASE consists of several (= turbo factor) spin echoes, each of which consists of a number (= EPI factor) of gradient echoes. All techniques (SE, FFE, TSE, TFE, EPI) could be considered as simplifications of GRASE, obtained by selecting proper turbo factor and EPI factor. GRASE offers full flexibility in choice of sequence. See Figure 63. The contrast in GRASE is expected to be closer to spin echo contrast than TSE contrast is. However, this has yet to be exhaustively proven.

FIGURE 63

All pulse sequences could be considered as simplifications of GRASE.

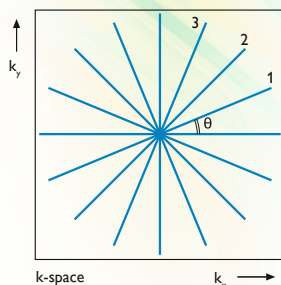


A

OTHER WAYS TO TRAVERSE K-SPACE

Instead of mapping k-space by sampling horizontal lines, alternative trajectories may be designed. In Figure 64 the k-space traversal during a spiral scan and a radial scan are shown. Such trajectories can be realized by manipulating G_x and G_y gradients during continuous data sampling. Since in these trajectories data points are not on a 2D-grid, interpolation to a 2D-grid is necessary before the 2D-Fourier transform can be performed. Or alternatively, a back-projection algorithm like in CT might be used.

Because the total k-space is mapped after one (or a few) excitations, spiral scan methods are very fast and therefore suited for dynamic imaging of fast processes and for cardiac imaging.

B

In a radial scan, more data points are acquired from the central – high intensity – region of k-space, which contributes to improve the signal-to-noise ratio and the contrast, but results in lower spatial resolution. This technique is less sensitive to motion and flow and allows the use of a short TE, since only a small phase encoding gradient is needed. The technique is actually a projection reconstruction technique, which requires a considerable reconstruction time or a strong reconstruction computer.

In a helical scan, a third dimension is added to the radial scan principle. If this is spatial encoding in z-direction an image at any z within the measured range can be calculated by interpolation. This method finds its analogy in modern CT helical scans. If the third dimension is time instead of depth, helical scan could be useful for monitoring dynamic processes.

FIGURE 64

K-space trajectory for
(A) a spiral scan and
(B) a radial scan.

Chapter 5

Practical Considerations in MR Imaging

INTRODUCTION

MR image quality is judged by clinical efficacy, not visual appearance. Magnetic resonance images are the result of a complex interaction of extrinsic (i.e. selectable) and intrinsic (i.e. patient characteristic) factors which produce an image with sufficient spatial resolution and object contrast to permit a physician to complete a diagnostic evaluation. This confluence permits manipulation of the image acquisition parameters to maximize clinical efficacy in a specific area of an image at the expense of overall image appearance.

The intrinsic factors include:

- proton density, PD or N(H)
- T_1 relaxation time
- T_2 relaxation time
- magnetic susceptibility
- flow phenomena.

The extrinsic factors include:

- repetition time, TR
- echo time, TE
- field of view, FOV
- matrix size
- number of signals averaged, NSA
- magnetic field strength
- properties of the detection coil(s)
- magnetic field inhomogeneities.

This chapter introduces the reader to these fundamental image acquisition parameters and provides a basis for understanding the relationships between them.

IMAGE QUALITY

A magnetic resonance image is composed of small elements, pixels, whose gray-scale intensity (brightness) is related to the amplitude of the MR signal arising from corresponding volume elements, voxels, in a tissue slice. The greater the signal intensity emitted by the voxel, the brighter the corresponding pixel in the image.

For an image to be diagnostically useful, anatomic features within the image must be distinguishable from each other. For optimizing image quality and imaging speed, the MR user can select many parameters, such as geometric characteristics of the slice(s), pulse sequence, scan mode, artifact reduction techniques, etc. in order to find the most appropriate balance.

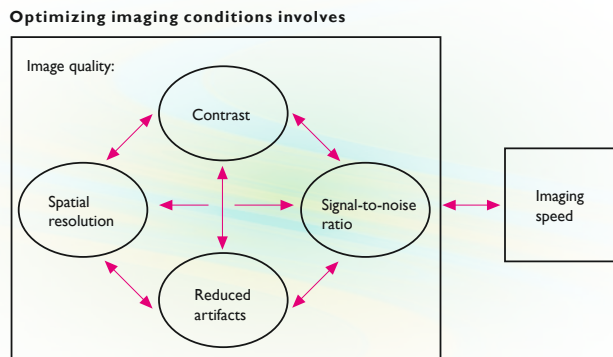
Ideally, an image would have high signal, low noise, high spatial resolution, excellent contrast and no artifacts. However, as illustrated in Figure 65, to achieve optimum conditions requires trade-offs – including consideration of imaging time. The steps required to improve spatial resolution and signal-to-noise ratio generally result in longer imaging times.

VOXEL SIZE AND SPATIAL RESOLUTION

The image matrix defines the number of pixels used to construct an image, determined by the steepness of the read-out gradient (x-axis) and the number of phase-encoding steps used (y-axis) for a given field of view (FOV). For example, in a 256 x 256 image matrix, 256 phase-encoding steps are included in the pulse program to create a matrix with 256 voxels along the y-axis. The actual volume of each voxel is determined by the field of view, the matrix size and the slice thickness selected. (See Figure 66)

FIGURE 65

Optimizing imaging conditions means finding a balance between the different several aspects of image quality and imaging speed.



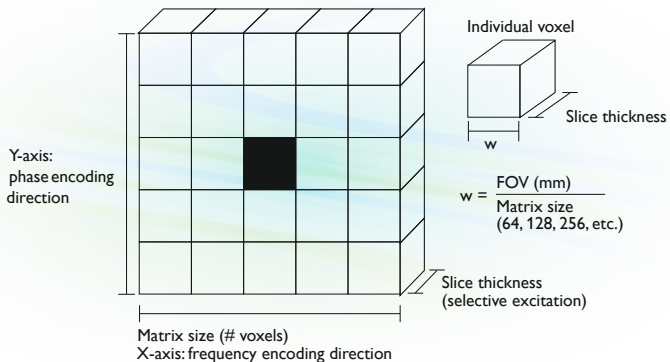


FIGURE 66
Definition of voxel size.

Spatial resolution defines the ability to resolve closely spaced anatomic details. Since the radio frequency signals from nuclei in a voxel are averaged, details within a voxel are lost during image acquisition and reconstruction. The larger the voxel dimensions the greater the amount of unresolved fine detail. However, resolution alone does not determine whether a detail is distinguishable within an image – contrast and signal-to-noise ratio are also determining factors.

Field homogeneity and the steepness of the gradients employed control the spatial resolution, which can be increased until the voxels become so small that the signal-to-noise ratio becomes the limiting factor. Resolution equals the field of view (FOV) divided by the image matrix. For an image acquired with a body coil, with a FOV of 50 cm and a 512 x 512 image matrix, the resolution is approximately 1.0 mm/pixel x 1.0 mm/pixel. Figure 67 shows two identical image slices acquired at two different resolution values.

While high spatial resolution is valuable, large image matrices require longer total imaging times, which increases the risk of patient movement during acquisition. Patient movement reduces spatial resolution by blurring image detail and can result in ghost-like image artifacts, as shown in Figure 82.

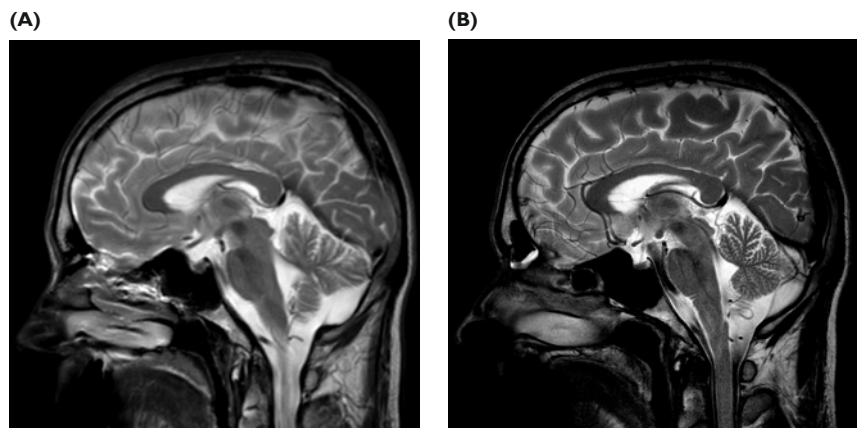


Figure 67

Two images of the sagittal brain with different spatial resolution:
(A) With 256 x 256 pixels and
(B) with 1024 x 1024 pixels.
latter image has a higher spatial resolution.

SIGNAL-TO-NOISE RATIO

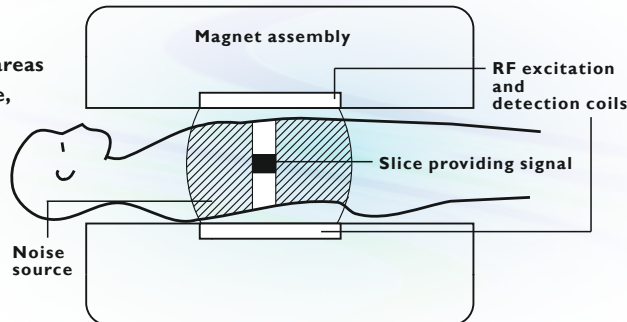
The brightness of each pixel in an MR image is determined by the signal intensity of its corresponding voxel in the tissue slice. However, the detection coil in an MR imaging system also detects RF emissions from tissue surrounding the voxel. This RF “noise” results from small, random electrical currents within the detection volume, reducing the ability to distinguish between low contrast anatomical features. (See Figure 68) In magnetic resonance imaging, the presence of background noise is the limiting factor in the detection of very weak signals.

In addition to the noise generated from within the patient, the RF coils also generate frequency-dependent noise through the resistance of the coil. This effect decreases as the strength of the applied static magnetic field increases. At typical field strengths, coil noise is very small compared to noise from the body.

The signal-to-noise ratio (SNR) is a function of both operational and data processing parameters. While data processing procedures (data filtering, sampling rate, zero filling, truncation, etc.) affect the signal-to-noise ratio, they are never as effective as reducing noise collection or increasing the relative signal to begin with.

FIGURE 68

Noise generation from areas outside the imaging slice, shown for a body coil.



The following operational parameters exert considerable influence on the SNR: voxel size, signal averaging, pulse sequence timing (TE, TR, flip angle), magnetic field strength, RF coils, half scan, reduced scan, and water-fat shift.

In a manner consistent with established computed tomography procedures, the voxel size can be decreased by decreasing slice thickness or increasing matrix size to improve spatial resolution. This, however, decreases signal intensity since it is directly proportional to voxel size. Background noise, by comparison, is independent of voxel size. Therefore, increasing the matrix size reduces the SNR. For example, as demonstrated by the images in Figure 69, doubling the matrix size from 128×128 to 256×256 while holding slice thickness constant would result in a fourfold decrease in voxel volume, a SNR reduction by a factor of $2\sqrt{2}$, and a twofold increase in the total imaging time. Conversely, you can decrease the matrix size to improve the SNR. This, however, reduces spatial resolution resulting in poorer visibility of anatomic detail.

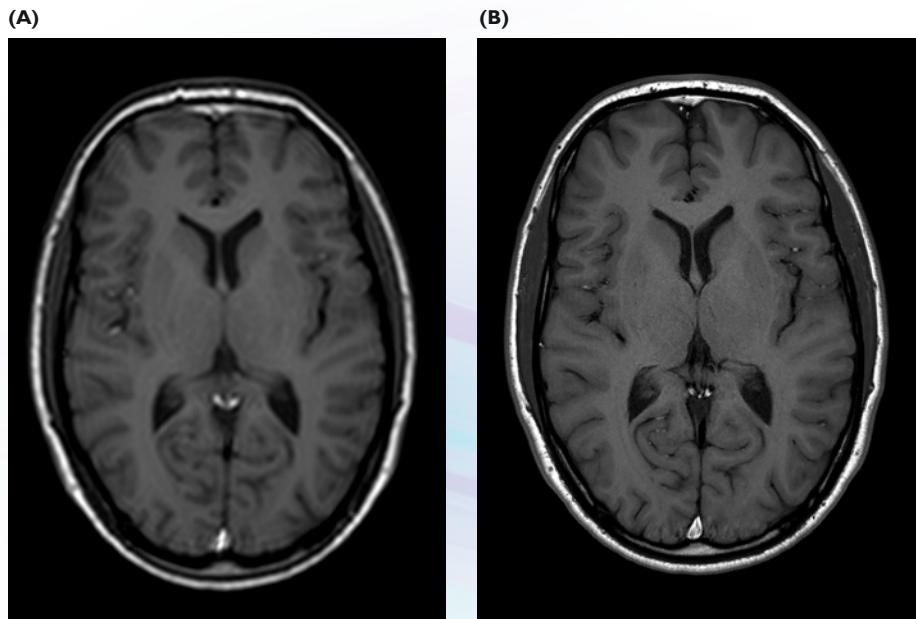


FIGURE 69

The effect of the matrix size on image appearance.

- A)** Axial slice in the brain acquired with a matrix of 128×128 .
- B)** The same slice, but acquired with a matrix size of 512×512 , resulting in higher spatial resolution, but lower signal-to-noise ratio.

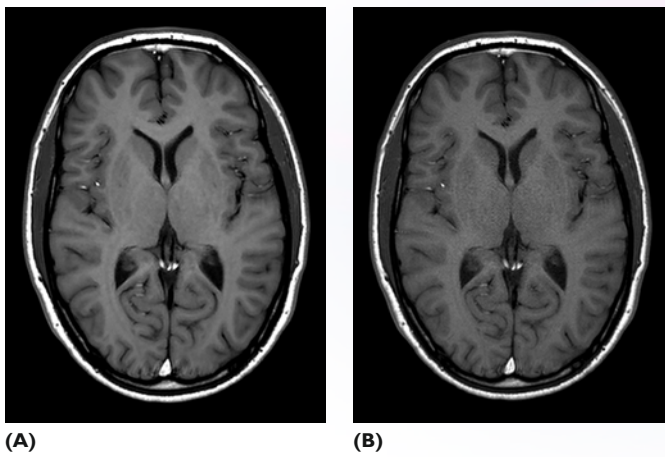


FIGURE 70

Two images, one with good signal-to-noise ratio and one with poor signal-to-noise ratio.

SIGNAL AVERAGING

Signal averaging means that signals are measured more than once and the signals from successive measurements are summed, producing a total intensity which increases linearly with the number of measurements. Noise, however, is a random process, whose intensity increases only as the square root of the number of averages. Therefore, by increasing the number of signal averages (NSA) from 1 to n, the SNR improves by \sqrt{n} . See Figure 70.

Signal averaging is not a time-efficient way to improve the signal-to-noise ratio, since significant improvements in SNR are only achieved with substantial increases in total imaging time, as shown in Table 3. It does, however, offer a way to reduce motion artifacts caused by respiratory motion or patient movement.

TABLE 3

Some values for number of signal averages NSA, relative signal-to-noise ratio and relative imaging time.

NSA	RELATIVE SNR	RELATIVE IMAGING TIME
1	1	1
2	1.41	2
4	2	4
6	4	16

PULSE SEQUENCE PARAMETERS

The magnitude of the transverse magnetization in an imaging voxel is a function of proton density and inherent relaxation phenomena. The dependence on proton density is obvious. The more nuclei present, the greater the signal.

The signal magnitude is also a function of T_1 and T_2 relaxation processes which control the magnitude and rate of decay of the transverse magnetization. By adjusting RF pulse timing, you can optimize SNR in a certain scan time. In spin echo measurements, two pulse timing parameters affect the magnitude of the MR signal: the repetition time, TR, and the echo time, TE.

The rate of recovery of the longitudinal magnetization is characterized by the T_1 relaxation time, and the degree of recovery at the end of TR is determined by the relationship of the repetition time, TR, to T_1 , the relaxation time. A short TR, one which is approximately the same as the shortest T_1 of interest, reduces the signal intensity, and since noise remains fixed, the SNR decreases. For example, at $TR \approx T_1$, the net magnetization has recovered to only about 63% of its maximum value. Of course, a short TR reduces the total imaging time, hence its use may be advantageous in specific studies.

The intensity of the MR signal is also dependent on the degree of spin-spin relaxation which has occurred, characterized by the T_2 relaxation time. The longer T_2 dispersion evolves, the weaker the net magnetization in the transverse plane. A long TE, one which is approximately equivalent to the T_2 relaxation time, produces an image whose relative contrast is primarily dependent on differences in T_2 relaxation rate (i.e. a T_2 -weighted image), and which has a greatly reduced signal intensity. At $TE \approx T_2$, the relative signal intensity is only about 37% of its maximum value.

MAGNETIC FIELD STRENGTH

Although this parameter is “fixed” in a given MR system, it is important to understand that signal strength varies as the square of the applied field. Noise is also a function of field strength, increasing linearly with the field strength. From this, it follows that the SNR improves linearly with applied field strength. In addition, the detected signal, and subsequently, the signal-to-noise ratio, are affected by the electronic characteristics of the detection coil and other electronic components.

EFFECT OF THE RF COILS

As discussed, the detection coils are sensitive to noise from surrounding tissue, with the magnitude of the noise related to the detection volume. While only the imaging slice is actively “excited” during an MR measurement, a much larger volume of the body is actually present in the detection volume of a coil. Thus, the physical configuration – size and shape – of the RF coil affects the relative magnitude of the noise. Surface coils, with their smaller sensitive volume provide a higher ratio of signal relative to background noise when compared to a volume coil such as the body coil. The size of the body coil and its distance from the patient permits a much greater contribution of noise from outside the selected slice, as depicted in Figure 71.

FIGURE 71

The impact of image coil configuration on the acquisition of background noise: the body coil picks up noise from a large volume, while a small, flexible surface coil only picks up noise from a much smaller volume.

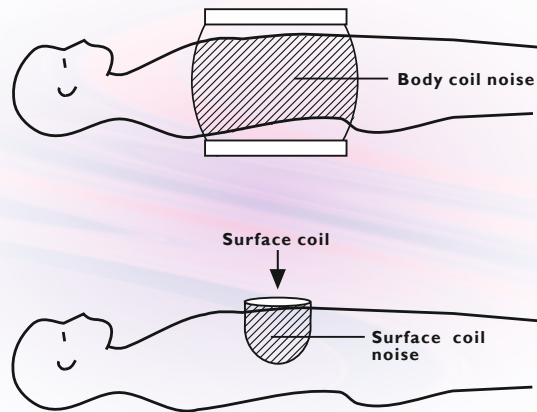


IMAGE CONTRAST

Regardless of spatial resolution and signal-to-noise ratio, MR images would have no clinical value without satisfactory image contrast. Superior soft tissue contrast is a major advantage of MR imaging versus alternate modalities such as computed tomography. Contrast is defined as the intensity difference between two tissues.

SOURCES OF OBJECT CONTRAST

Contrast in MR is a complex function of factors including intrinsic characteristics of the sample (proton density, relaxation times, T_1 and T_2 , magnetic susceptibility of the nuclei, and flow phenomena) and the programmable pulse sequence parameters (TR, TE, flip angle, etc.).

PROTON DENSITY

Proton density is perhaps the simplest factor influencing contrast. The net magnetization in a voxel is a function of the total number of protons present in that voxel. This determines the maximum possible signal intensity. For most images, proton density equals the number of mobile protons present in each voxel- mostly protons in water, fats, and in the hydration layers of biological macromolecules such as proteins. Non-mobile protons – e.g. protons in solids – have very long T_1 and very short T_2 relaxation rates which prohibit them from contributing to the measurable MR signal intensity. If no mobile protons were present, no signal would be emitted from the voxel. Objects with a low total mobile proton density include cortical bone, air and, sometimes, fibrous tissue. The corresponding image pixels for these voxels appear black regardless of the pulse program used.

By comparison, tissues with high mobile proton density, such as fatty tissue, blood, or cerebrospinal fluid (CSF), produce a free induction decay signal with a large initial amplitude. However, high proton density does not necessarily guarantee high signal intensity in the image, since the signal is subject to modulation by other factors, including T_1 and T_2 relaxation.

The inability to produce a high signal intensity does not preclude visualization of detail in a tissue slice. In CT, for example, air pockets are able to be identified because of the surrounding tissue. Similarly, MR images are able to provide some information on low proton density objects, such as calcifications or plastic implants, by contrast with surrounding tissue.

T₁ AND T₂ RELAXATION

As discussed in Chapter 2, after the nuclear spin system is excited, the signal amplitude is proportional to the transverse magnetization, which decays at a rate characterized by spin-spin relaxation time T₂. The rate of return of the longitudinal magnetization back to its equilibrium state is characterized by spin-lattice relaxation time T₁.

While proton density exerts a simple influence on image contrast, the influences of T₁ and T₂ relaxation are more complex, providing the most powerful source of contrast differentiation in MR images. T₁ and T₂ relaxation phenomena are responsible for the superior soft tissue contrast which MRI provides versus CT.

TR, TE AND CONTRAST IN SPIN ECHO IMAGING

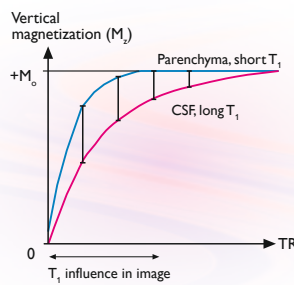


FIGURE 72

Recovery of longitudinal magnetization M_z for CSF and parenchyma after a 90° pulse. This shows how contrast is related to T₁ differences between tissues and can be controlled by selection of TR in a SE sequence.

Having re-established the framework for MR relaxation in biological samples, let's consider how the pulse sequence parameters, repetition time (TR) and echo time (TE), can be used to optimize contrast between different tissue types in a standard spin echo image.

T₁ relaxation can be used as a source of contrast in an image by variation of the repetition time. Objects with a long T₁ include cerebrospinal fluid or tumors, while those with a short T₁ include parenchyma and fat. Typical normal T₁ values for brain parenchymal tissue range between 500-800 ms for white matter and 600-950 ms for gray matter, depending on field strength (refer to Table 1). By comparison, typical CSF T₁ values are between 2000-4000 ms. By appropriate adjustment of imaging parameters (TR and TE), you can create a T₁-weighted image in which the image contrast is largely determined by differences in the T₁ relaxation of the tissues imaged.

Figure 72 illustrates how a variation of the repetition time affects contrast between brain parenchyma and CSF in a spin-echo imaging sequence. At long TR values, the difference between both magnetizations becomes smaller. Shorter TR values, however, provide ample differences for contrast differentiation. This qualitative approximation does not quantitatively account for small differences in proton density between the two tissue types. Proton density determines the maximum magnetization (M₀) that will be reached, in this example, for CSF and parenchyma.

It is important to remember that the value of TR also influences signal-to-noise ratio and total imaging time. Note that the best SNR is achieved at long TR values (e.g. 2500 ms), where signal intensity is the strongest, however, this adds significantly to total imaging time. The use of a shorter TR (e.g. 500 ms) permits background noise to become a more significant factor in image contrast. However, even if more signal averages are used ($NSA > 1$) to compensate for increased noise, imaging times are still acceptable.

Similarly, it is possible to effect changes in image contrast through manipulation of T_2 relaxation. In general, tissues with high proton density and long T_2 relaxation times appear brighter in spin echo images than tissues with short T_2 relaxation times. See Table 4. Tumors, cerebrospinal fluid, and inflammation all have relatively long T_2 relaxation times while parenchyma typically exhibits a short T_2 .

	DARK	BRIGHT
T_1 -weighted image	long T_1	short T_1
T_2 -weighted image	short T_1	long T_1

TABLE 4
Relation between image intensities and T_1 and T_2 of a tissue.

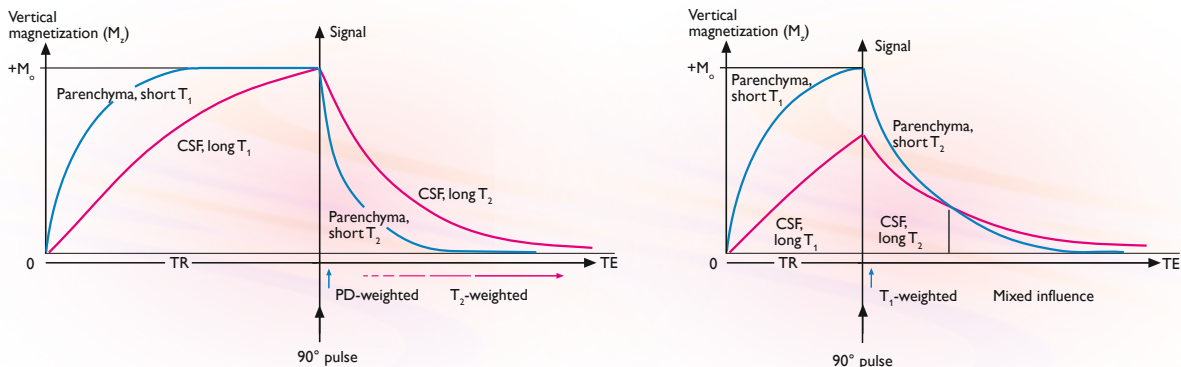
Figure 73 illustrates the effect of varying the echo time (TE) on a spin echo image for parenchyma and CSF. The complexity of the relationships governing image contrast are more apparent, since the impact of changes in the echo time is clearly dependent on the value of the repetition time. In Figure 73(a), a long TR was set, which permits nearly complete recovery of the net magnetization between successive pulse repetitions, assuring that the magnetization does not depend on the T_1 's of the tissues.

If TE is very short, the influence of T_2 relaxation is still negligible and hence signal intensities reflect proton density. When the TR value is long, the relative difference between long and short T_2 components of the image increases rapidly as TE is increased. At a sufficiently long TE value, only components with a long T_2 will remain visible – in our example, the parenchymal signal decays well before the CSF signal. For this case, tissue components with a longer T_2 value are always brighter in the final image than components with short T_2 values, regardless of the value of TE.

In Figure 73(b), a short TR was used. When a short repetition time is selected, a more complex relationship exists. Contrast is now also dependent on whether the object of interest has a long or short T_1 value. CSF which has a long T_1 value as well as a long T_2 , experiences incomplete recovery of the net magnetization between pulse repetitions. Therefore, when a short TE is used its signal is weaker than that of parenchyma. However, as TE is increased, the signal from parenchyma is affected more dramatically since it experiences greater T_2 decay, reducing the net magnetization in the transverse plane. Therefore, as TE is increased, the parenchymal signal decays rapidly until it “crosses over” and becomes weaker than the CSF signal. With long TE, CSF is once again the brighter object in the image.

FIGURE 73

- Contrast as a function of echo time for a SE sequence:**
- (A) With long TR vertical recovery is almost complete, thus eliminating T_1 influence, so that intensity differences are determined by T_2 differences**
 - (B) With a shorter TR the intensities contain mainly T_1 influence shortly after the 90°, while somewhat later this becomes both T_1 and T_2 influence.**



	short TE	long TE
short TR	T ₁ -weighted	mixed contrast
longTR	proton density weighted	T ₂ -weighted

Table 5 summarizes the image weighting factors for spin echo images. A T₁-weighted image usually corresponds to a short TR (typical 500 ms) and short TE (typical 20 ms). A T₂-weighted image generally employs a long TR (typical 2000 ms) and long TE (typical 90 ms). The combination of long TR and short TE yields a proton density weighted image.

Figure 74 demonstrates the effect of TE and TR on clinical image appearance.

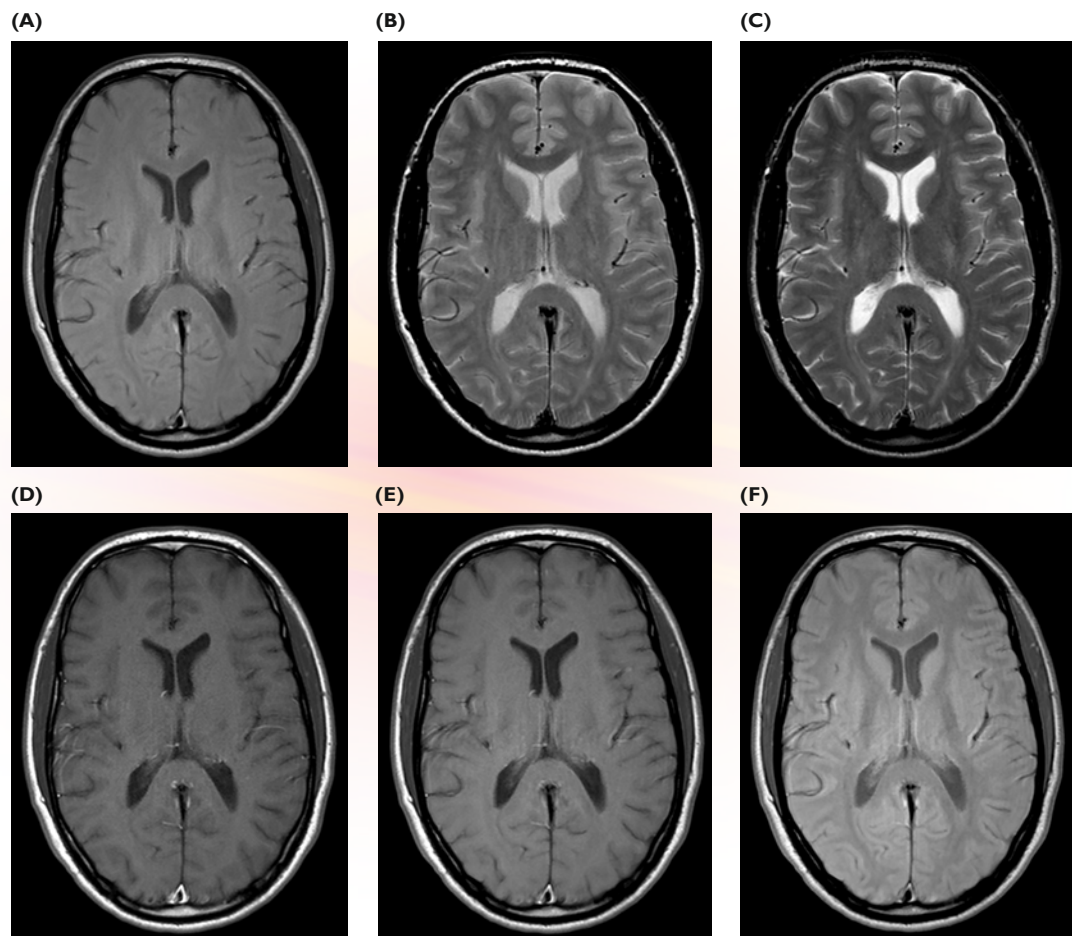


TABLE 5

Image appearance as a function of TR and TE for spin echo images.

FIGURE 74

Image appearance as a function of TR and TE for spin echo images:

- (A) TR 1500 ms, TE 20 ms
- (B) TR 1500 ms, TE 80 ms
- (C) TR 1500 ms, TE 122 ms
- (D) TR 400 ms, TE 20 ms
- (E) TR 800 ms, TE 20 ms
- (F) TR 2000 ms, TE 20 ms

TR, TE, PULSE FLIP ANGLE AND CONTRAST IN GRADIENT ECHO IMAGING (FFE)

In spin echo imaging, two selectable parameters determine image contrast – the repetition time and the echo time. In gradient echo imaging, a third – pulse flip angle – plays an equally significant role in contrast determination. Contrast phenomenology in gradient echo imaging is extremely complex.

To begin, recall that the application of gradient reversal to generate an echo signal does not reverse the spin dephasing effects of magnetic field inhomogeneities (refer to Chapter 4). Thus, in discussing contrast in gradient echo imaging, we are concerned with the T_2^* relaxation time instead of T_2 .

In gradient echo imaging, the pulse flip angle can be used as the principle lever controlling the dependence of the MR signal on the T_1 values of the tissues. A T_1 -weighted image can be generated using a large flip angle (30° - 90°) with a short echo time (8-15 ms) and a long TR. The contribution of T_1 to image contrast can be reduced by lowering the flip angle or increasing TR.

A T_2^* -weighted image can be acquired using a long echo time (30-60 ms) in conjunction with a small flip angle (5° - 15°) and a relatively long TR (200-400 ms). In this scheme, the echo time is set sufficiently long to permit evolution of the T_2^* spin dephasing, while the repetition time is set just long enough to assure essentially complete recovery of the partially-tipped longitudinal magnetization vector between successive pulses.

A predominantly proton density-weighted image requires reduction of the T_1 and T_2^* contributions, achieved through the use of very small flip angles (5° - 15°) and short echo time (8-15 ms) along with a long TR.

These conditions are summarized in Table 6.

TABLE 6

Comparison of parameter settings to achieve T_1 -, T_2^* and PD-weighted Images using FFE imaging with relatively long TR (200-400 ms).

IMAGE CONTRAST	PULSE FLIP ANGLE	TE (ms)
T_1 -weighted	Large (45 - 90°)	Short (8-15)
T_2^* -weighted	Small (5 - 20°)	Long (30-60)
PD-weighted	Small (5 - 15°)	Short (8-15)

If $TR \leq T_2^*$, another degree of complexity is added. As TR is reduced, the transverse magnetization will not completely disappear between successive RF pulses. Subsequent RF excitation flips both the recovered longitudinal magnetization and the residual transverse magnetization through an angle. In the process, some of the residual transverse magnetization is converted back into longitudinal magnetization, creating a signal enhancement. This steady-state signal enhancement will occur for protons which possess a long T_2^* , such as cerebrospinal fluid, whenever very short repetition times are used. In this case, the contrast is partially T_2^* -dependent, although it retains strong dependency on both proton density and the ratio of T_2^*/T_1 . Very short TR pulse sequences are frequently employed in imaging of CSF where the signal enhancement is pronounced. For volume imaging (scan mode 3D), T_1 -weighted images are obtained with a TR of typically 30 ms and T_2^* -weighted images with a TR of typically 60 ms.

In addition, short TR gradient echo sequences are commonly employed in cardiac imaging where temporal resolution is important for acquisition of multiple images in rapid succession.

FLOW PHENOMENA

T_1 , T_2 and proton density are the basic influences on image contrast in most MR images. However, other factors can dramatically influence the image appearance, including flow phenomena in blood or CSF.

Flow phenomena in MRI are generally categorized into two groups: inflow effects and phase effects. Inflow effects, also called time-of-flight, velocity or inflow/flow void, are dependent on RF pulse timing and signal type (spin-echo/gradient echo). Phase effects result from the velocity sensitive disruption of acquired phase characteristics which the spins accumulate as they move along a gradient. A variety of image effects, including signal enhancement (usually a time-of-flight effect) and ghosting, result from flow. In many cases, both inflow and phase effects are at work.

INFLOW EFFECTS

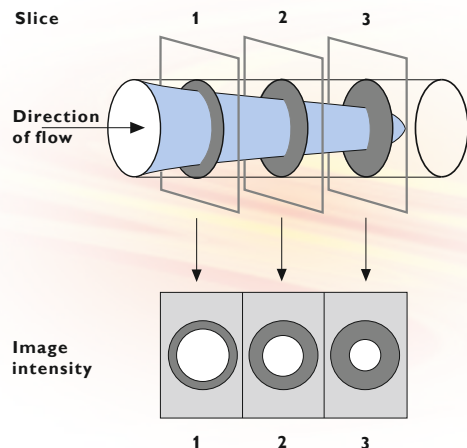
Time-of-flight effects can alter image appearance whether the flow is perpendicular to the imaging plane or within the imaging slice, and can produce either signal enhancement (bright blood) or a signal reduction (flow void).

FLOW ENHANCEMENT

During a SE or FFE examination, stationary spins are repeatedly excited by RF pulses and, depending on the imaging parameters, may become partially saturated. If the liquid within the voxel now moves perpendicularly through the imaging plane during the acquisition with uniform velocity, some of the nuclei in the voxel will be replaced by “fresh” nuclei which have not been previously excited by RF pulses, because they come from outside the excitation slice or volume. Since the replacement spins are not saturated, the signal from within the voxel is enhanced, a phenomenon called flow-related enhancement. (See Figure 75). Flow-related enhancement occurs in blood, CSF, and other fluids within the body. The magnitude of the enhancement is dependent on many factors, including the thickness of the image slice, the repetition time, the flip angle in FFE and field strength. In general, the longer the TR, the smaller the enhancement, since it is a function of partial saturation of the spins which do not leave the image slice. Inflow magnetic resonance angiography is based on this enhancement, as will be described in Chapter 6.

FIGURE 75

In smaller blood vessels usually a laminar flow pattern is observed, where blood flows most rapidly in the centre of the vessel and slower near vessel walls. Inflow signal enhancement will therefore be stronger in the centre of a blood vessel.



In certain cases, flow-related enhancement may confuse image interpretation ,or result in artifacts. For example, high signal intensity in the vessels can obscure intraluminal abnormalities such as dissections, tumors, and thrombi. It also tends to reduce contrast between small vascular structures and surrounding tissue. In these cases, it is possible to use presaturation pulses to reduce or eliminate the effects of flow-related enhancement. Typically, an additional 90° pulse is used to presaturate spins before they enter the imaging slice, eliminating the enhancement effect. REST (REgional Saturation Technique) is a pulse sequence to accomplish presaturation, which permits effective suppression of flow artifacts by saturating slabs on one or both sides of the image slice. An adequate signal void in blood vessels is then realized, enabling better clinical diagnosis. (See Figure 76).

FLOW VOID

If the flow velocity through the image slice in a spin echo measurement is increased, the nature of the flow effect changes. Now, the predominant effect is the result of spins leaving the image slice between the 90° excitation pulse and the 180° refocusing pulse. Since both pulses are required for a signal to be detected (and both pulses are usually slice selective), a decrease in signal is observed, a phenomenon called high-flow void, as shown in Figure 77. Note that signal reduction results from the use of slice selective 180° refocusing pulses, which act only upon the image slice, not outside the slice. Like inflow enhancement, outflow signal reduction is field-dependent and dependent on the slice thickness. However, it is sensitive to the echo time (TE) not the repetition time, since the magnitude of the signal loss is dependent on the time between the 90° and 180° pulses.

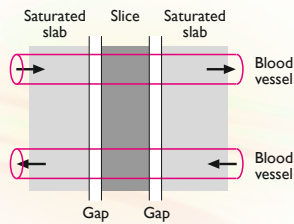
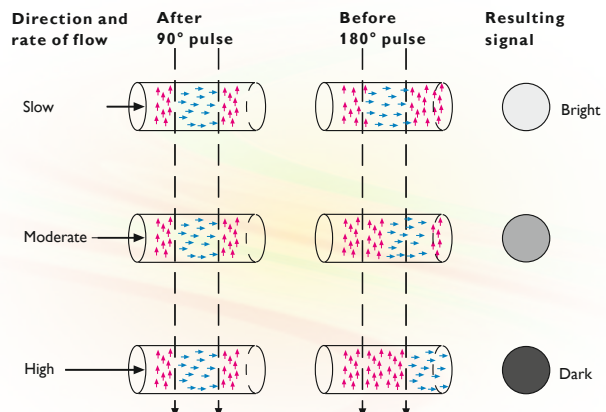


FIGURE 76

Schematic representation of parallel REST being used to saturate tissue slabs outside the region of interest in order to eliminate inflow enhancement.

FIGURE 77

Flow void signal reduction in spin echo: During the time between the 90° and the 180° pulse, blood in the selected slice is (partly) refreshed, so that only a fraction of the excited spins will “feel” the 180° pulse and be refocused to contribute to the signal.



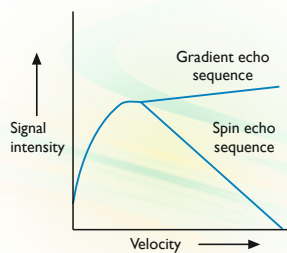


FIGURE 78

Graph of signal intensity versus flow rate for gradient echo and spin echo.

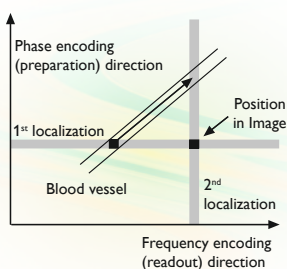


FIGURE 79

Misregistration is an in-view time-of-flight effect. It is due to the fact that phase encoding and frequency encoding are separated in time.

The behavior of the high velocity flow effects changes when a gradient echo acquisition is performed. Gradient reversal occurs over the full imaging volume; therefore, even if the excited nuclei leave the image slice after the initial 90° pulse, gradient refocusing can still occur outside the slice and a signal can be detected. Thus, rapidly flowing blood will appear bright relative to surrounding stationary tissue in most gradient echo sequences. This results from partial saturation of the stationary tissue and continual refreshment of the blood flowing through the image section. These effects are summarized in Figure 78.

MISREGISTRATION

Within an image slice, time-of-flight effects can also alter image appearance. In this case, the effects arise from the time lag between the application of the phase and frequency encoding gradients. This results in spatial misregistration of the individual voxels, as depicted in Figure 79. This occurs only when the vessel is oblique to the sides of the slice. The magnitude of the misregistration and resulting blurring or ghosting are especially prominent on second echo images, where the additional time lag permits greater movement within the image slice. Spatial misregistration can be eliminated by a special type of flow compensation, which involves additional gradients.

PHASE EFFECTS

The concept of “phase” relates the time-dependence of the magnitude and direction of movement of an object. This concept can be applied to moving nuclei in a vessel during an MR study. Figure 80 depicts laminar flow, which has a parabolic velocity profile across the vessel lumen. Note that the velocity of voxels near the vessel wall falls off quickly and that different velocities exist even within a single voxel. At the time the 180° refocusing pulse is applied during a spin echo measurement, each spin will have experienced a unique magnetic history which affects its specific Larmor frequency, since it experiences a different gradient at every position of its flow trajectory. Different frequencies result in different phases within one voxel and subsequently lead to loss of signal.

Phase phenomena are responsible for the signal enhancement behavior known as even echo rephasing. If after the 180° pulse, we allow two echoes to evolve – without using flow compensation – the second echo for flowing spins is commonly stronger than the first, due to correction of phase differences in the second echo. Even echo rephasing occurs only when the gradient that causes the dephasing is symmetrical (i.e. evenly distributed) on either side of the 180° pulse, and if the flow within the vessel is uniform. Pulsatile or accelerating flow eliminate the effects of even echo rephasing. In addition, only partial signal enhancement due to even echo rephasing will occur if any component of the flow is perpendicular to the imaging plane.

Flow compensation sequences can be used for both SE and FFE to correct for phase-based variations in signal intensity. Even in the case of higher order motion, such as acceleration, extra gradient waveforms can be applied during the spin preparation phase of the pulse sequence, permitting complete rephasing of mobile spins. The limitation of the approach is the time required for application of complex gradient waveforms, making the shortest TE longer and making it generally impractical to compensate for other than constant velocity flow.

TURBULENT FLOW

Both spin echo and gradient echo images are sensitive to signal loss due to turbulent flow. If a large spread in velocities exists, like in turbulence, signal loss occurs due to intravoxel dephasing, an irreversible loss of phase coherence. Turbulent flow or disturbed flow occur at sites such as stenotic lesions, vessel bifurcations, and valvular disorders resulting in regurgitation. Signal loss is a function of the viscosity of the flowing liquid, the vessel diameter, and the velocity of flow. The effect cannot be reduced by flow compensation. This phenomenon is shown in the image in Figure 83.

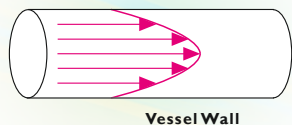


FIGURE 80

Laminar flow with a parabolic velocity profile in a blood vessel.

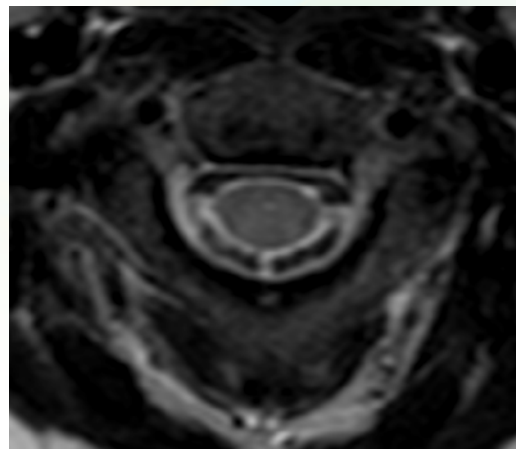


FIGURE 81

Transverse image of the C-spine showing flow voids in CSF.

MAGNETIC SUSCEPTIBILITY AND PARAMAGNETISM

Magnetic susceptibility represents the ability of a substance to become magnetized. In locations where neighboring tissues have large differences in magnetic susceptibility (e.g. air-tissue, bone-soft tissue, tissue-hemorrhage), artifacts occur on gradient echo images — air or bone appear distorted or enlarged.

Magnetic susceptibility is primarily a function of an atom's electron configuration, rather than its nuclear configuration, because the angular momentum possessed by the electrons is much greater than that of the nucleus. Most atoms have no unpaired electrons and possess only a small negative magnetic susceptibility. That indicates a slight tendency to produce a magnetic field aligned opposite to the direction of the applied field. This covers virtually all elements of interest in MR imaging.

By comparison, ions or molecules with one or more unpaired electrons, when placed in a magnetic field, generate a magnetic moment which tends to align with the applied field and which is 3-8 orders of magnitude stronger than the moment generated by the nucleus. These ions or molecules are referred to as paramagnetic, superparamagnetic, or ferromagnetic ions, depending on their specific electronic configuration. Of greatest interest in MRI are the endogenous and exogenous paramagnetic compounds such as methaemoglobin, melanin, gadolinium (Gd^{3+}), iron (Fe^{2+} , Fe^{3+}), and manganese (Mn^{2+}). These compounds may be present due to edema or hemorrhage, metallic implants, or the use of paramagnetic contrast agents. This last topic is discussed later in this chapter.

In solution, these molecules or ions tend to act as local relaxation enhancers for nearby protons. They affect both T_1 and T_2 relaxation through a process called proton-electron dipole-dipole interaction. This describes the interaction of the magnetic moments generated by the electrons with the magnetic moments generated by the protons. Paramagnetic ions do not generate any signal themselves. Their only effect is on neighboring nuclei. In addition, the proton-electron dipole-dipole interaction mechanism is only effective between two highly proximate species. Thus, paramagnetic relaxation generally only occurs in solutions when the two compounds can come into close contact.

The increase in T_1 or T_2 relaxation rate resulting from the presence of paramagnetic species is directly proportional to their concentration. At low-to-intermediate concentrations, paramagnetic ions predominantly affect T_1 relaxation. By increasing the efficiency of recovery of the longitudinal magnetization (i.e. shortening of T_1), the signal strength on T_1 images is increased. At higher concentrations, the effects on T_2 relaxation begin to dominate, even when relatively short echo times are used. By increasing spin dephasing, paramagnetics result in a sharp signal decrease in T_2 -weighted images. In all cases, the effects of paramagnetic materials are independent of field strength.

ARTIFACTS AND ARTIFACT REDUCTION TECHNIQUES

As with other imaging modalities, MR images are subject to artifacts resulting from acquisition or data handling problems or from biological processes within the patient. Most current systems deal effectively with the sources of technical and data handling errors, including truncation errors and eddy current distortion. Truncation errors occur at high-contrast interfaces and appear as ringing, or parallel high/low signal bands near sharp edges. High-contrast interfaces are the most difficult to represent mathematically, requiring large data sets. Occasionally, data truncation is utilized to create a manageable data set. This loss of data can result in approximation errors visualized as artifacts in the image in certain cases.

Eddy current distortion is the result of gradient switching during acquisition, and can produce distortions, image degradation and phase errors. Eddy currents can persist within the magnet cryostat, affecting subsequent acquisitions, though many modern imagers employ compensation routines (e.g. software predicted eddy current compensation) to eliminate eddy current effects in images.

Patient-related artifacts include motion artifacts, chemical shift artifacts, magnetic material effects. Flow phenomena sometimes give rise to artifacts, while on the other hand MR angiography is actually imaging of flow.

MOTION ARTIFACTS

Motion results in ghosting or blurring of image details in MR images. See Figure 82. There are a variety of sources of motion, including: patient motion (especially problematic in pediatric imaging), periodic respiratory or cardiac motion, swallowing or CSF flow.

The blurring associated with motion is generally slight and occurs in the direction of the motion. Ghost images generally occur in the direction of the phase-encoding gradient and are independent of the direction of the motion. Examples of motion artifacts include ghost images superimposed on nearby structures that result from pulsatile flow of CSF. Another example is ghosting that results from respiratory motion of the high-intensity subcutaneous fat of the ventral thoracic and abdominal wall.

FIGURE 82

Image showing ghosting due to motion of the patient's neck.



A variety of strategies have been developed for combating motion artifacts because of their common occurrence. These include:

Signal Averaging

Motion artifacts are “averaged out” in a manner similar to background noise. Since motion occurs randomly, heavy averaging tends to reduce the contribution of artifacts to the final image, although there is an increase in total imaging time.

Cardiac Triggering

In cardiac imaging, the acquisition is generally triggered by an electrocardiogram and is tied to the RR interval. This effectively eliminates the blurring and artifact problems inherent in cardiac imaging, although it does somewhat limit imaging strategies.

Respiratory Gating

Acquisition takes place only during the “gate”, when the respiratory movement is minimal. It is relatively effective at minimizing the effects of thoracic motion, but results in substantial increases in imaging time and, hence, is not commonly employed.

PEAR (Phase Encoded Artifact Reduction)

PEAR was developed to minimize the effects of respiratory artifacts without sacrificing imaging time. PEAR uses a bellows device to detect patient respiration, through either abdominal or chest wall changes and then generates an electronic respiration signal. The motion-sensitive data (low k-profiles) are collected in the quiet phase of respiration, the less motion-sensitive profiles during the rest of the time.

Respiratory Triggering

In analogy to cardiac triggering, respiratory triggering can also be used to generate an electronic signal upon expiration to start data acquisition.

Flow Compensation

Flow compensation is also referred to as gradient moment nulling or motion desensitization. It involves the balancing of the phase for both stationary and moving spins at the time of echo. The FLAG (Flow Adjustable Gradients) sequence accomplishes this task, compensating for constant velocity, constant acceleration and pulsatile motion.

REST (REgional Saturation Technique)

With REST, spins outside the slice of interest can be presaturated by using additional RF pulses preceding the standard sequence, so that these spins have no net magnetization during the acquisition. REST slabs can be parallel or perpendicular to the slice, or free. REST is used to eliminate artifacts caused by motion or blood flow.

Breath Holding and Abdominal Compression

Both techniques are employed whenever short acquisition sequences are employed, thereby minimizing the strain on the patient.

FOLD-OVER SUPPRESSION

Fold-over, also known as backfolding, aliasing or wrap-around, occurs if the dimension of the scanned object in the preparation direction is larger than the field of view: Tissues from outside the field of view are folded back into the image at the opposite side, where they do not belong. Fold-over can be suppressed either by using REST or by oversampling, i.e. the field of view in the preparation direction is doubled, so that it contains the unwanted parts, which are then ignored during image reconstruction.

CHEMICAL SHIFT ARTIFACTS

Nuclei of different elements resonate at specific frequencies. In addition, the specific resonance frequency is dependent upon molecular environment. The term “chemical shift” is used to describe the variations in resonant (Larmor) frequency which result from differences in molecular environment. The relative shift in Larmor frequency is caused by slight non-uniformity in the local magnetic field which results from nearby nuclei and electrons.

In clinical use, this phenomenon becomes a factor when imaging at fat-water interfaces. Virtually all regions of the body, except the central nervous system, have abundant fat-water interfaces. These two substances have slightly different resonant frequencies - about 3.4 parts per million (ppm) apart. When an image is reconstructed, the system cannot distinguish between frequency shifts which result from the spatial encoding read-out gradient and from chemical shift. As a result, a displacement occurs in the image along the interface between the lipids and water. This results in hypointense and hyperintense lines at the boundaries between organs and surrounding adipose tissue resulting from a 5-6 pixel displacement (for 1.5T; this is 1-2 pixels for 0.5T) of the signals in the measurement direction due to chemical shift. Chemical shift is highly dependent on the magnetic field strength, hence the chemical shift displacement is also field dependent (increases with increasing field) and is a function of the magnitude of the applied frequency encoding gradient (increases with decreasing gradient strength since the frequency difference per pixel decreases).

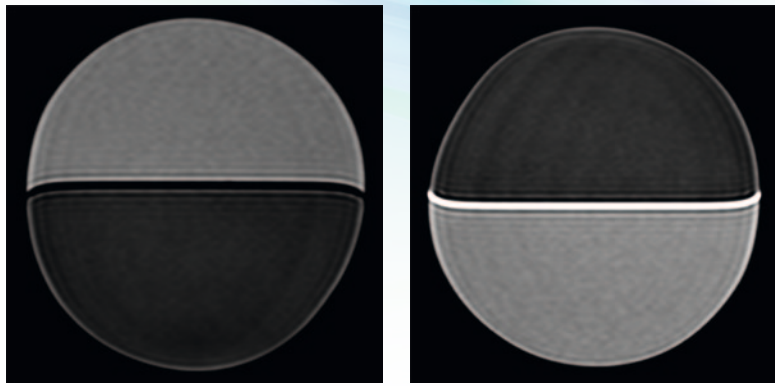


FIGURE 83

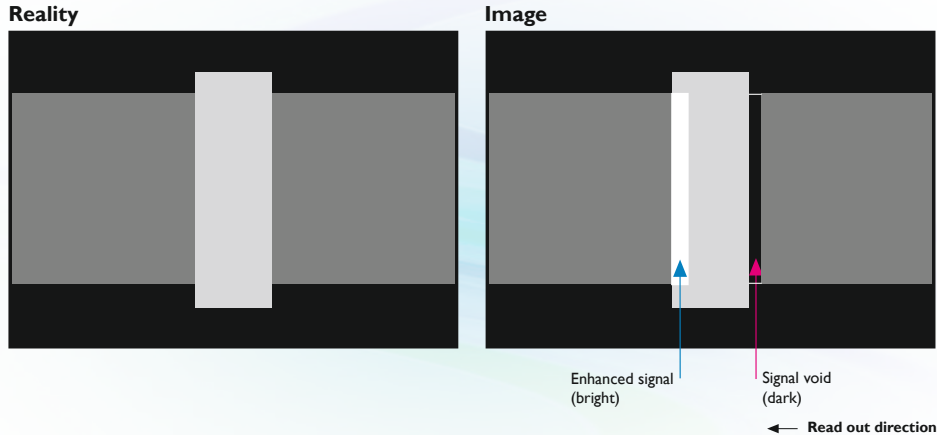
Images showing water-fat shift in a phantom: At the water-fat interface a dark line appears, while at the fat-water interface enhanced intensity is observed.

To illustrate this phenomenon, let's look at an example. For a read-out gradient of 1 mT/m, and a typical pixel size of 1 mm, the field difference per pixel is 1×10^{-6} T. The resulting frequency difference per pixel is $1 \times 10^{-6} \times 42.6$ MHz = 42.6 Hz. At 1.5T field strength, the chemical shift of 3.4 ppm between water and fat is about 220 Hz. Therefore, water and fat are displaced by about 5 pixels width which is clearly visible. At 0.5T field strength, this displacement is only 1 to 2 pixels, reflecting the relationship between chemical shift and field strength. (See Figures 83 and 84). On Philips MR systems, the water-fat shift parameter, WFS, can be set to limit the shift to a specified number of pixels at the expense of some loss in signal-to-noise ratio.

A second effect is that due to the frequency difference between water and fat, spins within a voxel can be out of phase – i.e. cancel intensities, when using FFE. This results in dark outlining of tissues. For FFE on a 0.5T system, water and fat are out of phase when TE is an odd multiple of 6.9 ms. For TE being an even multiple of 6.9 ms, water and fat are completely in phase.

FIGURE 84

Schematic explanation of water-fat shift, an example of a chemical shift artifact.



MAGNETIC MATERIAL ARTIFACTS

MR images are extremely sensitive to minute distortions in magnetic field homogeneity. The magnetic field can be locally distorted by ferromagnetic implants, such as hip prostheses or surgical wires, fillings in teeth, or even by minute residues such as filings from surgical saws. In addition, certain non-ferromagnetic objects, such as stainless steel biopsy needles with low nickel content, can also cause field distortion. These materials condense the magnetic field lines.

The effect of local magnetic field inhomogeneity is a geometric distortion of the final image. The appearance is similar to that of a picture being asymmetrically stretched or pushed from behind. The distortion results from eddy currents induced in the implant by the switching of the gradient currents. The appearance can sometimes be confusing since the distortion is often larger than the size of the object causing the distortion.

PARAMAGNETIC CONTRAST AGENTS

In most images, intrinsic parameters such as T_1 , T_2 and proton density are the primary sources of image contrast. The ability to acquire routine images without the use of radiopaque contrast agents is one of the major advantages of MR as a clinical modality. In certain instances, however, even MR fails to provide adequate discrimination between tissue structures. In these circumstances, the use of a relaxation enhancing contrast agent can be employed.

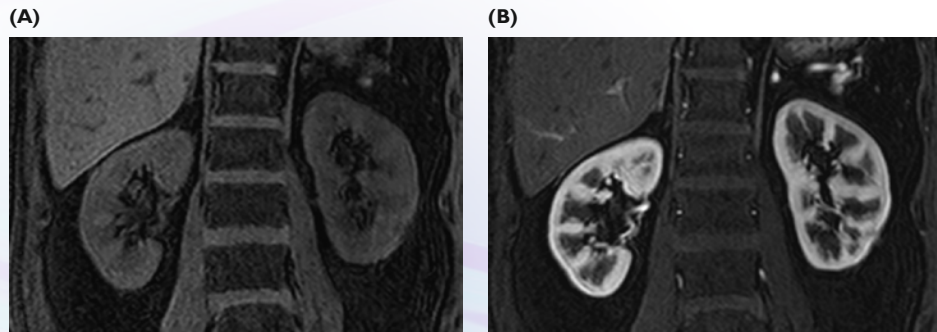
As discussed previously, ions or molecules with one or more unpaired electrons, when placed in a magnetic field, generate a magnetic moment which tends to align with the applied field and which is 3-8 orders of magnitude stronger than the moment generated by the nucleus. These ions or molecules are referred to as paramagnetic, superparamagnetic, or ferromagnetic ions, depending on their specific electronic configuration. Of greatest interest in MR are a class of exogenous paramagnetic compounds such as gadolinium (Gd^{3+}), iron (Fe^{2+} , Fe^{3+}), and manganese(Mn^{2+}).

The effects resulting from use of paramagnetic ions are the same as for endogenous paramagnetic species discussed earlier. While gadolinium (Gd^{3+}), iron (Fe^{2+} , Fe^{3+}), and manganese (Mn^{2+}) are all effective at accelerating T_1 relaxation, Gd^{3+} has gained the most widespread acceptance. The acute toxicity of Gd^{3+} at clinically relevant dosages restricts its use as a free ion. Chelation to molecules such as diethylene triamine pentaacetic acid (DTPA) reduces this toxicity and permits intravenous injection in clinical studies. The Gd^{3+} -DTPA complex has similar distributional properties to conventional iodinated contrast agents used in X-ray examinations. It has demonstrated broad potential, including the ability to enhance visualization of lesions within the brain, spine, breast and urinary tract. (See example in Figure 85).

When administered in a usual dose, the predominant effect of Gd-DTPA is to lower the T_1 of the tissues where it is accumulated. Therefore, a T_1 -weighted sequence should be employed to demonstrate the contrast enhancement. In practice, a spin echo sequence (typically with TR of 500 ms and TE 15-20 ms) is used to acquire both pre-contrast and post-contrast images. By comparison, a T_2 -weighted spin echo protocol demonstrates little enhancement effect.

FIGURE 85

Image (A) is made immediately after administration of Gd-DTPA, while image (B) is made after a while, showing contrast agent uptake.



At intermediate echo times (TE), the most sensitive sequence for detecting contrast enhancement is the medium- T_1 inversion recovery sequence, with TI intermediate between the lesion T_1 before and after contrast enhancement. If T_1 is lowered to a value similar to that of fat, the use of fat suppression by SPIR might be helpful to distinguish enhanced tissue from fat. With very short echo times, the spin echo sequences are now more effective at demonstrating the enhancement effects than IR sequences. In addition, the use of a dynamic, T_1 -weighted FFE scan in combination with subtraction of the pre-contrast reference image, allows for time-resolved monitoring of contrast wash-in/wash-out.

CAUTIONS AND CONTRA-INDICATIONS IN MAGNETIC RESONANCE IMAGING

During a magnetic resonance imaging examination, the patient is exposed to strong magnetic fields and radio frequency pulses. At present, there are no known effects of magnetic fields on biological systems. Fast changes in magnetic fields, which occur during gradient switching, cause Faraday currents in tissues. The most sensitive tissue to these currents is the retina, which can be activated, resulting in flash-like sensations.

The RF pulses used in MR imaging produce warming of tissues. This could result in local thermal injury and/or system thermal overload with an extra burden on the cardiovascular system. RF heating increases with the square of field strength, since the absorbed energy is roughly proportional to the square of the RF frequency used. Therefore, in high field strength systems, the repetition time may need to be set above a certain minimal value to maintain RF power deposition within regulatory limits. Users are instructed to refer to current regulatory guidelines for details on power deposition limits.

Non-aneurysmal surgical clips, vascular clips, and artificial joint prostheses are safe for MRI, although a localized image artifact may be present. Stainless steel and non-ferromagnetic metal implants (e.g., titanium), and many inferior vena caval filters and central venous lines or mediports are also considered safe. Of course, if there is any doubt concerning the safety of a specific device, the physician should check with the implant manufacturer before proceeding with an examination.

The main risk to patient safety during an MR exam is the potential projectile effect of ferromagnetic objects placed unattended within the magnetic field. Patients and medical staff should be carefully instructed prior to entering the imaging room to avoid potential hazards from certain metallic objects which can become projectiles.

Critically ill patients requiring close monitoring are not optimal candidates for MR since diagnostic ECG waveforms are distorted during the course of the MR exam. Operation of defibrillators, external pacemakers, and other monitoring instrumentation is also problematic within the magnetic fields frequently encountered in the MR examination room.

Conventional cardiac pacemakers, ferromagnetic aneurysm clips, neurostimulators, pre- 1964 Starr-Edwards prosthetic heart valves, and other implanted ferromagnetic devices are contraindications to MRI due to possible motion of ferromagnetic devices and electromagnetic interference or possible current induction in indwelling electrodes or wires. In addition, care must be taken within patients who have metallic foreign bodies embedded in the eye, or shrapnel.

Although no deleterious effects have been demonstrated in pregnant women or fetuses, current FDA guidelines suggest that MRI be used only when there are clear medical indications and it offers a definite advantage over other imaging modalities with known risks or hazards.

A small percentage of patients experience claustrophobia and may require sedation during examination. Thorough screening of each patient prior to the study is critical to determine to what extent sedation is required.

Chapter 6

Special Techniques

This chapter describes several special application areas of MRI:

- Magnetic resonance angiography or MRA, including phase velocity mapping.
- Cardiac imaging.
- Magnetic resonance spectroscopy or MRS, including spectroscopic imaging.
- Functional imaging

MAGNETIC RESONANCE ANGIOGRAPHY

The ultimate exploitation of flow effects in MRI is magnetic resonance angiography (MRA). Conventional intra-arterial X-ray angiography, in which blood vessels are imaged after introduction of a solution that is X-ray opaque, increases the contrast between blood vessels and surrounding tissue. However, in addition to radiation exposure, the patient is also subjected to attendant risks, including infection and internal bleeding. Six percent of angiography patients suffer minor consequences while 2.6 percent require surgical intervention to remedy complicating sequelae. By comparison, MRA procedures do not require insertion of catheters, do not employ contrast solutions, and can be readily performed on an outpatient basis.

Nearly all common MR angiography methods share several fundamental steps, including:

- acquisition of a flow-sensitive image with suppression of stationary background tissue for emphasizing vascular anatomy.
- generation of a projection image for visualization of the vasculature.

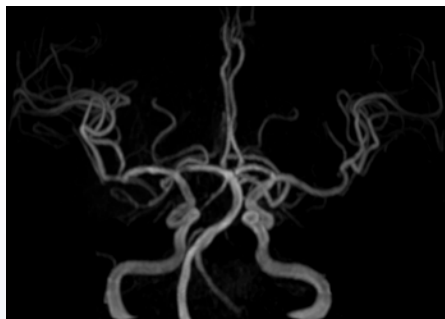
The requirement for a projection image stems from the vessel tortuosity inherent in many of the regions of interest in angiography (e.g. neurovascular anatomy). To adequately assess blood flow in areas such as the Circle of Willis, it is necessary to follow the vessel throughout its course. Use of a 3D-FT image acquisition permits the most flexible data set for projection images, since the image can be freely rotated for viewing alternate projections. Image acquisition relies on use of either inflow or phase effects to generate images with high signal intensity in the vascular anatomy and a low background signal from surrounding stationary tissue. Figure 86 demonstrates the potential of MRA for neurovascular exams, showing two different projections of the same anatomy, acquired during a single 3D-FT volume acquisition.

At present, there are two common methods for magnetic resonance angiography:

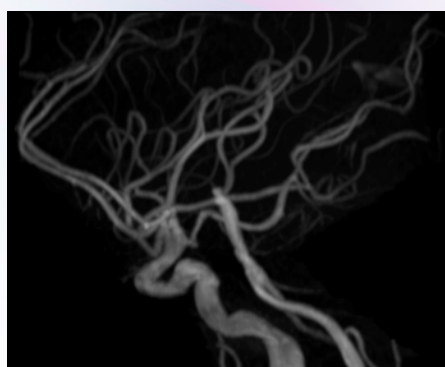
- Inflow MRA.
- Phase Contrast Angiography (PCA).

FIGURE 86

A coronal (A) and a sagittal (B) vascular projection of blood vessels in the head produced from one single MRA acquisition.



- (A) may be selectively imaged by the use of presaturation protocols. Second, image subtraction like in phase contrast MRA is not necessary, reducing scan time and computing requirements.



Inflow MRA can be applied in either M2D (multiple single slice) or 3D modes. Both M2D and 3D Inflow use gradient echo pulse sequences. The M2D technique is especially useful for imaging slow flow due to the good refreshment of flowing blood. A series of thin (2-3 mm) contiguous or overlapping slices are collected. (See Figure 87 for a description of overlapping slices.) The use of overlapping slices helps reduce the appearance of “staircase artifacts” – ragged edges – on the final image. 3D MRA can be applied to fast flowing (arterial) blood and to visualize small (high resolution), tortuous vessels. By using the 3D technique with thin slices, the voxel size decreases and intravoxel dephasing is reduced. This makes the 3D technique especially suitable for imaging aneurysms or the Circle of Willis where fine detail is necessary. Table 7 gives an overview of the characteristics of inflow MRA.

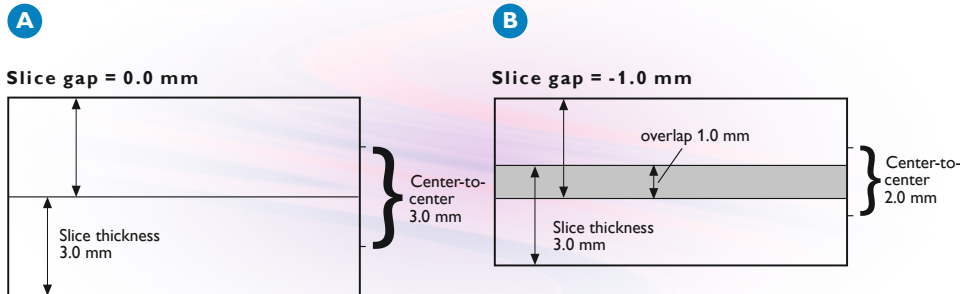


FIGURE 87

(A) Contiguous slices.
(B) Overlapping slices.

INFLOW MRA	Advantages	Disadvantages
General	<ul style="list-style-type: none"> - Reprojection and subvolumes possible - Presaturation works well 	<ul style="list-style-type: none"> - Thrombus may simulate flow - Tortuous vessels give less contrast
M2D	<ul style="list-style-type: none"> - Sensitive to slow flow - Reasonable scan times - No saturation effects 	<ul style="list-style-type: none"> - Thick slices - Large voxels; more intravoxel dephasing - Motion artifacts - Insensitive to in-plane flow - Long TE - Relatively poor SNR
3D	<ul style="list-style-type: none"> - Short scan times - High spatial resolution - Very short TE - Good SNR - Small voxels - Less dephasing (due to small voxels, short TE) - Sensitive to in-plane flow (small flip angle) 	<ul style="list-style-type: none"> - Insensitive to slow flow - Field distortion artifacts (air/bone) - Limited vessel track (<70 mm) - Sensitive to motion - Less static background suppression

TABLE 7

Advantages and disadvantages of inflow MRA.

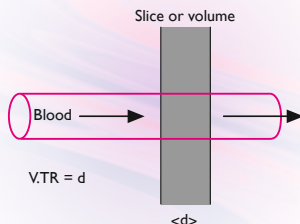


FIGURE 88

Blood refreshment in inflow

MRA depends on flow velocity, slice or volume thickness and TR.

The maximum contrast between flowing blood and stationary tissue is obtained when the blood is completely refreshed and read-out is immediately after excitation. As illustrated in Figure 88, the threshold minimum velocity is given by, $V_t = d/TR$, where d is the slice thickness and TR is the repetition time.

An important variable in this calculation is the thickness, d . In M2D Inflow, this is the thickness of one slice only. In 3D Inflow, this is the thickness of the volume, covered by a number of slices. This leads to a significant difference in contrast behavior between the two techniques:

- Using M2D over a thin slice or at high velocity, blood in the region d is completely replaced by unsaturated blood before the next RF pulse. This leads to bright appearance for blood relative to stationary tissue.
- Using 3D MRA over a large volume or at lower velocities, only part of the blood is replaced and part of the blood is increasingly saturated, depending on the number of excitations experienced. Consequently, blood will appear less bright compared to stationary tissue than with M2D. This effect can be partly compensated by using multichunk 3D, where the total volume is divided into subvolumes that are measured interleaved.

To optimize contrast, the repetition time (TR) should be short relative to the T_1 value of stationary tissue. This provides good suppression of the background with strong contrast to flowing blood. Maximum refreshment is provided when the imaging plane is orthogonal to the vessel orientation. Flip angle is also important in achieving maximum suppression of stationary tissue: for M2D a flip of $50^\circ\text{--}70^\circ$ is typical; for 3D a smaller flip, $15^\circ\text{--}25^\circ$ is more common. Finally, the thinner the slice the better the refreshment and the lower the intravoxel dephasing. Hence, thin slices are preferred for MRA inflow procedures. Background suppression can be improved by combining inflow MRA with MTC.

The phase of the transverse magnetization is made independent of the flow velocity by the use of velocity-compensated gradients. However, higher order flow terms, such as acceleration, do result in some spin dephasing. These high order flow terms may cause signal void in areas of turbulent flow. The use of the shortest possible echo times minimizes this signal loss.

Selective suppression of inflowing blood can be accomplished by positioning a saturation slab, as shown in Figure 89. In Inflow MRA, a REST slab can be used to suppress arterial or venous flow. The saturation slab orientation can be selected parallel to the slices, perpendicular, or free. In 2D inflow a single sided, parallel presaturation slab moves with the slice position ensuring good suppression. In 3D inflow its position is fixed. The slab thickness must be chosen large enough to insure complete saturation of the unwanted vessel, although the smaller the REST slab, the more accurate the saturation will be. For some applications, however, it is preferable to orient the presaturation slabs perpendicular to the imaging slice. An example of the use of perpendicular presaturation is imaging the carotids in the sagittal or coronal direction. A perpendicular presaturation slab is necessary to remove the venous flow.

Combination of inflow MRA with cardiac gating avoids artifacts like ghosting or signal voids due to pulsatile or retrograde flow. Cardiac triggering can be employed either to obtain temporal information about blood flow or just to get rid of pulsation artifacts.

Since the 2D method is a multiple single slice technique, the slices are reconstructed as they are collected. For routine transverse slices of the carotids, processing methods consist of projecting the stack of slices in a plane orthogonal to the slice direction. This method can also be used with sagittal or coronal images, with projections made along any orthogonal axis. Inflow image processing uses a maximum intensity projection (MIP) format with interpolation between the slices; the maximum intensity voxel along a given vector is used for that projective view. See Figure 90.

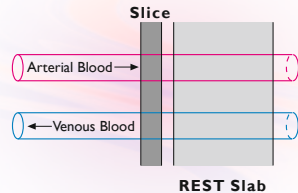


FIGURE 89

Use of a REST presaturation slab to selectively saturate inflowing venous blood.

FIGURE 90

Projected views in inflow MR angiography – the basis for maximum intensity projection reformatting.

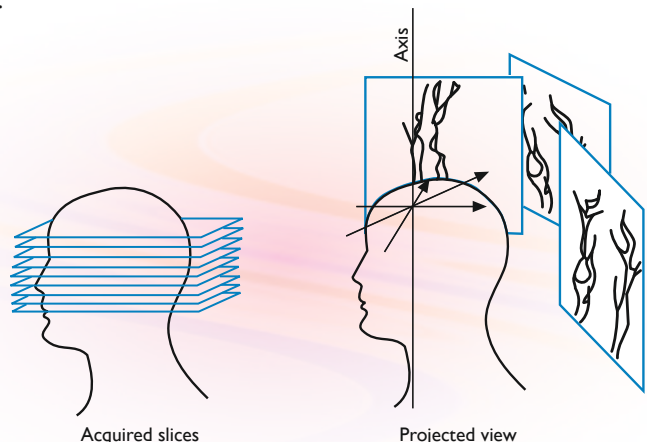


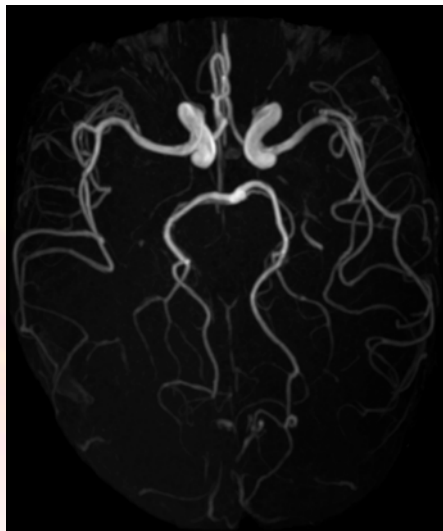
Figure 91 is an example of a maximum intensity projection of a 3D-inflow measurement. An alternative processing algorithm, Freestyle Reformatting, combines the basic functionality of the MIP format with the ability to perform reformatting in any planar orientation. This allows greater flexibility in evaluating the MRA data, particularly for viewing data independent of the centre of the imaged volume.

Black blood MR angiography is an alternate inflow method which uses spin echo acquisition to increase the signal of static tissue and create a signal void (i.e. no MR signal) for flowing blood. The data is processed using a minimum intensity projection algorithm to yield the final MR angiogram.

Black blood magnetic resonance angiography offers the advantage that turbulent flow, just as regular flow, will create a flow void - i.e. all blood will be black. However, the contrast between vessel and static tissue may be lower, arterial and venous flow may not easily be distinguished, and several "natural" regions of signal void (e.g. nasal sinuses) exist, which can complicate the generation of the minimum intensity projection image. Despite these disadvantages, black blood MRA can be a useful adjunct in the determination of some pathologies, such as severe stenotic lesions.

FIGURE 91

A 3D inflow angiogram of the head.



PHASE CONTRAST ANGIOGRAPHY (PCA) AND PHASE VELOCITY MAPPING

While inflow MRA depends on the refreshment of flowing blood into tissue slices for signal, Phase Contrast Angiography employs the phase shift in the MR signal that is induced by the flowing blood. The accumulation of flow-induced phase shift is proportional to velocity and there is a direct correlation with signal intensity. Therefore, with phase contrast methods, complete suppression of stationary tissue (if there is no velocity, there is no signal) can be achieved. This means that small vessels can be clearly visualized, even with slowly flowing blood. Plus, the user has control over the velocity sensitivity of the image which allows focusing on either fast or slow flow over a large area of interest. Figure 92 is an example of a PCA image.

In a normal MR image, signal intensity is the basis for image reconstruction. This image is referred to as a magnitude or modulus image. Alternately, images can be constructed based on the phase of the spins in each voxel. These images are called phase images. By applying flow sensitive gradients during acquisition of a phase image, it is possible to correlate the phase and the velocity of the moving spins via an “image”, called a phase velocity map, in which a phase image is “mapped” to depict velocity differences in moving spins across the image area.

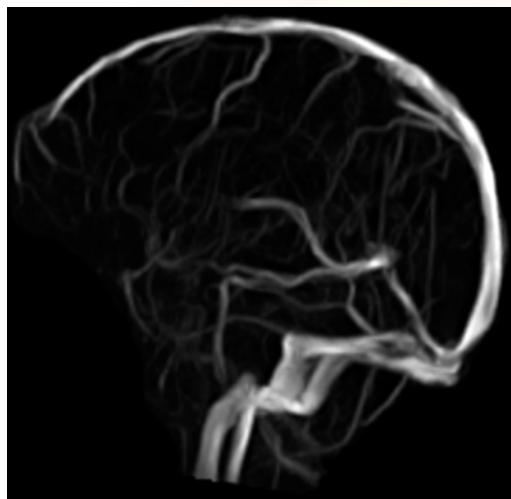


FIGURE 92

Phase contrast cranial venogram.

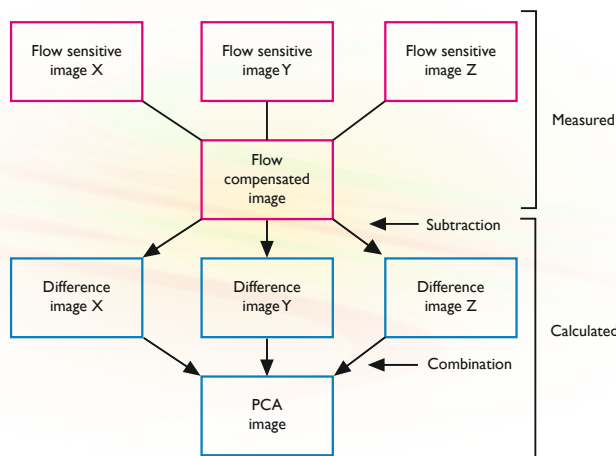
When static spins are subjected to a gradient reversal, the phase at the termination of the applied gradient is zero. By comparison, when moving spins are subjected to the same applied gradient system, the spins still possess a net phase at the termination of the applied gradient. This phase is dependent on the velocity of the spins during the time the gradient was applied.

Since magnetic field inhomogeneities and eddy currents also cause phase changes in an imaging slice, it is necessary to acquire a flow-compensated background image. By using flow compensation gradients to eliminate phase changes due to flow, a phase image can be created in which phase effects result exclusively from unwanted magnetic field aberrations. By subtracting this image from the velocity-sensitive image, we can thus produce a final image which accurately represents velocity effects within the image slice.

Phase Contrast Angiography (PCA) requires the acquisition of two, three or four images per slice, of which one, two or three are velocity-sensitive in a specified direction and the other velocity-compensated. A gradient is applied in the CC (cranial-caudal), AP (anterior-posterior), LR (left-right), all three directions or a combination of two of these to provide the flow encoded image. A flow compensated scan is subtracted from these flow sensitive scans. The results are combined into a composite image made of flows in 1, 2 or 3 directions. This image is processed to the PCA image. The construction of a PCA image is shown in Figure 93. Intensity in the PCA image is related to flow velocity, but this relation is quite complex. Higher velocities are represented as higher intensities, but there is no information on flow direction. Apart from the PCA image, that displays vasculature, an FFE image is also generated in the reconstruction, allowing comparison of vasculature and the soft tissue image

FIGURE 93

The construction of a PCA image.



PCA	Advantages	Disadvantages
General	<ul style="list-style-type: none"> - Variable velocity encoding allowing depiction of slow and fast flow - Excellent background suppression (if slice thickness >60 mm) - Minimized saturation effects; large track of vessels - Differentiation between flowing and stationary blood (hemorrhage) - Directional flow images 	<ul style="list-style-type: none"> - Long TE - Presaturation less effective, only for small track of vessel - More turbulence effects
PCA 2D	<ul style="list-style-type: none"> - Short scan times (one or few slices) - Useful as survey 	<ul style="list-style-type: none"> - No projection images - Large voxels due to thick slice - Low SNR - Signal loss with overlapping slices (due to thick slices)
PCA 2D mode cinema	<ul style="list-style-type: none"> - Variable velocity encoding - Time resolution - Hemodynamic flow information 	<ul style="list-style-type: none"> - Needs cardiac triggering; longer scan times
PCA 3D	<ul style="list-style-type: none"> - Small voxels - Reprojection and subvolumes possible 	<ul style="list-style-type: none"> - Long scan time - Motion sensitive - Field distortion artifacts (air/bone)

TABLE 8

Advantages and disadvantages of Phase Contrast Angiography.

PCA is applicable for both two-dimensional and three-dimensional acquisition. 2D-PCA is generally used for fast acquisition of one single thick slice and is especially valuable as a survey for more time-consuming 3D-PCA studies. 3D-PCA is implemented using acquisition of multiple thin, contiguous or overlapping slices with reduced intravoxel dephasing. This allows inspection of the vessels in any direction with complete background suppression. Table 8 lists some advantages and disadvantages of the PCA technique.

PCA is less subject to saturation effects than Inflow MRA. In addition, PCA is effective at imaging large sections of a vessel. Since scan orientation may be in-plane with the vessel, fewer slices are needed to cover larger areas. With PCA, cardiac synchronization is also required for optimal imaging of vessels with pulsatile flow.

Phase velocity maps can be used for quantitative assessments of fluid volume flowing through an imaging plane. A quantitative flow measurement requires an acquisition scheme similar to that of Figure 93, but instead of the PCA image, a phase velocity map is generated. By integrating flow velocity across a vessel diameter, a mean cross-sectional flow can be calculated, which can then be plotted as a function of time across a series of images. Figure 94 shows a typical flow-versus-time curve for flow in the ascending aorta and main pulmonary artery. By integration of the area under the curves, one can calculate fluid (blood) flow volumes through the vessel. This technique can be used for quantization of right and left ventricular stroke volumes during functional assessment in cardiac pathologies.

FIGURE 94

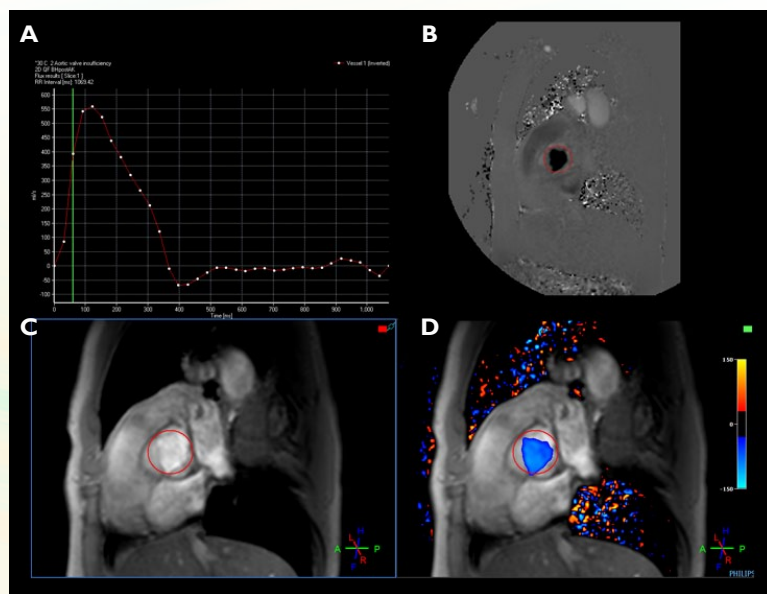
Quantitative flow –Aortic valve.

A) Flow versus time curve.

B) Phase Image

C) Modulus Image

D) Modulus image with color overlay



TRIGGERED ACQUISITION SEQUENCES – CARDIAC IMAGING

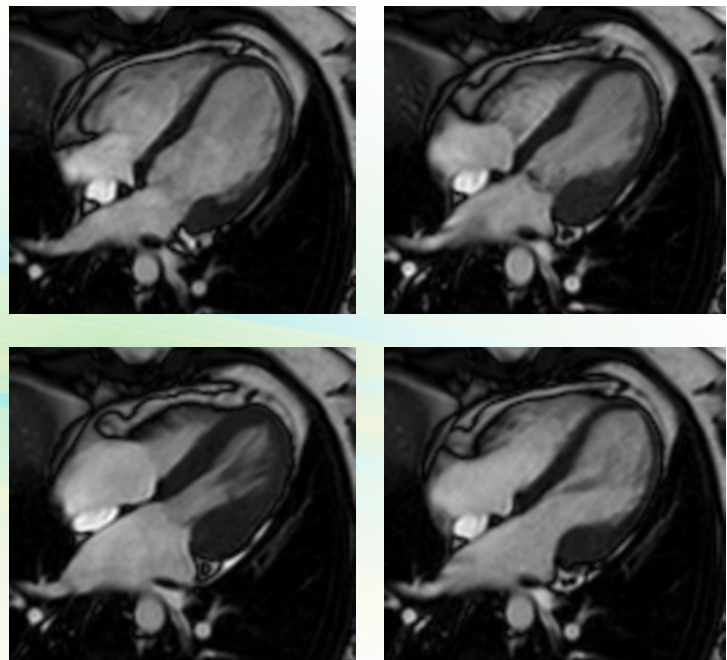
MR imaging has been established as a viable and, in some cases, unique imaging technique for cardiological examinations. Its utility is related to the ability to provide both precise morphology and assessment of global and regional ventricular function.

Since dynamic processes involve anatomical motion which reduce image quality; it is necessary to “freeze” the effects of motion. This is achieved using cardiac triggering – the coupling of image acquisition to a trigger signal – for cardiac studies, generally to an ECG signal. Using the assumption that most biological motion is rhythmic, triggering permits multiple images to be acquired within a single cardiac cycle, with same-phase images from consecutive cardiac cycles averaged together to improve signal-to-noise ratio in the final image. Since the images from multiple cardiac cycles are acquired at the same point into the cycle, the effects of motion are minimized. An image series can also be played back in cinematic loop fashion, called cine imaging, to provide physicians a way of viewing dynamic activities. (See Figure 95).

Triggered acquisitions are generally performed in conjunction with a gradient echo pulse sequence. Gradient echo imaging permits reduced repetition times for improved temporal resolution. Using a typical gradient echo pulse sequence, it is possible to acquire data from a single image slice in approximately 25 ms. With gated, cine MRI, a single slice, multiphase imaging series covering the full cardiac cycle, and with temporal resolution of 25 ms/image, can be acquired in approximately 5 minutes. A dual-slice acquisition with temporal resolution of approximately 50 ms/image can be acquired in the same time period.

FIGURE 95

Four images representing 4 different phases from the cardiac cycle obtained by cine acquisition.



The technique of retrospective gating employs uninterrupted multiphase acquisition over the entire cardiac cycle. During reconstruction, the profiles will be assigned to different heart phases. This permits obtaining end diastole information and elimination of the “lightening” effects that occur in conventionally-triggered imaging, since, due to non-steady state imaging the intensities for different phases differ.

MAGNETIC RESONANCE SPECTROSCOPY CHEMICAL SHIFT

Nuclei of different elements resonate at different Larmor frequencies, since they differ in gyromagnetic ratio. But even spins of the same isotope experiencing the same local magnetic field may resonate at slightly different frequencies, if their molecular environment – chemical bonding – is different. An example of this effect is already discussed as the water-fat shift. The relative difference is a result of the influence of nearby nuclei. These frequency differences are called chemical shifts. An MR spectrum has chemical shift on the horizontal axis and intensities on the vertical.

The chemical shift is expressed in units of 10^{-6} or ppm (parts per million) which makes it independent of magnetic field strength. Chemical shifts for ^1H are typically in the range of a fraction of a ppm to about 10 ppm, see Table 9. They always refer to a standard substance. Comparison of values for the chemical shift measured in a sample with values in tables allows identification of chemical substances. Concentrations of substances may be estimated from line intensities after calibration of the measurement system.

TABLE 9

For in-vivo spectroscopy these values are an indication for the spectral ranges for different nuclei.

NUCLEUS	RANGE in ppm	RANGE in Hz for 1.5T
^1H	10	640
^{31}P	30	770
^{13}C	200	5000
^{19}F	2000	120000

In order to be able to distinguish close peaks, the magnetic field homogeneity has to be at least 0.1 ppm. Since a patient is a very inhomogeneous sample, local shimming in the volume of interest is required.

LOCALIZATION

In MR spectroscopy (MRS) of living organisms, one encounters the problem of how to localize such spectra to any particular area in the body. It is useless, for example, to determine the ^{31}P spectrum of the human head. It is more likely of interest to record a spectrum of a particular part of the brain, as is illustrated in Figure 96. The use of a surface coil is the simplest way of localization, see Figure 97, but this localization is restricted to areas close to the body surface and does not allow for flexible adaptation of size and shape of the volume of interest.

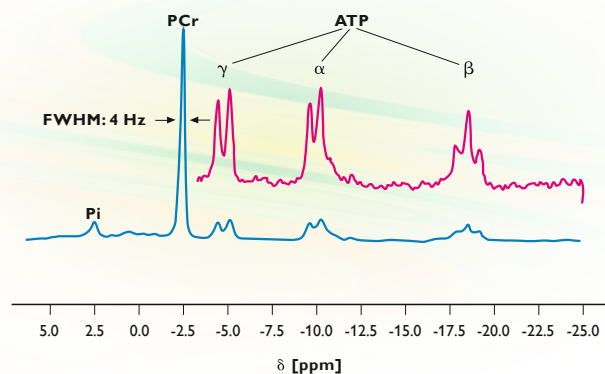


FIGURE 96

A 25.9 MHz ^{31}P surface coil spectrum of the human calf.

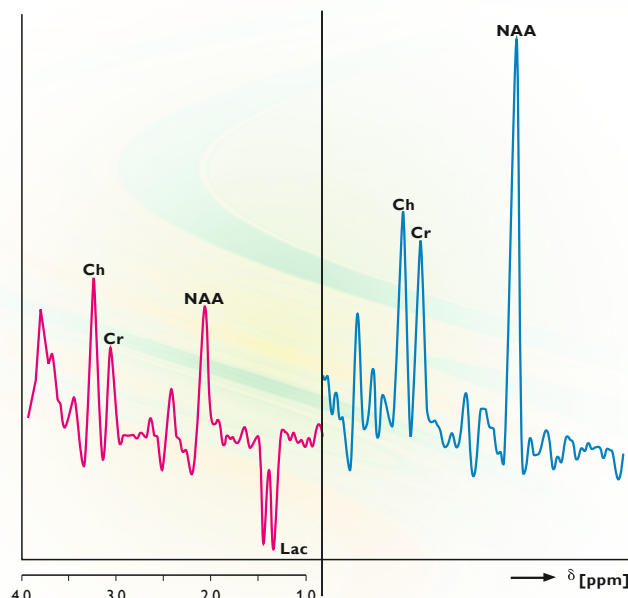


FIGURE 97

Single voxel ^1H spectra taken from a symptomatic (left) and a control region (right) in the brain of a patient suffering from seizures and showing a high intensity lesion in a T_2 -weighted image. The spectra are acquired from a $2 \times 2 \times 2 \text{ cm}^3$ voxel.

It is possible to define a volume of interest on a survey image and then acquire spectra from that region only. This is called image localized spectroscopy. The selection of the spectroscopy volume is achieved by a combination of carefully designed excitation pulse sequences and gradient sequences. Several techniques are in use, but only two will be further explained here, one which is mostly used in ^{31}P spectroscopy and one which is particularly useful for ^1H spectroscopy.

VOLUME SELECTIVE ^{31}P SPECTROSCOPY

The ILOPS (Image LOcalized Phosphorus Spectroscopy) sequence is mostly used for ^{31}P spectroscopy. In the one-dimensional version of this technique a slice selective inversion pulse is followed by a non selective 90° pulse and data acquisition. This is repeated, without an inversion pulse. Subtraction of the two measurements will cancel all signal originating from outside the selected slice. In ILOPS, this technique is extended to confine the volume of interest in three directions, which requires that the experiment is carried out eight times. The resulting eight signals are then combined with the appropriate signs, so that all signals except the signal from the selected volume element cancel and only the signal of the selected volume element remains.

ILOPS is useful in ^{31}P spectroscopy, since signal acquisition can start immediately after the 90° excitation pulse, so that signal losses due to the relatively short T_2 relaxation time of many ^{31}P metabolites remain small. Because of the low ^{31}P metabolite concentrations in the tissue, an improvement of signal-to-noise ratio by multiple signal acquisition is always needed, so that the fact that eight measurement cycles are required to obtain a spectrum of the selected volume element will not lead to increased measurement times.

LOCAL ^1H SPECTROSCOPY – SUPPRESSION OF THE WATER RESONANCE

For the localization of ^1H signal a technique is used which localizes the signal from a selected region of interest in one single acquisition. This method, PRESS (Point RESolved Spectroscopy) or PRIME (PRe Inversion Multi Echo), comprises a slice selective excitation pulse, followed by two slice selective refocusing pulses. As all slice selections are orthogonal, only the signal from the volume, which is intersected by all three selected slices is preserved. This technique not only localizes one single excitation, but suppresses signal from outside the volume of interest much better than other techniques, which rely on add-and-subtract schemes for localization. An important feature of a single excitation localization technique is the ability to use the sequence for localized shimming. The timing between the pulses determines the actual echo time at which the signal is acquired. In proton spectroscopy, an echo time between 10 and 25 ms is considered a short echo time, whereas other echo times, which are often used are 136 or 272 ms. At these typical values, the signals in the proton spectrum have a well-defined phase, which results in well-resolved proton resonances.

A problem in ^1H spectroscopy is that ^1H nuclei are present in very high concentrations (80 M) in water in tissue. This has to be compared with the concentrations of the biochemical compounds (metabolites) measured with spectroscopy, which range from 20 mM maximum to 1 mM (lower detection limit of in-vivo NMR). The water line has such a high intensity in the spectrum that the resonances of all other ^1H compounds are practically invisible, since these are present in almost 10,000 times lower concentrations. However, it is these compounds which are of interest for investigating metabolism.

Water suppression techniques in volume selective proton spectroscopy are quite analogous to fat suppression techniques in imaging, in particular the SPIR technique. To suppress the water, a slice-selective pulse is given to the water resonance. By adjusting the bandwidth of this pulse to 1 ppm, only the water signal or metabolite signal in a range of 0.5 ppm around the position of water is affected. This pulse may be a 180° inversion pulse followed by a delay to null the water resonance, when the first excitation pulse of the PRESS sequence is generated. Another method consists of a slice-selective 90° excitation pulse just at the water resonance frequency followed by a strong dephasing gradient, which spoils all the water magnetization in the transverse plane. These techniques are capable of suppressing the water signal to the extent that the much smaller metabolite signals become clearly visible.

SPECTROSCOPIC IMAGING

Spectroscopic imaging (SI) combines MR spectroscopy with spatial encoding in two or three directions, so that spectroscopic information is displayed in images: For each peak in the spectrum a spatial distribution of the peak intensity can be displayed, with the intensities represented on a gray-scale. Comparison of these metabolite images with normal MR images yields additional information. An example is given in Figure 98. The size of the voxels in spectroscopic imaging is considerably larger than in normal MRI. In ^1H spectroscopic imaging the minimum voxel size is 1 cm^3 , while the maximum matrix size is 32×32 . Spectroscopy of the brain, particularly proton spectroscopic imaging, already gave insight in the detailed metabolism of several pathologies in the brain. Grading and staging of intracranial brain tumors, assessment of stroke and other ischemic injuries, multiple sclerosis, epilepsy and several inborn brain deficiencies in neonates have been successfully studied by localized brain spectroscopy and spectroscopic imaging. Some of these studies have been combined with other modalities (e.g. PET studies), to value the extra information MRS or MRSI may give.

FIGURE 98

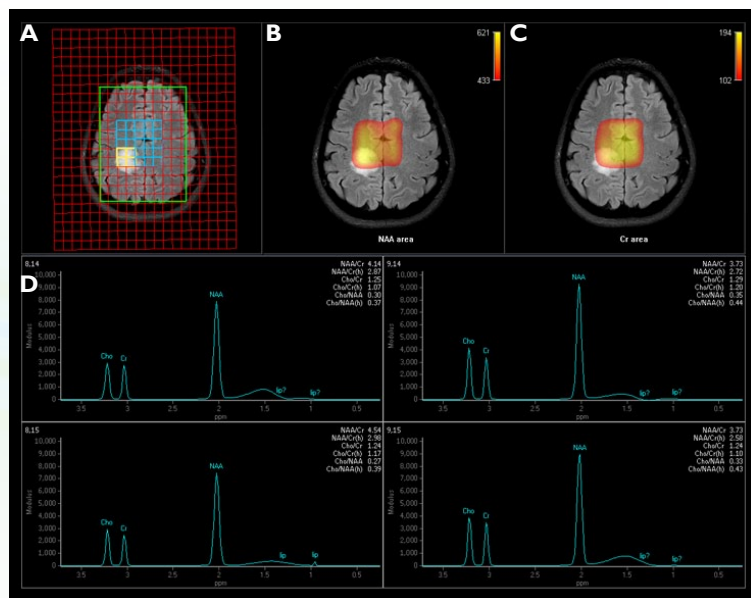
Example of spectroscopic imaging in the brain

A) Grid overlay

B) N-acetyl aspartate image

C) P-creatine image

D) Proton metabolite spectrum



FUNCTIONAL IMAGING

Functional imaging of the brain is one of the most exciting recently developed applications of magnetic resonance imaging. The visualization of activated cortical brain regions during external stimulations or performing specific tasks opens a completely new perspective for the use of MRI.

Functional brain imaging comprises a variety of approaches, which result in information of the human brain, which goes beyond morphology only. Recently developed techniques offer functional information of the brain with an unprecedented accuracy, spatial and temporal resolution. These techniques share the characteristic that the signal is derived from the proton signal as in normal MRI. However, contrast is no longer a function of proton density, T_1 and T_2 only. Other physiological processes play a major role in the generation of contrast.

Each technique has its own specific instrumental requirements and applications. Image processing may also require completely new approaches to optimize the information content of measurements. The potential of these techniques is embedded in the fact that by the introduction of fast scanning techniques, most measurements can be combined in a single examination, offering the possibility for a comprehensive brain study that goes far beyond any current diagnostic imaging modality.

FUNCTIONAL BRAIN IMAGING

The direct observation of activated cortical brain regions without the use of contrast agents is one of the most spectacular new applications in the field of whole body MRI. Several contrast mechanisms have been described to explain this phenomenon. Two models are currently used to describe the observed signal increase in the activated brain regions.

During activation, the blood flow in activated regions may increase by 20-40%. The increase in oxygen consumption during an activated state of brain tissue is only 5%. This incommensurate change in local blood flow and local oxygen extraction increases the oxygen tension in the activated area. Due to decreased susceptibility of oxygenated blood, activated brain tissue will be characterized by a longer T_2^* than non-activated brain tissue. By using heavily T_2^* weighted sequences, activated brain areas will show an increase in signal intensity. By subtracting non-activated from activated images, the area of activation will show up brightly.

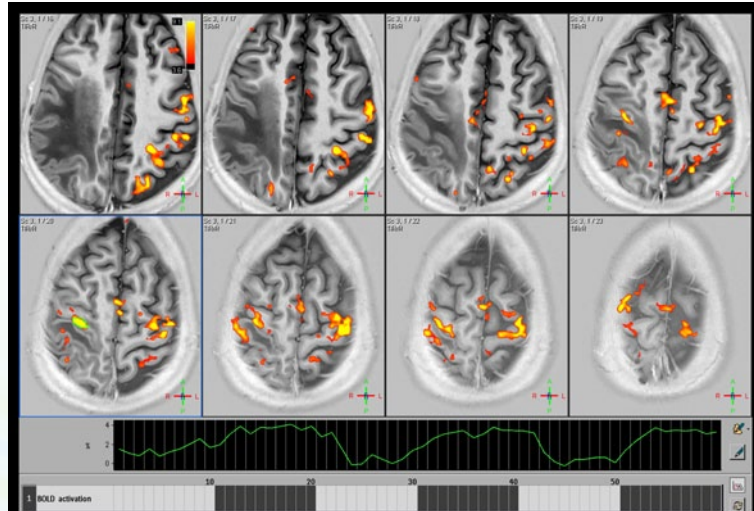
This type of imaging is called Blood Oxygen Level Dependent (BOLD) contrast imaging. An important characteristic of this type of contrast is the field dependence: Susceptibility effects scale linearly with field strength.

Not only changes in susceptibility may be used to generate contrast during brain stimulations. The substantial increase in local blood flow during a stimulation may result in a direct time-of-flight effect: increased blood flow related to increased energy demand in activated brain regions may be registered by MR techniques that are sensitive to flow changes. The increase in blood flow may be visualized in heavily T₁-weighted sequences. This may result in local signal enhancement in venous structures associated with the activated region (time-of-flight contrast in functional imaging).

Most applications of functional imaging have been restricted to simple task activation studies. Motor cortex activations, stimulation of the optical nerve centre and the speech centre have been used to illustrate the potential use of MR to image function. Some cognitive task studies have been performed (e.g. silent speech protocols), but in general the signal changes observed in such task performance are smaller than in optical or sensory type of stimulations. An example of an application is given in Figure 99.

FIGURE 99

Functional Imaging in the motor cortex of the brain, with finger tapping. Color activation of the motor cortex, displayed on a T₁ anatomical image.



FUNCTIONAL IMAGING USING CONTRAST AGENTS

The underlying principle of detecting changes in the brain related to activation of neurons by the measurements of a bolus passage of (a new) contrast agent is completely different from the way in which contrast agents are used to delineate lesions. The increase in regional blood flow and volume in the activated areas results in an increased concentration of contrast agent. It is a short change of tissue susceptibility due to the passage of the contrast agent, which results in a local shorter T_2^* upon stimulation. During the bolus passage the signal in a T_2^* -weighted gradient echo (or EPI) sequence will decrease, whereas the signal intensity will partially restore directly after the passage.

After determining the dynamics of bolus passage on a pixel by pixel basis, the dynamic data set can be converted into a regional Cerebral Blood Volume (rCBV) map, which displays relative blood volume in the brain. One step beyond this application is to combine the magnitude of the signal changes with the mean transit times, which can be interpreted as Cerebral Blood Flow (CBF) information. The first rCBV application was to delineate activated regions in the brain, like the use of optical stimulation protocols to visualize the optical cortex. A much more important application of rCBV maps is the assessment of tissue perfusion in acute stroke or degenerative white matter disorders.

PERFUSION IMAGING

Contrast agents may be used to generate rCBV or CBF maps, but other techniques are available to detect tissue perfusion without using any contrast agent. The increased blood volume or blood flow in microvasculature in the brain may result in subtle apparent T_1 changes, which can be exploited to generate contrast. As these techniques have not been performed on humans yet, the future applications are quite uncertain.

DIFFUSION IMAGING

Diffusion weighted imaging is an application which generates contrast by signal attenuation related to a variation in the diffusion coefficient of water molecules in the image plane. The diffusion coefficient varies per tissue e.g. between CSF and grey matter by a factor of four. More interestingly, the diffusion coefficient may be altered due to pathology or exhibit an anisotropic behavior in some parts of the brain, e.g. in white matter fibre tracts.

Restricted diffusion related to ischemic processes in the brain or to the anisotropic structure of the elongated nerve bundles can be measured by heavily diffusion weighted imaging. Most diffusion weighted imaging sequences have a bipolar pair of diffusion sensitizing gradients in common. Some applications in brain diffusion imaging attract quite some attention, the most important being related to the very early detection of an ischemic insult (stroke), long before edematous effects can be seen on normal T_2 images.

180° pulse	31	Contrast Agent	107, 131
¹ H Spectroscopy	127	Contrast Enhancement	66
³¹ P Spectroscopy	126	Contrast Wash-in	109
3D Imaging	55	Cross-relaxation	29
90° pulse	31	Crosstalk	49, 69

A

Abdominal Compression	104	Dead Time	67, 68
Actively Shielded	43	Delay Time	75
Actively Shielded Gradient	40	Detection Coil	30
Aliasing	105	Diffusion	132
Artifacts	69, 73, 84, 103	Dual Echo	78
		Dynamic Imaging	72

B

B_0	20	Echo	30, 31
B_1	22	Echo Planar Imaging (EPI)	79
Backfolding	105	Echo Time (TE)	31, 68, 73, 83, 89, 92, 94, 96, 99
Bandwidth	48, 49	Eddy Currents	40, 103, 107, 120
Binomial Pulses	127	Effective Echo Time	77
Black Blood MR Angiography	118	Effective Transverse Relaxation Time	28
Blood Oxygen Level Dependent (BOLD) Contrast	130	EPI	see Echo Planar Imaging
Blurring	103	Even Echo Rephasing	101
BodyCoil	90		
BOLD	see Blood Oxygen Level Dependent Contrast		
Bound Water Pool	29		
Breath Holding	104	Fast Field Echo (FFE)	61, 63, 79, 96
		Fast Flow	119
		Fat-Water Interfaces	105

C

Carbon	33	FFE	see Fast Field Echo
Cardiac Imaging	123	FID	see Free Induction Decay
Cardiac Triggering	104, 123	Field of View (FOV)	83, 84, 85
CBF	see Cerebral Blood Flow	Field Strength	83, 87, 90
Cerebral Blood Flow	131	First Echo	68
Chemical Shift	105, 124	FLAIR	see Fluid Attenuated Inversion Recovery
Cine Imaging	123	Flip Angle Sweep	74
Coil	40, 83, 86, 90	Flip Angle	22, 62, 87, 96, 116
Contiguous	69	Flow	97, 113, 129
Contrast	84, 85, 91, 116, 129, 130	Flow Artifacts	99

D

Dead Time	67, 68
Delay Time	75
Detection Coil	30
Diffusion	132
Dual Echo	78
Dynamic Imaging	72

E

Echo	30, 31
Echo Planar Imaging (EPI)	79
Echo Time (TE)	31, 68, 73, 83, 89, 92, 94, 96, 99
Eddy Currents	40, 103, 107, 120
Effective Echo Time	77
Effective Transverse Relaxation Time	28
EPI	see Echo Planar Imaging
Even Echo Rephasing	101

F

Fast Field Echo (FFE)	61, 63, 79, 96
Fast Flow	119
Fat-Water Interfaces	105
FFE	see Fast Field Echo
FID	see Free Induction Decay
Field of View (FOV)	83, 84, 85
Field Strength	83, 87, 90
First Echo	68
FLAIR	see Fluid Attenuated Inversion Recovery
Flip Angle Sweep	74
Flip Angle	22, 62, 87, 96, 116
Flow	97, 113, 129
Flow Artifacts	99

Flow Compensation	101, 104, 120	Helical Scan	80
Flow Enhancement	98	Homogeneity	38, 43, 85, 107
Flow Phenomena	83		
Flow Velocity	120		
Flow Void	97, 99	ILOPS see Image LOCALIZED PHOSPHORUS SPECTROSCOPY	
Flow-related Enhancement	98	Image	84
FLuid Attenuated Inversion Recovery (FLAIR)	65	Image LOCALIZED PHOSPHORUS SPECTROSCOPY (ILOPS)	126
Fluorine	33	Image LOCALIZED SPECTROSCOPY	126
Fold-over Suppression	105	Image Quality	83, 84
Fourier Transform	70, 80	Image Reconstruction	52
Fourier Transformation	30, 52	Imaging Sequence	59
FOV,	see Field of View	Imaging Speed	84
Free Induction Decay (FID)	30, 60	Implants	107, 109
Free Water Pool	29	Inflow Effects	69, 97
Freestyle Reformatting	117	Inflow MRA	114
Frequency	20	Inhomogeneities	28, 30, 61, 62, 71, 77, 83, 96, 120
Frequency Encoding Gradient	51	Interference	55
Frequency Spectrum	29	Inversion Prepulse	64, 75
Functional Imaging	129	Inversion Pulse	64, 65, 75
		Inversion Recovery (IR)	65, 75
		Inversion Time (TI)	65
G			
Gauss	20	IR	see Inversion Recovery
Gd-DTPA	108	IR-TSE	65
Ghost Images	97, 103		
Ghosting	39		
Gradient	39	K	
Gradient and Spin Echo (GRASE)	79	K-Space	56
Gradient Coil	37, 39	K-Space Shutter	70
Gradient Echo Imaging	96	Keyhole Imaging	72
Gradient Echo	61, 63, 66, 73, 96, 100, 123		
GRASE	see Gradient and Spin Echo		
G_x	see Measurement Gradient		
G_y	see Phase Encoding Gradient		
Gyromagnetic Ratio	20, 124		
		L	
Half-Fourier Imaging	71	Laminar Flow	100
Halfscan	70, 71, 87	Larmor Frequency	20, 22, 30
		Localization	125
		Longitudinal Relaxation	24
H			
Half-Fourier Imaging	71		
Halfscan	70, 71, 87		
		M	
		Magnet	37, 38
		Magnetic Field Gradient	47

Magnetic Field Homogeneity	38, 43, 107
Magnetic Field Inhomogeneity	83, 120
Magnetic Material Artifacts	107
Magnetic Moment	19
Magnetic Resonance Angiography (MRA)	98, 113
Magnetic Shielding	37, 43
Magnetic Susceptibility	83, 102
Magnetization Transfer Contrast (MTC)	29, 116
Matrix	54, 83, 84, 87, 128
Maximum Intensity Projection (MIP)	117
Measurement Gradient (G_x)	51, 53, 58, 63, 105
Minimum Intensity Projection	118
MIP	see Maximum Intensity Projection
Misregistration	100
Molecular Motion	25
Motion Artifacts	103
MR Spectroscopy (MRS)	125
MRA	see Magnetic Resonance Angiography
MRS	see MR Spectroscopy
MTC	see Magnetization Transfer Contrast
Multi-chunk	116
Multi-echo	68
Multi-slice	68, 73, 76, 77
Multiphase Imaging	123
Multiplanar Reformatting	56
M_{xy}	23
M_z	23
N	
Natural Abundance	32
Net Magnetization	20, 23
NMR,	see Nuclear Magnetic Resonance
Noise	86
NSA	see Number of Signals Averaged
Nuclear Magnetic Resonance (NMR)	13
Number of Phase Encoding Steps	70, 71
Number of Signals Averaged (NSA)	83, 88
O	
Overcontiguous Slices	56
Overlapping Slices	69
Oxygen	33
P	
Pacemaker	110
Packages	69
Paramagnetic	102
Passively Shielded	43
Patient Monitoring	37
PCA	see Phase Contrast Angiography
PEAR	see Phase Encoded Artifact Reduction
Perfusion	132
Permanent magnet	38
Phase	119
Phase Cycling	66
Phase Contrast Angiography (PCA)	119
Phase Effects	97, 100
Phase Encoded Artifact Reduction (PEAR)	104
Phase Encoding	56
Phase Encoding Gradient (G_y)	52, 55, 60
Phase Velocity Map	119, 122
Phosphorous	33
Physiology	37
Pixel	84
Point RESolved Spectroscopy (PRESS)	127
PPM	124
PRe Inversion Multi Echo (PRIME)	127
Precession	20
Preparation Gradient	63
Prepulse	29, 64, 75
Presaturation	114
Presaturation Pulse	99
PRESS	see Point RESolved Spectroscopy
PRIME	see PRe Inversion Multi Echo
Profile	56, 58
Profile Order	77

Projection Reconstruction	51	Ringing	103
Proton	20	Rotating Frame	22
Proton Density	83, 89, 91, 92		
Pulse	31	S	
Pulse Program	59	Saturation	61
Pulse Sequence	59	Saturation Pre-pulse	75
Q		SE	see Spin Echo
Quadrature Coil	41	Second Echo	68
Quantum Number	19	Sensitivity	32, 33
R		Shimming	39
Radial Scan	80	Short TI Inversion Recovery (STIR)	65
Radio Frequency Pulse	see RF Pulse	Shots	76
Raw Data	54, 56	Signal Averaging	87, 88, 93, 104
RCBV	see Regional Cerebral Blood Volume	Signal Detection	29
Read-out Gradient	see Measurement Gradient	Signal-to-Noise Ratio (SNR)	70, 71, 72, 79, 84, 85, 86
Reconstruction	37, 42	Single Shot	78, 79
Rectangular Field of View	71	Slice Gap	69
Reduced Acquisition	70	Slice Interference	49, 55
Reduced Scan	87	Slice Orientation	48
Refocusing Pulse	31, 60, 76	Slice Selection	48
Reformatting	117	Slice Selection Gradient	51, 52, 55
Regional Cerebral Blood Volume (RCBV)	131	Slice Thickness	49
REgional Saturation Technique (REST)	99 104 , 117	Slow Flow	115, 119
Relaxation	23, 30	SNR	see Signal-to-Noise Ratio
Relaxation time	27	Solids	91
Repetition Time (TR)	60, 68, 73, 76, 83, 87, 89	Spatial Encoding	47
Rephasing Field	61	Spatial Resolution	70, 71, 72, 84, 85
Rephasing Gradient	50	Spectral Presaturation with Inversion Recovery (SPIR)	66
Resistive Magnet	38	Spectrometer	42
Resonance Frequency	22	Spectroscopic Imaging	128
Respiratory Gating	104	Spin Density	23, 30
Respiratory Triggering	104	Spin Echo (SE)	30, 60, 77, 79, 99, 100
REST	see REgional Saturation Technique	Spin Echo Imaging	92
Retrospective Gating	124	Spin Preparation	63
RF Pulse	22, 48	Spin Quantum Number	19
RF Shielding	37, 44	Spin-Lattice Relaxation Time (Tl)	24, 83, 89, 92
		Spin-Spin	27
		Spin-Spin Interactions	30 32 60

Spin-Spin Relaxation Time	27, 30, 92	Turbo Field Echo (TFE)	73, 79
SPIR see Spectral Presaturation with Inversion Recovery		Turbo Spin Echo (TSE)	76, 79
Spiral Scan	80	Turbulent Flow	101
Spoiler Gradient	66		
Spoiler Pulse	66		
Steady State	62, 74	Velocity Sensitivity	119
STIR	see Short T1 Inversion Recovery	Volume Imaging	55, 97
Superconducting Magnet	39	Volume Selective Refocusing (VSR)	127
Surface Coil	41, 90	Voxel Size	84
Susceptibility	129	VoxeL	55, 84, 87, 128
Synergy Coil	42	VSR	see Volume Selective Refocusing

T

T_1	see Spin-Lattice Relaxation Time
T_1 Values	23, 24
T_1 -FFE	66
T_1 -Weighted	64, 75, 92, 95, 96, 108
T_2^* Effective Transverse Relaxation Time	28, 30, 60, 61, 96
T_2	see Spin-Spin Relaxation Time
T_2 Values	23
T_2^* -Weighted	96
T_2 -FFE	66
T_2 -Weighted	77, 93, 95, TE
see Echo Time	
Tesla	20
TFE	see Turbo Field Echo
Throughput	67
TI	see Inversion Time
Time-of-Flight Effects	97, 130
Tissue Presaturation	64
TR	see Repetition Time
Transverse Relaxation	27, 60
Transverse Spin-Spin Relaxation	27
True T_2 Value	32
TSE, see Turbo Spin Echo	76, 79
TSI	see Spectroscopic Imaging
Turbo Factor	78, 79

V

Velocity Sensitivity	119
Volume Imaging	55, 97
Volume Selective Refocusing (VSR)	127
Voxel Size	84
VoxeL	55, 84, 87, 128
VSR	see Volume Selective Refocusing

W

Warming of Tissues	109
Water and Fat Dephasing	106
Water Suppression	127
Water-Fat Shift (WFS)	87, 106
WFS,	see Water-Fat Shift

Z

Zero-filling	70
--------------	----

Basic principles of MR imaging

This book offers an introduction to the basic principles of magnetic resonance imaging. It is written for individuals with a clinical or scientific background, but does not assume prior knowledge of classical physics, quantum mechanics, or complex mathematics.



© 2010 Koninklijke Philips Electronics N.V. All rights are reserved.

Philips Healthcare reserves the right to make changes in specifications and/or to discontinue any product at any time without notice or obligation and will not be liable for any consequences resulting from the use of this publication.

Printed in The Netherlands.
4522 962 65271 * SEP 2010